Semiclassical Mechanics of the Wigner $6j$-Symbol

Vincenzo Aquilanti

Dipartimento di Chimica, Università di Perugia, Perugia, Italy 06100

Hal M. Haggard, Austin Hedeman, Nadir Jeevanjee, Robert G. Littlejohn, and Liang Yu

Department of Physics, University of California, Berkeley, California 94720 USA

E-mail: `robert@wigner.berkeley.edu`

Abstract. The semiclassical mechanics of the Wigner $6j$-symbol is examined from the standpoint of WKB theory for multidimensional, integrable systems, to explore the geometrical issues surrounding the Ponzano-Regge formula. The relations among the methods of Roberts and others for deriving the Ponzano-Regge formula are discussed, and a new approach, based on the recoupling of four angular momenta, is presented. A generalization of the Yutsis-type of spin network is developed for this purpose. Special attention is devoted to symplectic reduction, the reduced phase space of the $6j$-symbol (the 2-sphere of Kapovich and Millson), and the reduction of Poisson bracket expressions for semiclassical amplitudes. General principles for the semiclassical study of arbitrary spin networks are laid down; some of these were used in our recent derivation of the asymptotic formula for the Wigner $9j$-symbol.

1. Introduction

The Wigner $6j$-symbol (or Racah W-coefficient) is a central object in angular momentum theory, with many applications in atomic, molecular and nuclear physics. These usually involve the recoupling of three angular momenta, that is, the $6j$-symbol contains the unitary matrix elements of the transformation connecting the two bases that arise when three angular momenta are added in two different ways. Such applications and the definition of the $6j$-symbol based on them are described by Edmonds (1960). More recently the $6j$- and other $3nj$-symbols have found applications in quantum computing (Marzuoli and Rasetti 2005) and in algorithms for molecular scattering calculations (De Fazio *et al* 2003, Anderson and Aquilanti 2006), which make use of their connection with discrete orthogonal polynomials (Aquilanti *et al* 1995, 2001a,b).

The $6j$-symbol is an example of a spin network, a graphical representation for contractions between tensors that occur in angular momentum theory. The graphical notation has been developed by Yutsis *et al* (1962), El Baz and Castel (1972), Lindgren and Morrison (1986), Varshalovich *et al* (1981), Stedman (1990), Danos and Fano (1998), Wormer and Paldus (2006), Balcar and Lovesey (2009) and others. The $6j$-symbol is the simplest, nontrivial, closed spin network (one that represents a rotational

invariant). Spin networks are important in lattice QCD and in loop quantum gravity where they provide a gauge-invariant basis for the field. Applications in quantum gravity are described by Rovelli and Smolin (1995), Baez (1996), Carlip (1998), Barrett and Crane (1998), Regge and Williams (2000), Rovelli (2004) and Thiemann (2007), among others.

Alongside the Yutsis school of graphical notation and the Clebsch-Gordan school of algebraic manipulation there is a third approach to the evaluation of rotational ($SU(2)$) invariants. The third method, sometimes called chromatic evaluation, grew out of Penrose's doctoral work on the graphical representation of tensors and is closely related to knot theory. We will not have further occasion to mention this school, see Penrose (1971) for its introduction, Rovelli (2004) for an overview and Kauffman and Lins (1994) for its full development.

The asymptotics of spin networks and especially the $6j$-symbol has played an important role in many areas. By "asymptotics" we refer to the asymptotic expansion for the spin network when all j's are large, equivalent to a semiclassical approximation since large j is equivalent to small $\hbar$. The asymptotic expression for the $6j$-symbol (the leading term in the asymptotic series) was first obtained by Ponzano and Regge (1968), or, more precisely, they obtained several formulas, valid inside and outside the classically allowed region and in the neighborhood of the caustics. In the same paper those authors gave the first spin foam model (a discretized path integral) for quantum gravity. The formula of Ponzano and Regge is notable for its high symmetry and the manner in which it is related to the geometry of a tetrahedron in three-dimensional space. It is also remarkable because the phase of the asymptotic expression is identical to the Einstein-Hilbert action for three-dimensional gravity integrated over a tetrahedron, in Regge's (1961) simplicial approximation to general relativity. The semiclassical limit of the $6j$-symbol thus plays a crucial role in simplicial approaches to the quantization of the gravitational field.

For all these reasons, the asymptotic formula of Ponzano and Regge for the $6j$-symbol has attracted a great deal of attention. Ponzano and Regge obtained their formula by inspired guesswork, supporting their conclusion both with numerical evidence and arguments of consistency and plausibility. The formula itself is of the one-dimensional WKB-type, a reflection of the fact that the $6j$-symbol fundamentally represents a dynamical system of one degree of freedom.

The Ponzano-Regge formula was first derived by Neville (1971), using the recursion relations satisfied by the $6j$-symbol and a discrete version of WKB theory. Similar techniques were later used by Schulten and Gordon (1975a,b), who also presented stable algorithms for evaluating the $6j$-symbol numerically. A proof of a different sort was later given by Biedenharn and Louck (1981), based on showing that the Ponzano-Regge formula satisfies a set of defining properties of the $6j$-symbol.

More recently there have appeared more geometrical treatments of the asymptotics of the $6j$-symbol, that is, those based on geometric quantization (Kirillov 1976, Guillemin and Sternberg 1977, Woodhouse 1991), symplectic geometry and symplectic and Poisson reduction (Abraham and Marsden 1978, Arnold 1989, Marsden and Ratiu 1999) and other techniques. Among these are the works by Roberts (1999) and by Charles (2008). In addition, the $6j$-symbol has been taken as a test case for asymptotic studies of amplitudes that occur in quantum gravity (Barrett and Steele 2003, Freidel and Louapre 2003), in which the authors developed integral representations for the $6j$-symbol as integrals over products of the group manifold. There have also been quite a few other studies of asymptotics of particular spin

networks, including Barrett and Williams (1999), Baez *et al* (2002), Rovelli and Speziale (2006), Hackett and Speziale (2007), Conrady and Freidel (2008), Alesci *et al* (2008), Barrett *et al* (2009), among others. We also mention the works of Gurau (2008), which applies standard asymptotic techniques (Stirling's approximation, etc) directly to Racah's sum for the $6j$-symbol; of Ragni *et al* (2010) on the computation of $6j$-symbols and on the asymptotics of the $6j$-symbol when some quantum numbers are large and others small; and of Littlejohn and Yu (2009) on uniform approximations for the $6j$-symbol.

In addition there has been some work on the q-deformed $6j$-symbol, important for the regularization of the Ponzano-Regge spin-foam model (Turaev and Viro 1992, Ooguri 1992a,b) and for its possible connection to quantum gravity with cosmological constant. In particular, Taylor and Woodward (2004) applied the recursion and WKB method of Schulten and Gordon to the q-deformed $6j$-symbol. The results are geometrically interesting (the tetrahedron of Ponzano and Regge is moved from $\mathbb{R}^3$ to S^3 when the q-deformation is turned on), but it seems that at present there is no geometrical treatment of the asymptotics of the q-deformed $6j$-symbol, analogous to what is available for the ordinary $6j$-symbol. There is also the recent work of Van der Veen (2010) on the asymptotics of general q-deformed spin networks, which treats the problem from the standpoint of knot theory and representation theory. Among other things, this work creates a broad generalization of the Schwinger-Bargmann generating function of the $6j$-symbol.

In Aquilanti *et al* (2007) we applied multidimensional WKB theory for integrable systems to the asymptotics of the $3j$-symbol, and in this paper we apply similar techniques to the $6j$-symbol. These methods bear the closest relationship to the works of Roberts (1999) and of Charles (2008). The point of this paper is not another derivation of the Ponzano-Regge formula, although one is provided, but rather to clarify the relationship among some of the methods used in the past, to reveal useful calculational techniques, and to lay the basis for the development of new results. Among the latter we mention our own work on uniform approximations for the $6j$-symbol (Littlejohn and Yu, 2009), our recent derivation of the asymptotic form for the $9j$-symbol (Haggard and Littlejohn, 2010), both of which relied on techniques explained in this paper, and our work on the Bohr-Sommerfeld quantization of the volume operator in loop quantum gravity (Bianchi and Haggard, 2011). Previous and current work on the volume operator includes Chakrabarti (1964), Lévy-Leblond and Lévy-Nahas (1965), Lewandowski (1996), Major and Seifert (2001), Carbone *et al* (2002), Neville (2006), Brunnemann and Rideout (2008, 2010) and Ding and Rovelli (2010).

In addition, this paper is distinguished by its use of what we call the "$4j$-model" for the $6j$-symbol, in contrast to the "$12j$-model" used by Roberts (1999). The $4j$-model is less symmetrical than the 12-model, but it is closer to the manner in which the $6j$-symbol is commonly used in recoupling theory. In addition, in loop quantum gravity (Rovelli 2004) angular momenta represent area vectors, which in the case of four-valent nodes correspond by Minkowski's (1897) theorem to a tetrahedron. In this context the $4j$-model is closer to the applications than the $12j$-model, indeed, it played an important role in the work of Bianchi and Haggard (2011).

In this paper we refer to Aquilanti *et al* (2007) as I, for example writing eqn. (I.13) for an equation from that paper. We note two errata in I, namely, $\sigma(x)$ in (I.89) should read $\sigma(u)$, and j_3 and j_4 should be swapped in the $6j$-symbol in (I.112).

2. Spin network notation

We begin by explaining our notation for spin networks, which is based on that of Yutsis *et al* (1962) with modifications due to Stedman (1990). At the end of this section we compare our conventions for spin networks with others in the Yutsis tradition.

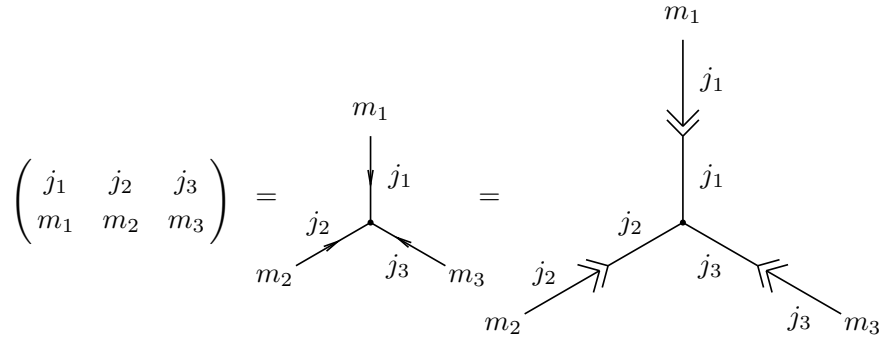### 2.1. The 3j-symbol and Wigner intertwiner

Figure 1. The 3j-symbol contains the components of the standard three-valent intertwiner.

The $3j$-symbol is a number that can be regarded as the components of an intertwiner $W : \mathcal{C}_{j_1} \otimes \mathcal{C}_{j_2} \otimes \mathcal{C}_{j_3} \to \mathbb{C}$ with respect to the standard basis $|j_1 m_1\rangle \otimes |j_2 m_2\rangle \otimes |j_3 m_3\rangle$, as indicated in Fig. 1. In this paper $\mathcal{C}_j$ denotes a carrier space for unitary irrep j of $SU(2)$, so that $\dim \mathcal{C}_j = 2j+1$. We call W the "Wigner" intertwiner. We will gradually explain the features of Fig. 1 as we proceed.

The standard notation for the $3j$-symbol is on the left of Fig. 1, while the central diagram is the standard Yutsis spin network for the $3j$-symbol, with small arrows presented as in the Yutsis notation. The indices (m_1, m_2, m_3) in the central diagram are covariant, that is, they transform under rotations as the components of a dual vector (in contrast to an ordinary vector). In a Hilbert space we regard ordinary wave functions or ket vectors as "vectors," while bra vectors are regarded as "dual vectors." Thus, contravariant indices are those that transform as the components of a vector. In the Yutsis notation the arrows indicate the transformation properties of the corresponding m index, and there are rules for "raising and lowering" indices, that is, reversing the direction of the arrow. The rules do not, however, make use of the metric as in ordinary tensor analysis. Our definition of the arrow (explained below) is different from that of Yutsis, but designed so that the two notations agree as much as possible. In particular, our notation for the $3j$-symbol is the same as the Yutsis diagram in Fig. 1.

A trivalent node of a spin network such as those illustrated in Fig. 1 is assumed to have a positive or counterclockwise orientation, unless otherwise indicated (thus we dispense with the $+$ sign used by Yutsis).

2.2. Bras, kets and scalar products

The diagram on the right of Fig. 1 makes use of the standard basis vectors $|j_i m_i\rangle$ in $\mathcal{C}_{j_i}$, $i = 1, 2, 3$. The spin networks for these basis vectors and their duals are shown in

$$|jm\rangle \;=\; \overset{j}{\longleftarrow}\; m \qquad \langle jm| \;=\; \overset{j}{\longrightarrow}\; m^{*}$$

$$|\psi\rangle \;=\; \overset{j}{\longleftarrow}\; \psi \qquad \langle \psi| \;=\; \overset{j}{\longrightarrow}\; \psi^{*}$$

Figure 2. Spin networks for bras and kets.

Fig. 2. The large, broadly open arrow is a "chevron" (Stedman 1990). When pointing outward (inward), the chevron indicates a ket (bra) vector. Also shown in Fig. 2 is the spin network for an arbitrary vector $|\psi\rangle$ in $\mathcal{C}_j$, and the dual bra vector $\langle\psi|$ obtained by Hermitian conjugation. In the Dirac notation it is customary to label bras by the same symbol as kets, it being understood that the two are related by Hermitian conjugation. This convention is so deeply ingrained that we dare not change it. But in spin networks there are two different ways of converting kets into bras and vice versa, and this presents some notational challenges. One can see in Fig. 2 that Hermitian conjugation applied to bras and kets is notationally the changing of bra chevrons to ket chevrons and vice versa, and the starring of identifying symbols, with a double star being removed. Full rules for Hermitian conjugation of any spin network are given in Sec. 2.9.

The lines of a spin network will be referred to as "edges," including cases like those shown in Fig. 2.

An edge of a spin network ending in an unstarred m index represents a contraction with the basis ket $|jm\rangle$, so the m index transforms under rotations as a covariant index. The explicit insertion of basis kets may be seen in Fig. 1. An edge ending in a starred m index represents the insertion of a basis bra $\langle jm|$, so starred indices are contravariant. Thus, the star on an m index indicates its transformation property, and invariant contractions can only take place between a pair of starred and unstarred m indices.

$$\langle \psi| \;=\; \overset{j}{\longrightarrow}\; \psi^{*} \;=\; \psi^{*}\; \overset{j}{\longleftarrow}$$

Figure 3. Orientation of a spin network does not matter.

As illustrated in Fig. 3, the orientation of a spin network on the page does not affect its value. The spin network in the figure has been rotated by $180°$.

$$\langle \phi|\psi\rangle \;=\; \phi^{*}\; \overset{j}{\longleftarrow}\!\!\overset{j}{\longleftarrow}\; \psi \;=\; \phi^{*}\; \overset{j}{\longleftarrow}\; \psi$$

$$\langle \psi|\phi\rangle \;=\; \left(\phi^{*}\; \overset{j}{\longleftarrow}\; \psi\right)^{*} \;=\; \phi\; \overset{j}{\longrightarrow}\; \psi^{*}$$

Figure 4. Spin networks for scalar products or contractions. Illustration of rules for complex conjugation.

As illustrated in the final diagram in Fig. 1 and in Fig. 4, when a bra chevron and a ket chevron are juxtaposed, it represents the scalar product or contraction. In effect, the bra chevron acts as a receptacle for the ket chevron, and vice versa. After

the contraction the two edges may be joined, with a small arrow remaining to indicate which was the bra and which the ket in the contraction. One might suppose that the star would carry the same information, but, as shown below, it is possible to change the direction of the arrow without changing the stars. Figure 4 also presents another example of Hermitian conjugation (complex conjugation, in this case). Since the small arrow represents the contraction of a bra and a ket chevron, when the chevrons are reversed, the direction of the arrow changes.

$$\langle jm|jm'\rangle = \quad m^* \xrightarrow{\quad j \quad} \! \ll \! \xleftarrow{\quad j \quad} m' \quad = \quad m^* \xrightarrow{\quad j \quad} m'$$

$$= \quad \delta_{mm'} \quad = \quad m'^* \xrightarrow{\quad j \quad} m$$

Figure 5. Orthonormality relations for basis vectors.

As a special case of the scalar product, the orthonormality relations of the basis vectors are illustrated in Fig. 5. The final spin network follows from the symmetry of the Kronecker delta, or, alternatively, by the reality of $\delta_{mm'}$ and the rules for complex conjugation.

The j labels on the edges of the spin networks indicate which carrier space $\mathcal{C}_j$ the ket or bra lies in, or in which carrier space a contraction has taken place. If there are distinct carrier spaces with the same j label, then additional distinguishing information must be supplied.

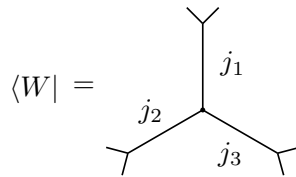*2.3. Intertwiners*

$$\langle W| \quad = \quad$$

Figure 6. Spin network for the Wigner or $3j$-intertwiner.

An $SU(2)$ intertwiner (the only kind we are interested in) is a linear map between two vector spaces that commutes with the action of $SU(2)$ on the two spaces. The only case of interest here is where the target space is $\mathbb{C}$, consisting of scalars, that is, invariants under rotations. The Wigner intertwiner $W : \mathcal{C}_{j_1} \otimes \mathcal{C}_{j_2} \otimes \mathcal{C}_{j_3} \to \mathbb{C}$ is of this type. But a linear map from a Hilbert space to $\mathbb{C}$ can be thought of as a dual or bra vector, for example, we can associate the map W with a bra vector $\langle W|$ belonging to $\mathcal{C}_{j_1}^* \otimes \mathcal{C}_{j_2}^* \otimes \mathcal{C}_{j_3}^*$. The spin network notation for $\langle W|$ is shown in Fig. 6. The components of the Wigner intertwiner, that is, the $3j$-symbol, are obtained by inserting basis kets, the ket chevron first, into the bra chevrons of the intertwiner, as in the final diagram of Fig. 1.

More generally, a $\mathbb{C}$-valued intertwiner on a Hilbert space $\mathcal{H}$ can be regarded as an $SU(2)$-invariant bra vector on this space, that is, a member of $\mathcal{H}^*$. By Hermitian conjugation we obtain an $SU(2)$-invariant ket vector in $\mathcal{H}$. Thus, there is a one-to-one correspondence between the subspace of $\mathcal{H}$ of rotationally invariant vectors and the

set of $\mathbb{C}$-valued intertwiners on $\mathcal{H}$. The subspace $\mathcal{Z}$ introduced in Sec. 3.4 below is a subspace of this type, consisting of rotationally invariant vectors.

2.4. Tensor products and resolution of identity

$$\sum_m |jm\rangle\langle jm| \;=\; \sum_m \overset{j}{\longleftarrow}\ m\ m^*\ \overset{j}{\longrightarrow}\!\!< \;=\; \overset{j}{\longleftarrow}\!\!<$$

Figure 7. Resolution of identity, and an illustration of the outer product.

The outer product of a ket with a bra is represented in spin network language simply by placing the spin networks for the ket and the bra on the same page, as illustrated in Fig. 7. The orientations of the bra and ket spin networks is immaterial, but in the figure they have been placed with their m indices adjacent in order to emphasize the summation (a contraction over two indices, one covariant, one contravariant). The final diagram is the spin network for the identity operator on space $\mathcal{C}_j$.

$$\sum_m \overset{j}{\longleftarrow}\ m\ m^*\ \overset{j}{\longleftarrow} \;=\; \overset{j}{\longleftarrow}$$

Figure 8. Summing on m to join two edges.

Figure 7 illustrates another technique, the replacement of a sum on m by a joining of edges. The general usage is shown in Fig. 8. The directions of the arrows and the stars on one of the m's must be coordinated as shown for the identity to be used as shown. The small arrow in the final diagram in Fig. 8 (a fragment of a spin network) is a reminder of the directions of the arrows before the sum. This small arrow is omitted in the final diagram of Fig. 7 (the identity diagram) because the chevrons already indicate the direction of the edge. Recall that edges are also joined on contracting a bra with a ket, as in Fig. 4.

$$\overset{j}{\longleftarrow}\!\!\ll\!\!\overset{j}{\longleftarrow}\ \psi \;=\; \overset{j}{\longleftarrow}\ \psi$$

$$\phi^*\overset{j}{\longrightarrow}\!\!\ll\!\!\overset{j}{\longrightarrow}\!\!< \;=\; \phi^*\overset{j}{\longrightarrow}\!\!<$$

$$\phi^*\overset{j}{\longrightarrow}\!\!\ll\!\!\overset{j}{\longleftarrow}\!\!\ll\!\!\overset{j}{\longleftarrow}\ \psi \;=\; \phi^*\overset{j}{\longleftarrow}\ \psi$$

Figure 9. Summing on m to join two edges.

The use of the identity diagram is illustrated in Fig. 9. The first row illustrates its action on kets (as a map : $\mathcal{C}_j \to \mathcal{C}_j$), where bra and ket chevrons are combined as in Fig. 4. The small arrow is omitted after the joining of the bra and ket chevrons because the remaining chevron indicates the direction of the edge. The second row of the figure illustrates its action on bras (the map : $\mathcal{C}_j^* \to \mathcal{C}_j^*$), and the third row illustrates its action as a map : $\mathcal{C}_j^* \otimes \mathcal{C}_j \to \mathbb{C}$, that is, the scalar product map : $\langle\phi| \otimes |\psi\rangle \mapsto \langle\phi|\psi\rangle$. All

of these usages are encompassed by the same spin network. The identity spin network can also be seen as an element of $\mathcal{C}_j \otimes \mathcal{C}_j^*$, that is, the space dual to $\mathcal{C}_j^* \otimes \mathcal{C}_j$ on which it, viewed as a $\mathbb{C}$-valued linear operator, acts (the third line of Fig. 9).

In general a spin network has some number of edges that terminate in incoming or outgoing chevrons. Examples are the identity diagram in Fig. 7 and the Wigner intertwiner in Fig. 6. In all cases there are multiple interpretations of the spin network as a linear operator mapping one vector space to another, depending on how many of the incoming and outgoing chevrons have ket and bra chevrons plugged into them (specifying the domain), and how many are left free (specifying the range). The domain is the tensor product of some number of $\mathcal{C}_j$ times some number of $\mathcal{C}_j^*$, and so is the range. In the extreme case that all incoming and outgoing chevrons on the spin network have kets and bras plugged into them the result is simply a number and the range is $\mathbb{C}$. In that case the spin network, as a $\mathbb{C}$-valued linear operator, can be seen as a vector in the space dual to the domain.

This facile identification of closely associated operators, and their reinterpretation as elements of vector spaces, is an important advantage of spin networks. It is difficult and awkward to do something similar with the Dirac notation.

In general, a tensor is a multilinear operator acting on a tensor product of some set of vector spaces and their duals. Thus, a spin network is a notation for a tensor on some product of the $\mathcal{C}_j$ and their duals. The edges of the spin network terminating in ket or bra chevrons indicate the nature of the space the tensor acts on. In general, the tensor product of two tensors in spin network notation is indicated by the placing of the two spin networks together on the page, in any orientation. The outer product of a bra and a ket illustrated in Fig. 7 is a special case. Partial or complete contractions of tensors are indicated by joining some or all ket chevrons with bra chevrons.

2.5. *The* $2j$ *symbol and intertwiner*

We now consider another intertwiner, which leads to an important mapping between kets and bras, alternative to Hermitian conjugation. The intertwiner acts on the Hilbert space $\mathcal{C}_j \otimes \mathcal{C}_j'$, the tensor product of two carrier spaces of the same j. In general we wish to consider the second carrier space as distinct from the first, which is the purpose of the prime on the second factor. To within a normalization and phase, there is a unique vector in this space that is invariant under rotations; we call it $|K\rangle$, and express it in terms of the Clebsch-Gordan coefficients by

$$|K\rangle = \sqrt{2j+1} \sum_{mm'} |jm\rangle \otimes |jm'\rangle \, C^{00}_{jjmm'}. \tag{1}$$

This vector can also be expressed in terms of the "$2j$-symbol," which we define in terms of the usual $3j$-symbol by

$$\begin{pmatrix} j & j \\ m & m' \end{pmatrix} = \begin{pmatrix} j & j & 0 \\ m & m' & 0 \end{pmatrix} = C^{00}_{jjmm'} = \frac{(-1)^{j-m}}{\sqrt{2j+1}} \, \delta_{m,-m'}. \tag{2}$$

The terminology "$2j$-symbol" is not entirely standard, but it has been used by Stedman (1990). The invariant vector $|K\rangle$ can also be written,

$$|K\rangle = \sum_{mm'} |jm\rangle \otimes |jm'\rangle \, (-1)^{j-m} \, \delta_{m,-m'} = \sum_m |jm\rangle \otimes |j,-m\rangle \, (-1)^{j-m}. \tag{3}$$

By Hermitian conjugation we convert $|K\rangle$ into the bra $\langle K|$, which is otherwise an intertwiner $K : \mathcal{C}_j \otimes \mathcal{C}_j' \to \mathbb{C}$. Just as the components of the intertwiner W are

$$m \xrightarrow{\quad j \quad\;\; j \quad} m' = (-1)^{j-m} \delta_{m,-m'}$$

$$= m \xrightarrow{\quad j \quad} \xrightarrow{\quad j \quad\;\; j \quad} \xleftarrow{\quad j \quad} m'$$

Figure 10. Components of the map K, a standard bivalent intertwiner.

the $3j$-symbol, the components of the intertwiner K are the $2j$-symbol, multiplied however by $\sqrt{2j+1}$ because of a normalization convention. Figure 10 shows first the spin network for the components of K, which is conceived of as a standard bivalent node or intertwiner. The small arrows indicate that the components on the first line can be considered the result of plugging basis kets into the intertwiner itself, as seen on the second line. The short line extending above the node is a "stub" (Stedman 1990), whose purpose is to orient the node. The convention is that if we start at the stub and move in a positive (counterclockwise) direction, the first and second edges we encounter are respectively the first and second operands of K, conceived of as a map $: \mathcal{C}_j \otimes \mathcal{C}'_j \to \mathbb{C}$.

We note that if V and W are vector spaces, then $V \times W$ is not the same as $V \otimes W$, but if we have a bilinear map on $V \times W$ it can be extended to a linear map on $V \otimes W$ by linear superposition. For example, in the previous paragraph we have regarded K as a bilinear map $: \mathcal{C}_j \times \mathcal{C}'_j \to \mathbb{C}$, and computed its components as $K(|jm\rangle, |jm'\rangle)$. The first and second operands of this expression correspond to the first and second edges as specified by the stub.

$$\langle K | \;=\; \rangle\!\!\xrightarrow{\quad j \quad\;\; j \quad}\!\!\langle$$

Figure 11. Spin network for map $K : \mathcal{C}_j \otimes \mathcal{C}'_j \to \mathbb{C}$.

Figure 10 also gives the numerical values of the components of K, and in the final diagram, the network for K itself, with two kets inserted. The network for K in isolation is illustrated in Fig. 11, regarded as a bra vector on $\mathcal{C}_j \otimes \mathcal{C}'_j$, that is, as an element of $\mathcal{C}_j^* \otimes \mathcal{C}_j'^*$.

$$m \xrightarrow{\quad j \quad\;\; j \quad} m' = \sqrt{2j+1}$$

Figure 12. The stub can be regarded as a vestigial edge of a $3j$-symbol with value $j = 0$.

The stub in Fig. 10 can be regarded as a vestigial edge of a $3j$-symbol or W-intertwiner with the value $j = 0$, although one must beware of the normalization convention. This is illustrated in Fig. 12, which is equivalent to (2). The value does not depend on the direction of the arrow on the zero edge (see below for rules for

reversing arrows).

$$\phi \xrightarrow{\;\;j\;\;} \!\!\Longrightarrow \xrightarrow{\;j\;}\Big|\xrightarrow{\;j\;} \Longleftarrow \xrightarrow{\;j\;} \psi \;=\; \phi \xrightarrow{\;j\;}\Big|\xrightarrow{\;j\;} \psi$$

$$=\; (-1)^{2j}\,\psi \xrightarrow{\;j\;}\Big|\xleftarrow{\;j\;} \phi \;=\; (-1)^{2j}\,\phi \xrightarrow{\;j\;}\Big|\xleftarrow{\;j\;} \psi$$

Figure 13. The intertwiner K acquires a phase $(-1)^{2j}$ if the two operands are swapped.

The components of $K : \mathcal{C}_j \otimes \mathcal{C}'_j \to \mathbb{C}$, seen in Fig. 10, acquire a phase of $(-1)^{2j}$ if m and m' are swapped. This is equivalent to the statement

$$K(|\phi\rangle, |\psi\rangle) = (-1)^{2j} K(|\psi\rangle, |\phi\rangle), \tag{4}$$

for all $|\psi\rangle$, $|\phi\rangle$, which is illustrated in spin network language in Fig. 13. The final diagram differs from the preceding simply by a $180°$ rotation, so the value is the same. But this leads to the rule, that a spin network acquires a phase of $(-1)^{2j}$ when the stub at a bivalent node is inverted. In particular, the arrow on the null edge in Fig. 12 can be inverted without changing the value.

2.6. Kets to bras

$$\succ\!\!\xrightarrow{\;j\;}\Big|\xrightarrow{\;j\;} \Longleftarrow \xrightarrow{\;j\;} \psi \;=\; \succ\!\!\xrightarrow{\;j\;}\Big|\xleftarrow{\;j\;} \psi$$

$$\equiv\; \succ\!\!\xrightarrow{\;j\;} \psi \;\neq\; \succ\!\!\xrightarrow{\;j\;} \psi^{*}$$

Figure 14. The intertwiner K can be used to convert a ket to a bra.

The intertwiner $K : \mathcal{C}_j \otimes \mathcal{C}_j \to \mathbb{C}$ has an alternative interpretation as a map $K_1 : \mathcal{C}_j \to \mathcal{C}_j^{*}$, where for simplicity we have dropped the prime on the second factor, and where the 1-subscript distinguishes the new map from the old. This alternative interpretation is natural in spin network language, as seen in Fig. 14. The spin network for $|\psi\rangle \in \mathcal{C}_j$ is plugged into the second operand of the spin network for K, resulting in a spin network with one free bra chevron. The choice of the second operand of K for this purpose is conventional. The result is an element of $\mathcal{C}_j^{*}$, that is, it is a bra. As indicated in the figure, we abbreviate this spin network by drawing the same spin network for $|\psi\rangle$ that we started with, except the ket chevron is converted into a bra chevron.

In other words, when we use K_1 to convert a ket into a bra, we just flip the ket chevron, leaving everything else the same. In particular, we do not put a star on the label of the ket. This distinguishes the map $K_1 : \mathcal{C}_j \to \mathcal{C}_j^{*}$ from the metric or Hermitian conjugation, which is also a map $: \mathcal{C}_j \to \mathcal{C}_j^{*}$. When the metric is used to convert a ket to a bra, not only is the ket chevron flipped to a bra chevron, but a star is appended to the label. These two maps are quite distinct; in particular, K_1 is a linear map, while the metric is an antilinear map. As indicated in Fig. 14, the results are not the same.

When a ket is turned into a bra, the components with respect to some basis change from contravariant to covariant. But since there is more than one way to do

this, any notation based on the position (upper or lower) of the indices is inadequate to represent the result.

Figure 15. An arbitrary spin network with one edge terminating in a ket chevron.

The map K_1 can be used to turn a ket chevron into a bra chevron on any spin network, not only on kets themselves. A notation for an arbitrary spin network with an edge terminating in a ket chevron is shown in Fig. 15. The circle around the X indicates the rest of the spin network, which may include other edges terminating in ket or bra chevrons.

Figure 16. Converting a ket chevron into a bra chevron with the map $K_1 : \mathcal{C}_j \rightarrow \mathcal{C}_j^*$.

To convert the ket chevron in Fig. 15 into a bra chevron we simply insert it into the second operand of $K : \mathcal{C}_j \otimes \mathcal{C}_j \rightarrow \mathbb{C}$, as shown in Fig. 16. The remainder of the spin network, indicated by the X, does not change.

2.7. Bras to kets

Figure 17. Spin network for the maps $K^{-1} : \mathcal{C}_j^* \otimes \mathcal{C}_j^* \rightarrow \mathbb{C}$ and $K_1^{-1} : \mathcal{C}_j^* \rightarrow \mathcal{C}_j$.

Figure 18. Spin network for the quantity $K^{-1}(\langle\phi|, \langle\psi|)$.

The map $K_1 : \mathcal{C}_j \rightarrow \mathcal{C}_j^*$ has an inverse, the map $K_1^{-1} : \mathcal{C}_j^* \rightarrow \mathcal{C}_j$, that takes bras into kets. We associate K_1^{-1} with a closely related map $K^{-1} : \mathcal{C}_j^* \otimes \mathcal{C}_j^* \rightarrow \mathbb{C}$ that is expressed by the spin network in Fig. 17. This spin network and the meaning of the -1 on K^{-1} are to be defined, but the spin network represents a linear operator $: \mathcal{C}_j^* \otimes \mathcal{C}_j^* \rightarrow \mathbb{C}$ with the ordering of the two operands being specified by the stub. The action of K^{-1} on two bras is illustrated in Fig. 18.

$$\phi^* \xrightarrow{\quad j \quad} \!\!\ll\!\! \xrightarrow{\quad j \quad\; j \quad} \;=\; \phi^* \xrightarrow{\quad j \quad\; j \quad}$$

$$\equiv \; \phi^* \xrightarrow{\quad j \quad} \; \neq \; \phi \xrightarrow{\quad j \quad}$$

Figure 19. Action of K_1^{-1} on a bra.

We now define the network in Fig. 17 by requiring that K_1^{-1} act on a bra by inserting it into the first operand of that network, as illustrated in Fig. 19, and by requiring that K_1^{-1} actually be the inverse of K_1. Figure 19 shows the action of K_1^{-1} on an arbitrary bra $\langle\phi|$. The use of the first operand of K^{-1} for this purpose is a convention, but one that makes our overall notation for mapping kets to bras and vice versa consistent (see Fig. 22 below). As indicated, we abbreviate the result by taking the original network for the bra $\langle\phi|$ and simply flipping the direction of the chevron. We do not unstar the identifying symbol. As indicated, the result differs from Hermitian conjugation applied to $\langle\phi|$, which is the ket $|\phi\rangle$ (without the star).

$$\xleftarrow{\quad j \quad\; j \quad} \!\!\gg\!\! \xrightarrow{\quad j \quad\; j \quad} \!\!\ll\; = \; \xleftarrow{\quad j \quad}\!\!\ll$$

Figure 20. The requirement that $K^{-1} \circ K = \mathrm{Id}$.

The requirement that K_1^{-1} actually be the inverse of K_1 is illustrated in Fig. 20. The stub on the network for K^{-1} is inverted so that the output of the first step is fed into the first operand of K^{-1}.

$$\xrightarrow{\quad j \quad\; j \quad\; j \quad} \;=\; \xrightarrow{\quad j \quad}$$

Figure 21. Two arrow flips, with stubs oppositely oriented, annihilate each other.

The identity represented by Fig. 20 is usually encountered in practice in the form shown in Fig. 21 (a fragment of a spin network). The $2j$-node inverts the direction of the arrow. Two such inversions, with stubs pointing in opposite directions, annihilate one another.

$$\xleftarrow{\quad j \quad\; j \quad} \!\!\gg\!\! \xrightarrow{\quad j \quad\; j \quad} \!\!\ll\!\! \xrightarrow{\quad j \quad\; j \quad}$$

$$= \; \xleftarrow{\quad j \quad\; j \quad\; j \quad\; j \quad} \;=\; \xleftarrow{\quad j \quad\; j \quad}$$

Figure 22. Flipping the chevrons on K gives K^{-1}.

We have made an independent definition of the spin network in Fig. 17, but it is the same as the spin network for K, shown in Fig. 11, with both bra chevrons flipped. Since we now have a convention for flipping bra chevrons (by applying K_1^{-1}), for consistency we must show that the two results are the same. This is done in Fig. 22, which uses the identity of Fig. 21.

$$m^* \xrightarrow{j} \Longleftarrow \xrightarrow{j|j} \Longrightarrow \xrightarrow{j} m'^*$$

$$= m^* \xrightarrow{j|j} m'^* = (-1)^{j-m}\,\delta_{m,-m'}$$

Figure 23. The components of K^{-1} have the same numerical values as the components of K.

By inserting resolutions of the identity into the diagram in Fig. 20 it is easy to work out the components of K^{-1}. These are displayed in Fig. 23. Notice that they have the same numerical values as the components of K (see Fig. 10).

Figure 24. Converting a bra chevron to a ket chevron on an arbitrary spin network.

By using K^{-1} we can convert a bra chevron into a ket chevron on any spin network, not only on bras and kets themselves. This is illustrated in Fig. 24, which may be compared to Fig. 16.

Figure 25. Reversing the arrow on an edge of a spin network incurs a phase of $(-1)^{2j}$.

Finally, by using Figs. 16, 24 and 21, it may be shown that when we reverse the arrow on an edge of a spin network, we incur a phase of $(-1)^{2j}$. This is done in Fig. 25.

2.8. Raising and lowering indices

When we convert a ket to a bra by the action of K_1, then the bra has components with respect to the standard basis $|jm\rangle$ that are simple functions of the components of the original ket with respect to the standard basis $\langle jm|$. Mapping the one set of components to the other is "lowering the index." Using K_1^{-1} to convert a bra to a ket similarly amounts to "raising the index." More generally the procedure can be

applied to an edge of any spin network terminating in a starred (contravariant) or an unstarred (contravariant) index. The index can refer to any basis, not just the standard one.

Figure 26. Expressing contravariant components in terms of covariant components.

Figure 27. Rules for raising and lowering indices.

Figure 26 shows how to the express contravariant components in terms of the covariant components in the standard basis. By plugging in the numerical values of the components of K, we obtain the first line of Fig. 27. Similarly we derive the second line of Fig. 27 for expressing covariant components in terms of contravariant components.

Figure 28. The completely covariant and completely contravariant components of the $3j$-intertwiner are numerically equal.

Figure 29. The completely covariant and completely contravariant components of the $2j$-intertwiner are numerically equal.

If these rules are used to raise all three covariant components of the $3j$-intertwiner (Fig. 1), then we find that the completely contravariant components have the same

values, namely, the $3j$-symbol. This is illustrated in Fig. 28. To show this it is necessary to use the symmetry of the $3j$-symbol (see Varshalovich *et al* 1981, Eq. (8.2.4.6)). Then by setting one of the j's to zero and using Fig. 12, we find that the same is true for the completely covariant and completely contravariant components of the $2j$-intertwiner, as shown in Fig. 29. The same result is obtained by comparing Figs. 10 and 23.

2.9. Hermitian conjugation of spin networks

Consider a spin network of arbitrary complexity involving only $2j$- and $3j$-nodes. The network is allowed to have any number of edges terminating in bra or ket chevrons, or in starred or unstarred labels such as m indices. By using the identities above, possibly with the insertion or removal of $2j$-nodes and the extraction of phases of the form $(-1)^{2j}$, it is possible to bring the spin network into a standard form, in which all edges joining $3j$-nodes have arrows pointing toward the $3j$-node, all edges joining $2j$-nodes have arrows pointing away from the $2j$-node, all edges terminating in a starred symbol have arrows pointing toward that symbol, and all edges terminating in an unstarred symbol have arrows pointing away from that symbol. Next, by inserting resolutions of the identity, which involve m-sums, it is possible to express the spin network as sum over the completely covariant components of $3j$-symbols and completely contravariant components of $2j$-symbols, times a tensor product of bras and kets.

In this form it is easy to take the Hermitian conjugate. Under Hermitian conjugation, bras go to kets and vice versa, while the covariant components of $3j$-symbols and contravariant components of $2j$-symbols do not change, since they are real. By using Figs. 28 and 29, however, these components can be rewritten as the completely contravariant components of $3j$-symbols and the completely covariant components of $2j$-symbols. The m-sums can now be done, reversing the earlier insertions of resolutions of the identity. Then the other steps leading to the standard form can be reversed.

The result is a simple rule for the Hermitian conjugation of any spin network of the given form: All ket chevrons are changed to bra chevrons and vice versa, the directions of all arrows are reversed, and all edges terminating in a symbol have a star added to the symbol, with a double star being removed.

2.10. Discussion of spin network rules

Our rules for spin networks differ from those of Yutsis *et al* and most of the literature in the Yutsis tradition primarily by our ability to express abstract vectors (kets), dual vectors (bras) and tensors in addition to the components of those objects. Also, we indicate the nature of an m index (covariant or contravariant) by the presence or absence of a star, rather than the direction of the arrow. One result is that our rules for reversing the direction of the arrow are more uniform than in the Yutsis tradition, where such a reversal picks up a phase $(-1)^{2j}$ only on internal edges. In our approach, the rule applies everywhere, including edges terminating in an m index. In addition, our rules for Hermitian conjugation are simpler than those in the Yutsis tradition, where phase factors must be introduced. The simplification is due to the explicit introduction of $2j$-symbols, and the use of stubs.

To translate a Yutsis spin network into one of ours, it is necessary only to put stars on m indices terminating edges with outward pointing arrows.

The standard form of a spin network discussed in Sec. 2.9 has all $3j$-nodes with inward pointing arrows, and all $2j$-nodes with outward pointing ones. If we assume the standard form, then the arrows become superfluous and can be dropped. Only the stubs and $2j$-nodes remain, in comparison to a Yutsis-style spin network. This is the procedure advocated by Stedman (1990). For the purposes of this paper we will keep the arrows, since we wish to have finer control on the spin network than that offered by the standard form.

3. Models for the $6j$-symbol

For given values of the six j's, the $6j$-symbol is just a number, but to study its semiclassical limit it is useful to write it as a scalar product $\langle B|A\rangle$ of wave functions in some Hilbert space. This can be done in many different ways, corresponding to what we call different "models" of the $6j$-symbol. In this section we describe a class of such models that are related to one another. We begin by summarizing our notation for the Schwinger representation of angular momentum operators. Then we present what we call the "$12j$-model," which was used by Roberts (1999) in his derivation of the Ponzano-Regge formula. Next we describe the "$4j$-model" which we will use for the semiclassical analysis of this paper. We also mention an $8j$-model for the $6j$-symbol.

3.1. The Schwinger Representation

Our notation for the Schwinger representation of angular momentum operators is similar to that used in I. We denote the Schwinger Hilbert space by $\mathcal{S} = L^2(\mathbb{R}^2)$; it is the space of wave functions $\psi(x_1, x_2)$ for two harmonic oscillators of unit frequency and mass. The usual annihilation and creation operators are $\hat{a}_\mu = (\hat{x}_\mu + i\hat{p}_\mu)/\sqrt{2}$, $\hat{a}_\mu^\dagger = (\hat{x}_\mu - i\hat{p}_\mu)/\sqrt{2}$, for $\mu = 1, 2$; we use hats on operators to distinguish them from their classical counterparts. We define operators

$$\hat{I} = \frac{1}{2}\hat{a}^\dagger\hat{a}, \qquad \hat{J}_i = \frac{1}{2}\hat{a}^\dagger\sigma_i\hat{a}, \tag{5}$$

where $i = 1, 2, 3$ and where $\hat{a}$ (without the μ index) is a 2-vector (or column spinor) of operators, with $\hat{a}^\dagger$ the adjoint (or row spinor) and with obvious contractions against the Pauli matrices σ_i. These operators satisfy the commutation relations $[\hat{I}, \hat{J}_i] = 0$, $[\hat{J}_i, \hat{J}_j] = i\epsilon_{ijk}\hat{J}_k$. We set $\hbar = 1$. Note that $\hat{I} = (\hat{H}_1 + \hat{H}_2 - 1)/2$, where $\hat{H}_\mu$, $\mu = 1, 2$, are the two harmonic oscillators. There is also the operator relation $\hat{\mathbf{J}}^2 = \hat{I}(\hat{I} + 1)$. We denote the squares of 3-vectors in bold face. The operators $\hat{\mathbf{J}}$ generate an $SU(2)$ action on $\mathcal{S}$, which carries one copy of each irrep $j = 0, 1/2, 1, \ldots$, that is,

$$\mathcal{S} = \sum_j \oplus \mathcal{C}_j. \tag{6}$$

The irreducible subspace $\mathcal{C}_j$ is an eigenspace of $\hat{I}$ with eigenvalue j. In the semiclassical analysis of spin networks, the spaces $\mathcal{C}_j$ that the spin networks refer to are interpreted as one of the irreducible subspaces of a Schwinger Hilbert space $\mathcal{S}$. Similarly, $\mathcal{C}_j^*$ is interpreted as a subspace of a space $\mathcal{S}^*$. In this way the bra and ket vectors referred to by the spin network are interpreted as wave functions on $\mathbb{R}^2$, and the spin network itself can be interpreted as a wave function in $\mathbb{R}^{2N}$.

In the various nj-models we take tensor products of the Schwinger Hilbert space, writing $\mathcal{S}_r$ for the r-th copy. Similarly, we put an r index on various operators, for example, $\hat{a}_r$, $\hat{I}_r$, $\hat{\mathbf{J}}_r$, $r = 1, \ldots, n$, or, with two indices, $\hat{a}_{r\mu}$, $\mu = 1, 2$.

3.2. The 12j-model of the 6j-symbol

We begin with the standard spin network (Yutsis *et al* 1962) of the $6j$-symbol, shown in Fig. 30. According to the remarks in Sec. 2.10, this spin network can be reinterpreted according to our conventions, presented in Sec. 2, without modification. We will refer to the labeling of the six j's in the $6j$-symbol shown in Fig. 30 as the "symmetric" labeling.
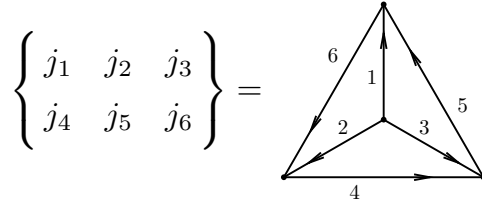
$$\begin{Bmatrix} j_1 & j_2 & j_3 \\ j_4 & j_5 & j_6 \end{Bmatrix} =$$

Figure 30. The Yutsis spin network for the $6j$-symbol, in a symmetrical labeling of the j's. The numbers 1, 2, etc on the spin network refer to j_1, j_2, etc.

We perform an operation on each edge of the spin network that is illustrated for edge 1 in Fig. 31. After the second equality edges are labeled by 1 and $1'$. These refer to two distinct carrier spaces, say, $\mathcal{C}_{j_1}$ and $\mathcal{C}'_{j_1}$, with the same value of j (that is, j_1). The introduction of such distinct carrier spaces does not change the value of the $6j$-symbol, which is just a number. In the second equality we have expressed the lower ket chevron as a bra chevron transformed by K_1^{-1}, as in Fig. 24. In the final diagram the arrows are directed toward both $3j$-nodes connected by the original edge, and a $2j$-node has been inserted. We do this on all six edges of the spin network in Fig. 30. The resulting diagram is somewhat busy so we do not attempt to draw it, but each edge of the original diagram now looks like the final diagram in Fig. 31.
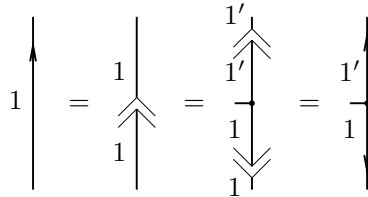
Figure 31. By inserting $2j$-symbols in each edge of a Yutsis diagram, all $3j$-symbols can be put into standard form (purely contravariant).

$$\xrightarrow{\quad 1 \quad | \quad 1' \quad} = \sum_{m_1 m'_1} \xrightarrow{\quad j_1 \quad} m_1 \; m_1^* \xrightarrow{\quad j_1 \quad | \quad j_1 \quad} m_1'^* \; m'_1 \xrightarrow{\quad j_1 \quad}$$

Figure 32. Breaking lines to represent $6j$-symbol as a sum over $2j$- and $3j$-symbols.

We now break up the final diagram in Fig. 31 in two different ways. The first way is illustrated in Fig. 32, in which the primed and unprimed lines are broken into summations over primed and unprimed quantum numbers m. This is done for all

six edges of the original spin network. The $6j$-symbol is represented as a product of six copies of a $2j$-symbol and four of a $3j$-symbol. Using the definition (2) for the $2j$-symbol, the result is

$$
\left\{ \begin{array}{ccc} j_1 & j_2 & j_3 \\ j_4 & j_5 & j_6 \end{array} \right\} = \left(\prod_{r=1}^{6} \sqrt{2j_r + 1} \right) \sum_{\text{all } m\text{'s}}
$$

$$
\times \left(\begin{array}{ccc} j_1 & j_2 & j_3 \\ m_1 & m_2 & m_3 \end{array} \right) \left(\begin{array}{ccc} j_1 & j_5 & j_6 \\ m_1' & m_5' & m_6 \end{array} \right) \left(\begin{array}{ccc} j_2 & j_6 & j_4 \\ m_2' & m_6' & m_4 \end{array} \right) \left(\begin{array}{ccc} j_3 & j_4 & j_5 \\ m_3' & m_4' & m_5 \end{array} \right) (7)
$$

$$
\times \left(\begin{array}{cc} j_1 & j_1 \\ m_1 & m_1' \end{array} \right) \cdots \left(\begin{array}{cc} j_6 & j_6 \\ m_6 & m_6' \end{array} \right)
$$

This formula may be compared to Edmonds (1960), eq. (6.2.3). Edmonds uses what he calls a "metric tensor" (really the components of K or K^{-1}, multiplied by $(-1)^{2j}$, see his eq. (3.7.1)), which relative to our $2j$-symbol introduces an overall phase of $\prod_{r=1}^{6}(-1)^{2j_r}$. He also swaps m_r and m_r' for $r = 4, 5, 6$ relative to our definitions, which introduces further phases. The product of these phases is 1, showing that the formulas agree.

Another way of breaking up the $6j$-symbol is to stop with the third diagram of Fig. 31 in the transformation of the six edges of the $6j$-symbol. Again the resulting diagram is too busy to draw, but it can be regarded as the complete contraction of two tensors, one the tensor product of six $2j$-intertwiners, all terminating in ket chevrons, the other the tensor product of four $3j$-intertwiners, all terminating in bra chevrons. There are twelve ket chevrons and twelve bra chevrons altogether, which we think of as living in twelve carrier spaces $\mathcal{C}_{j_r}$ and $\mathcal{C}'_{j_r}$ and their duals, where $r = 1, \ldots, 6$. These can be viewed as subspaces of twelve Schwinger Hilbert spaces, $\mathcal{S}_r$, $\mathcal{S}'_r$, $r = 1, \ldots, 6$, and their duals. Then the $6j$-symbol takes on the form $\langle B|A \rangle$, where states $|A\rangle$, $|B\rangle$ belong to the total Hilbert space $\mathcal{H}_{12j} = (\prod_r \otimes \mathcal{S}_r) \otimes (\prod_r \otimes \mathcal{S}'_r)$. These states are illustrated in Fig. 33, where the state $|B\rangle$ has been turned into ket form by Hermitian conjugation.
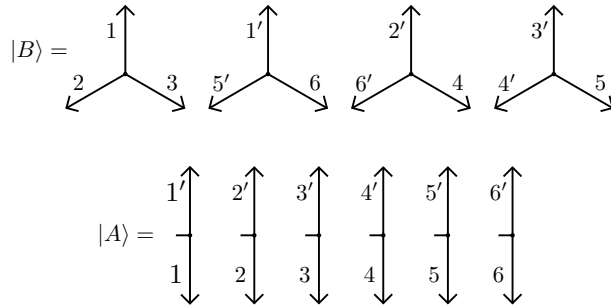

Figure 33. The two states that appear in Roberts' (1999) expression for the $6j$-symbol.

The usual custom in physics is to specify a state by the operators and quantum numbers of which the state is a simultaneous eigenstate. This requires that the eigenstate be nondegenerate, so that it is determined to within a normalization and phase. This in turn requires, in a certain sense, that the number of independent operators should be equal to the number of degrees of freedom of the system. We

will not attempt to be precise about this statement, but will illustrate the principle in several examples.

One example is the first $3j$-state appearing in Fig. 33, which lies in the Hilbert space $\mathcal{S}_1 \otimes \mathcal{S}_2 \otimes \mathcal{S}_3$ and is a simultaneous eigenstate of $\hat{I}_r$, $r = 1, 2, 3$ with eigenvalues j_r, $r = 1, 2, 3$. It is also an eigenstate of the vector of operators

$$\hat{\mathbf{J}}_{123} = \hat{\mathbf{J}}_1 + \hat{\mathbf{J}}_2 + \hat{\mathbf{J}}_3, \tag{8}$$

the total angular momentum on this Hilbert space, with eigenvalue $\mathbf{0}$. That this simultaneous eigenstate is nondegenerate follows from standard angular momentum theory; and the number of operators (six) equals the number of degrees of freedom in the Hilbert space (two for each $\mathcal{S}_r$, $r = 1, 2, 3$). Thus we write this state as illustrated in Fig. 34, indicating both operators and eigenvalues. This is otherwise the state $|W\rangle$, illustrated in bra form in Fig. 6. As for the normalization and phase, these must be supplied by context. For the $3j$-state illustrated in Fig. 34, these are given in terms of the $3j$-symbol by Fig. 1; in particular, the state is normalized.

$$\left| \begin{matrix} \hat{I}_1 & \hat{I}_2 & \hat{I}_3 & \hat{\mathbf{J}}_{123} \\ j_1 & j_2 & j_3 & \mathbf{0} \end{matrix} \right\rangle =$$

Figure 34. Ket notation for invariant state of the $3j$-type.

Similarly, the first $2j$-state in Fig. 33 lies in the Hilbert space $\mathcal{S}_1 \otimes \mathcal{S}'_1$ and is a simultaneous eigenstate of the operators $\hat{I}_1$ and $\hat{I}'_1$ with eigenvalues j_1 and j_1, as well as of the total angular momentum operator on this space,

$$\hat{\mathbf{J}}_{11'} = \hat{\mathbf{J}}_1 + \hat{\mathbf{J}}'_1, \tag{9}$$

with eigenvalue $\mathbf{0}$. This state is a simultaneous eigenstate of five operators, but in a sense only two of the three components of $\hat{\mathbf{J}}_{11'}$ are independent, so we should count only four independent operators, which agrees with the number of degrees of freedom in the Hilbert space (again, two each for $\mathcal{S}_1$ and $\mathcal{S}'_1$). We write this state as illustrated in Fig. 35; the normalization and phase are given by the components of K^{-1} shown in Fig. 23. In particular, with the square root factor in Fig. 35, this state is normalized.

$$\left| \begin{matrix} \hat{I}_1 & \hat{I}'_1 & \hat{\mathbf{J}}_{11'} \\ j_1 & j_1 & \mathbf{0} \end{matrix} \right\rangle = \frac{1}{\sqrt{2j_1 + 1}}$$

Figure 35. Ket notation for invariant state of the $2j$-type.

In this notation we can write the equations of Fig. 33 in the form

$$|B\rangle = \left| \begin{matrix} \hat{I}_1 & \hat{I}_2 & \hat{I}_3 & \hat{\mathbf{J}}_{123} \\ j_1 & j_2 & j_3 & \mathbf{0} \end{matrix} \right\rangle \left| \begin{matrix} \hat{I}'_1 & \hat{I}'_5 & \hat{I}_6 & \hat{\mathbf{J}}_{1'5'6} \\ j_1 & j_5 & j_6 & \mathbf{0} \end{matrix} \right\rangle \left| \begin{matrix} \hat{I}'_2 & \hat{I}'_6 & \hat{I}_4 & \hat{\mathbf{J}}_{2'6'4} \\ j_2 & j_5 & j_6 & \mathbf{0} \end{matrix} \right\rangle \left| \begin{matrix} \hat{I}'_3 & \hat{I}'_4 & \hat{I}_5 & \hat{\mathbf{J}}_{3'4'5} \\ j_3 & j_4 & j_5 & \mathbf{0} \end{matrix} \right\rangle, \tag{10}$$

and

$$|A\rangle = \left(\prod_{r=1}^{6} \sqrt{2j_r + 1}\right) \left| \begin{matrix} \hat{I}_1 \ \hat{I}_1' \ \hat{\mathbf{J}}_{11'} \\ j_1 \ j_1 \ \mathbf{0} \end{matrix} \right\rangle \cdots \left| \begin{matrix} \hat{I}_6 \ \hat{I}_6' \ \hat{\mathbf{J}}_{66'} \\ j_6 \ j_6 \ \mathbf{0} \end{matrix} \right\rangle. \tag{11}$$

One can see that Edmonds' form of the 6j-symbol (7) is equal to $\langle B|A\rangle$.

This scalar product was the starting point for Roberts' (1999) analysis of the asymptotics of the 6j-symbol. We shall comment below on further aspects of Roberts' calculation.

3.3. The Triangle and Polygon Inequalities

We make a remark on a generalization of the triangle inequalities before presenting the 4j-model of the 6j-symbol. If (ℓ_1, ℓ_2, ℓ_3) are three nonnegative lengths, the usual triangle inequalities are $|\ell_i - \ell_j| \leq \ell_k \leq \ell_i + \ell_j$, where $(i, j, k) = (1, 2, 3)$ and cyclic permutations. We generalize these as follows. Let $\{\ell_i, i = 1, \ldots, n\}$ be a set of lengths, $\ell_i \geq 0$, $i = 1, \ldots, n$. Then this set is said to satisfy the "polygon inequality" if

$$\max\{\ell_i\} \leq \frac{1}{2} \sum_{i=1}^{n} \ell_i. \tag{12}$$

This is equivalent to the triangle inequalities when $n = 3$. In general, it represents the necessary and sufficient condition that line segments of the given, nonnegative lengths can be fitted together to form a polygon with n sides (in $\mathbb{R}^N$, $N > 0$).

3.4. The 4j-model of the 6j-symbol

A different way of writing the 6j-symbol as a scalar product begins with Fig. 36, in which the j's in the 6j-symbol of Fig. 30 have been relabeled. We will refer to the labeling in Fig. 36 as the "asymmetric" labeling, which is more appropriate for the 4j-model. After the relabeling, we have reversed the arrow on the edge j_3 of the spin network (labeled simply by 3), incurring a phase $(-1)^{2j_3}$, and broken four edges into scalar products of a bra and a ket. Then, on the second line of Fig. 36, we have unfolded the bra and the ket, written the bra as the Hermitian conjugate of a ket, and adjusted phases. The result expresses the 6j-symbol as a phase times a scalar product of two states lying in the Hilbert space $\mathcal{H}_{4j} = \prod_{r=1}^{4} \otimes \mathcal{S}_r$. It is understood that the ket terminating a line labeled r lies in the j_r-irreducible subspace of $\mathcal{S}_r$.

These same states arise in the recoupling of four angular momenta with a resultant of zero. Let $\mathcal{Z}$ be the subspace of $\mathcal{C}_{j_1} \otimes \mathcal{C}_{j_2} \otimes \mathcal{C}_{j_3} \otimes \mathcal{C}_{j_4}$ upon which

$$\hat{\mathbf{J}}_{\text{tot}} = \sum_{r=1}^{4} \hat{\mathbf{J}}_r = 0. \tag{13}$$

This is the subspace of rotational invariants, that is, $\mathcal{Z}$ is the set of states $|\psi\rangle \in \mathcal{C}_{j_1} \otimes \mathcal{C}_{j_2} \otimes \mathcal{C}_{j_3} \otimes \mathcal{C}_{j_4}$ that are invariant under rotations. According to the rules for addition of angular momenta, subspace $\mathcal{Z}$ is nontrivial (dim $\mathcal{Z} > 0$) if $\sum_{r=1}^{4} j_r = $ integer and if the set $\{j_r\}$ satisfies the polygon inequality (12). In accordance with the remarks in Sec. 2.3, the subspace $\mathcal{Z}$ can also be interpreted as the space of 4-valent intertwiners, that is, $SU(2)$-invariant maps : $\mathcal{C}_{j_1} \otimes \mathcal{C}_{j_2} \otimes \mathcal{C}_{j_3} \otimes \mathcal{C}_{j_4} \rightarrow \mathbb{C}$. The notation $\mathcal{Z}$ is a mnemonic for "zero" (the eigenvalue of $\hat{\mathbf{J}}_{\text{tot}}$).

As far as recoupling theory is concerned the spaces $\mathcal{C}_{j_r}$ can be any carrier spaces of $SU(2)$ for the given values of j_r, but in our application we shall interpret the space

$$\begin{Bmatrix} j_1 & j_2 & j_{12} \\ j_3 & j_4 & j_{23} \end{Bmatrix} = (-1)^{2j_3}$$

$$= (-1)^{2j_2} \left(\text{} \right)^{\dagger} \left(\text{} \right)$$

Figure 36. Asymmetric labeling of the 6j-symbol, and decomposition of spin network.

$\mathcal{C}_{j_r}$ as the irreducible subspace j_r of the r-th copy of the Schwinger Hilbert space $\mathcal{S}_r$. Then $\mathcal{Z}$ becomes a subspace of $\mathcal{H}_{4j}$. We shall assume that the fixed values of the four j_r, $r = 1, \ldots, 4$ are chosen such that $\dim \mathcal{Z} > 0$. We should properly label $\mathcal{Z}$ by the four j_r values since $\mathcal{H}_{4j}$ contains as many subspaces of the type $\mathcal{Z}$ as there are choices of the four j's. For simplicity, however, we will suppress this dependence in the notation, it being understood that j_r, $r = 1, \ldots, 4$ are given.

Standard recoupling theory gives three ways of constructing an orthonormal basis in $\mathcal{Z}$. One uses Clebsch-Gordan coefficients to couple angular momenta according to the pattern $1 + 2 = 12$, $12 + 3 = 123$, $123 + 4 = 0$, resulting in the normalized state $|B\rangle$ lying in $\mathcal{Z}$, expressed in terms of a spin network in Fig. 37. A second way couples according to the pattern $2 + 3 = 23$, $1 + 23 = 123$, $123 + 4 = 0$, producing the normalized state $|A\rangle$ illustrated in Fig. 37. A third way, which we will not consider further, uses the intermediate coupling $1 + 3 = 13$.

$$|A\rangle = (-1)^{j_1 - j_2 - j_3 + j_4} \sqrt{2j_{12} + 1} \quad \text{}$$

$$|B\rangle = (-1)^{2(j_1 + j_2 + j_4)} \sqrt{2j_{23} + 1} \quad \text{}$$

Figure 37. Two ways of recoupling four angular momenta with a total of zero.

The quantum numbers j_{12} and j_{23} of the intermediate angular momenta range in

integer steps between the bounds

$$
\begin{aligned}
j_{12,\min} \leq j_{12} \leq j_{12,\max}, \\
j_{23,\min} \leq j_{23} \leq j_{23,\max},
\end{aligned}
\tag{14}
$$

where the maximum and minimum values are given in terms of the four fixed j_r, $r = 1, \ldots, 4$ by

$$
\begin{aligned}
j_{12,\min} = \max(|j_1 - j_2|, |j_3 - j_4|), \quad j_{12,\max} = \min(j_1 + j_2, j_3 + j_4), \\
j_{23,\min} = \max(|j_2 - j_3|, |j_1 - j_4|), \quad j_{23,\max} = \min(j_2 + j_3, j_1 + j_4).
\end{aligned}
\tag{15}
$$

Then the dimension of $\mathcal{Z}$ is given by

$$
D = \dim \mathcal{Z} = j_{12,\max} - j_{12,\min} + 1 = j_{23,\max} - j_{23,\min} + 1.
\tag{16}
$$

An expression for $\dim \mathcal{Z}$ can be given that is symmetrical in (j_1, j_2, j_3, j_4). Using the fact that $|x| = \max(x, -x)$, the difference between $j_{12,\max}$ and $j_{12,\min}$ becomes the shortest distance between one set of four numbers, $\{j_1 - j_2, j_2 - j_1, j_3 - j_4, j_4 - j_3\}$, and another set of two numbers, $\{j_1 + j_2, j_3 + j_4\}$. But this is the minimum of the distance between all eight possible pairs taken from the two sets. Thus

$$
D = \dim \mathcal{Z} = 2\min(j_1, j_2, j_3, j_4, s - j_1, s - j_2, s - j_3, s - j_4) + 1,
\tag{17}
$$

where s is the semiperimeter,

$$
s = \frac{1}{2}(j_1 + j_2 + j_3 + j_4).
\tag{18}
$$

More precisely, if D computed by (17) is ≤ 0, then subspace $\mathcal{Z}$ is trivial ($\dim \mathcal{Z} = 0$); otherwise $D = \dim \mathcal{Z}$. The formula (17) bears an interesting relationship to the Regge symmetries of the $6j$-symbol (Varshalovich *et al* 1981, Eq. (9.4.2.4)).

Now by comparing Figs. 36 and 37 we see that the $6j$-symbol is proportional to a scalar product,

$$
\langle B|A \rangle = (-1)^{j_1 + j_2 + j_3 + j_4} \sqrt{(2j_{12} + 1)(2j_{23} + 1)} \begin{Bmatrix} j_1 & j_2 & j_{12} \\ j_3 & j_4 & j_{23} \end{Bmatrix}.
\tag{19}
$$

This is the scalar product that we shall use for the semiclassical analysis of the $6j$-symbol in this paper. In a different notation, we can write $\langle j_{23}|j_{12} \rangle$ instead of $\langle B|A \rangle$, which emphasizes the fact that this is a unitary matrix element connecting two bases on $\mathcal{Z}$. The usual orthonormality relations satisfied by the $6j$-symbol (see Edmonds eq. (6.2.9)) are equivalent to the unitarity of $\langle j_{23}|j_{12} \rangle$.

Notice that in this $4j$-model, the angular momenta $\hat{\mathbf{J}}_r$, $r = 1, 2, 3, 4$ are independent operators, while the two remaining angular momenta,

$$
\hat{\mathbf{J}}_{12} = \hat{\mathbf{J}}_1 + \hat{\mathbf{J}}_2, \qquad \hat{\mathbf{J}}_{23} = \hat{\mathbf{J}}_2 + \hat{\mathbf{J}}_3,
\tag{20}
$$

are not, rather they are functions of the first four. As usual in the Schwinger representation, the quantum number j_r, $r = 1, \ldots, 4$ specifies the eigenvalues of both $\hat{I}_r$ and $\hat{\mathbf{J}}_r^2$, that is, j_r and $j_r(j_r + 1)$, respectively. And the quantum numbers j_{12} and j_{23} specify the eigenvalues of the operators $\hat{\mathbf{J}}_{12}^2$ and $\hat{\mathbf{J}}_{23}^2$, that is, $j_{12}(j_{12} + 1)$ and $j_{23}(j_{23} + 1)$, respectively. But there are no operators $\hat{I}_{12}$ or $\hat{I}_{23}$.

The states $|A\rangle$ and $|B\rangle$ in Fig. 37 can be expressed as eigenstates of complete sets of operators,

$$
|A\rangle = \left| \begin{matrix} \hat{I}_1 \, \hat{I}_2 \, \hat{I}_3 \, \hat{I}_4 \, \hat{\mathbf{J}}_{12}^2 \, \hat{\mathbf{J}}_{\text{tot}} \\ j_1 \, j_2 \, j_3 \, j_4 \, j_{12} \quad \mathbf{0} \end{matrix} \right\rangle, \qquad |B\rangle = \left| \begin{matrix} \hat{I}_1 \, \hat{I}_2 \, \hat{I}_3 \, \hat{I}_4 \, \hat{\mathbf{J}}_{23}^2 \, \hat{\mathbf{J}}_{\text{tot}} \\ j_1 \, j_2 \, j_3 \, j_4 \, j_{23} \quad \mathbf{0} \end{matrix} \right\rangle,
\tag{21}
$$

in a notation like that used in (10) and (11). As mentioned, these states are normalized, and their phases are specified by Fig. 37.

Notice that each state $|A\rangle$ and $|B\rangle$ has a list of eight independent operators (counting the three components of $\hat{\mathbf{J}}_{\text{tot}}$), corresponding to the eight degrees of freedom in the $4j$-model. We will call these lists of operators the A-list and B-list, and write them collectively as

$$
\begin{aligned}
\hat{A} &= (\hat{I}_1, \hat{I}_2, \hat{I}_3, \hat{I}_4, \hat{\mathbf{J}}_{12}^2, \hat{\mathbf{J}}_{\text{tot}}), \\
\hat{B} &= (\hat{I}_1, \hat{I}_2, \hat{I}_3, \hat{I}_4, \hat{\mathbf{J}}_{23}^2, \hat{\mathbf{J}}_{\text{tot}}),
\end{aligned}
\tag{22}
$$

We denote elements of these lists with subscripts, for example, $\hat{A}_i$ or $\hat{B}_i$, $i = 1, \ldots, 8$. The operators in the either of the lists (22) do not commute with one another (because the components of $\hat{\mathbf{J}}_{\text{tot}}$ do not commute; otherwise all commutators are zero), but they do possess simultaneous eigenstates in $\mathcal{Z}$, which are unique to within a phase, namely, the states (21).

3.5. The $8j$-model of the $6j$-symbol

We obtain an $8j$-model of the $6j$-symbol by inserting $2j$-symbols into edges 12 and 23 of the spin network of Fig. 36 and then treating them in the same way as the $2j$-symbols in the $12j$-model. The result is the Hilbert space $\mathcal{H}_{8j} = (\prod_{r=1}^{4} \otimes \mathcal{S}_r) \otimes \mathcal{S}_{12} \otimes \mathcal{S}_{12}' \otimes \mathcal{S}_{23} \otimes \mathcal{S}_{23}'$. This model has more symmetry than the $4j$-model but less than the $12j$-model. Operators $\hat{I}_{12}$ and $\hat{I}_{23}$ exist in this model (as well as operators $\hat{I}_{12}'$ and $\hat{I}_{23}'$), unlike the $4j$-model. This gives the $8j$-model certain advantages over the $4j$-model. We shall not consider the $8j$-model further in this paper.

4. The Classical Manifolds

In this section we study the classical mechanics that will be relevant for the semiclassical analysis of the $6j$-symbol in a $4j$-model. We begin by presenting our notation for the Schwinger phase space and products of it that are used to represent coupled, classical angular momenta. Other spaces that will be important are obtained by Poisson and symplectic reduction. Then we examine the geometry of the A- and B-manifolds in phase space that support the states (21), including a rather general analysis of why they are Lagrangian. Finally we discuss the Bohr-Sommerfeld quantization of these manifolds.

4.1. The Schwinger Phase Space and Other Spaces

The classical phase space for two harmonic oscillators (the Schwinger phase space) is $\Phi = (\mathbb{R}^4, dp \wedge dx)$, with coordinates $(x, p) \in \mathbb{R}^4$, for $x, p \in \mathbb{R}^2$. See Sec. I.3 for more details on our use of the Schwinger representation, as well as Cushman and Bates (1997) for a more detailed discussion of the geometry of two harmonic oscillators and the role played by the Hopf map. Here $dp \wedge dx$ means $\sum_{\mu=1}^{2} dp_\mu \wedge dx_\mu$, and similarly for other obvious contractions over $\mu = 1, 2$. Complex coordinates $z_\mu = (x_\mu + ip_\mu)/\sqrt{2}$, $\bar{z}_\mu = (x_\mu - ip_\mu)/\sqrt{2}$ are also useful, allowing us to write $\Phi = (\mathbb{C}^2, id\bar{z} \wedge dz)$.

Interesting functions on Φ (classical observables) include

$$
I = \frac{1}{2} \bar{z} z, \qquad J_i = \frac{1}{2} \bar{z} \sigma_i z,
\tag{23}
$$

where $i = 1, 2, 3$, obviously the classical analogs of (5), and where z or $\bar{z}$ without indices indicates a 2-component "spinor," that is, an element of $\mathbb{C}^2$. In comparison to (5) notice the absence of the hats, indicating that these are classical observables. These satisfy the Poisson bracket relations $\{I, J_i\} = 0$ and $\{J_i, J_j\} = \epsilon_{ijk} J_k$, as well as the identity $\mathbf{J}^2 = I^2$. The Hamiltonian flow of I is a $U(1)$ action on Φ, while the flows of J_i, $i = 1, 2, 3$, generate an $SU(2)$ action on Φ. Both actions are easily expressed in the complex coordinates z: that of $U(1)$ is $z \mapsto \exp(-i\psi/2)z$, where ψ is the variable conjugate to I, while that of $SU(2)$ is $z \mapsto uz$ for $u \in SU(2)$.

The orbit of the $U(1)$ action generated by I passing through any point $z \neq 0$ on Φ is a circle on which ψ is a coordinate, covered once when $0 \leq \psi < 4\pi$. The level set $I = J$ for $J > 0$, where $I : \Phi \to \mathbb{R}$ is the function and $J \in \mathbb{R}$ is the contour value, is a 3-sphere to which the orbits of I are confined. The definition (23) of J_i is interpreted as a map $\pi : \Phi \to \mathbb{R}^3$, where the three components J_i of $\mathbf{J}$ are coordinates on $\mathbb{R}^3$ (thus, this space is "angular momentum space"). This map is a Poisson map (Marsden and Ratiu 1999), giving $\mathbb{R}^3$ the Poisson structure $\{J_i, J_j\} = \epsilon_{ijk} J_k$. We denote $\mathbb{R}^3$ with this Poisson structure by Λ, as indicated by the diagram,

$$
\begin{array}{ccc}
(I = J) & \subset & \Phi \\
\downarrow{\scriptstyle \pi_H} & & \downarrow{\scriptstyle \pi} \\
\Sigma & \subset & \Lambda
\end{array}
\qquad (24)
$$

The map π can also be interpreted as the momentum map (Abraham and Marsden 1978) of the $SU(2)$ action on Φ, so that Λ or angular momentum space is identified with $\mathfrak{su}(2)^*$. When π is restricted to a level set $I = J > 0$ in Φ (a 3-sphere), it projects onto the 2-sphere $|\mathbf{J}| = J$ in Λ. This is the projection map π_H of the Hopf fibration, in which the orbits of I are the fibers (or "Hopf circles"). It is also the map of symplectic reduction (Abraham and Marsden 1978) of the level set $I = J$ in Φ by the $U(1)$ action, so that the 2-spheres $|\mathbf{J}| = J$ in Λ are symplectic manifolds. The symplectic form on one of these 2-spheres is $J \, d\Omega$, where $d\Omega$ is the element of solid angle (to within a sign). We denote one of these spheres with its symplectic structure (for some value $J > 0$) by Σ; these spheres are also the symplectic leaves of the Poisson structure in Λ.

In an nj-model of a spin network we take Cartesian products of the Schwinger phase space Φ to obtain the phase space for n independent classical angular momenta. We will illustrate the notation for the $4j$-model. We write $\Phi_{4j} = \Phi^4$ for the entire phase space; apart from the symplectic structure, this is $\mathbb{C}^8 = \mathbb{R}^{16}$. Coordinates on Φ_{4j} are $x_{\mu r}$, $p_{\mu r}$, $z_{\mu r}$, etc, $\mu = 1, 2$, $r = 1, \ldots, 4$. We denote the r-th copy of Φ by Φ_r, and define functions I_r, J_{ri} on Φ_r on the pattern of (23), that is, just by adding r subscripts to all the variables in those equations. Naturally these can also be viewed as functions on Φ_{4j}. The vector $\mathbf{J}_r$ is the r-th classical angular momentum.

We generalize the diagram (24) to the $4j$-model as follows,

$$
\begin{array}{ccc}
(I_r = J_r) & \subset & \Phi_{4j} \\
\downarrow {\scriptstyle \pi_H} & & \downarrow {\scriptstyle \pi} \\
\mathrm{CL} \quad \subset \quad \Sigma_{4j} & \subset & \Lambda_{4j} \\
\downarrow {\scriptstyle \pi_{KM}} & & \\
\Gamma & &
\end{array}
\tag{25}
$$

where π means dividing Φ_{4j} by the $U(1)^4$ action generated by I_r, $r = 1, \ldots, 4$. Thus $\mathbf{J}_r$, $r = 1, \ldots, 4$ are coordinates on $\Lambda_{4j} = (\mathbb{R}^3)^4$, in which the Poisson bracket of two functions f and g is given by

$$
\{f, g\} = \sum_{r=1}^{4} \mathbf{J}_r \cdot \left(\frac{\partial f}{\partial \mathbf{J}_r} \times \frac{\partial g}{\partial \mathbf{J}_r} \right).
\tag{26}
$$

Similarly, for four positive contour values $J_r > 0$, $r = 1, \ldots, 4$, the level set $I_r = |\mathbf{J}_r| = J_r$, $r = 1, \ldots, 4$, in Φ_{4j} is $(S^3)^4$ (indicated simply by $I_r = J_r$ in the diagram). The map π restricted to this space is a power of the Hopf map (simply denoted π_H in the diagram), which projects $(S^3)^4$ onto the space $\Sigma_{4j} = (S^2)^4$, a symplectic manifold in Λ_{4j}. Notice that the radii of the spheres (the 3-spheres in Φ_{4j} and the 2-spheres in Λ_{4j}) need not be equal for different r. The spaces CL and Γ in (25) will be explained later.

Other important classical observables on Φ_{4j} are $\mathbf{J}_{12} = \mathbf{J}_1 + \mathbf{J}_2$ and $\mathbf{J}_{23} = \mathbf{J}_2 + \mathbf{J}_3$, their squares, $\mathbf{J}_{12}^2$ and $\mathbf{J}_{23}^2$, and the total angular momentum $\mathbf{J}_{\mathrm{tot}} = \sum_{r=1}^{4} \mathbf{J}_r$.

4.2. Level Sets and Contour Values

The A- and B-lists of operators in (22) correspond to lists of classical observables (without the hats),

$$
\begin{aligned}
A &= (I_1, I_2, I_3, I_4, \mathbf{J}_{12}^2, \mathbf{J}_{\mathrm{tot}}), \\
B &= (I_1, I_2, I_3, I_4, \mathbf{J}_{23}^2, \mathbf{J}_{\mathrm{tot}}).
\end{aligned}
\tag{27}
$$

We will denote the members of these lists by A_i, B_i, $i = 1, \ldots, 8$. As discussed in I and in Littlejohn (1990), the Lagrangian manifolds that support the semiclassical approximations to the states $|A\rangle$ and $|B\rangle$ are the level sets in Φ_{4j} of these lists of classical observables, with quantized values of the contour values. We will defer the question of quantization to Sec. 4.6, and for now just examine these level sets for some suitable contour values. We will call the level sets of the A- and B-lists the A- and B-manifolds.

It will be convenient to distinguish notationally the functions in the two lists, regarded as maps : $\Phi_{4j} \to \mathbb{R}$, from the contour values, which are real numbers. Our notation is summarized in Table 1. The vector of functions $\mathbf{J}_{\mathrm{tot}}$ is given the value $\mathbf{0}$ because that is the only contour value we will consider. The other contour values are variable. The conventions in the table solve some notational problems in I, but the notation requires care. For example, the magnitude of the vector $\mathbf{J}_r$, regarded

function	value
I_r	J_r
$\mathbf{J}_{12}^2$	J_{12}^2
$\mathbf{J}_{23}^2$	J_{23}^2
$\mathbf{J}_{\text{tot}}$	$\mathbf{0}$

Table 1. Notation for functions : $\Phi_{4j} \to \mathbb{R}$ and values (real numbers) of those functions. In the first row, $r = 1, \ldots, 4$.

as a function : $\Phi_{4j} \to \mathbb{R}$, is not J_r (because J_r is a number, not a function), but on the level set $I_r = J_r$ it is true that that $|\mathbf{J}_r| = J_r$, in view of the identity between functions, $\mathbf{J}_r^2 = I_r^2$. If we wish to refer to the magnitude or the square of the vector $\mathbf{J}_r$, regarded as a function on Φ, we will write $|\mathbf{J}_r|$ or $\mathbf{J}_r^2$ (in bold face), not J_r or J_r^2. We will denote the lists of contour values collectively by a or b, so that

$$a = (J_1, J_2, J_3, J_4, J_{12}^2, \mathbf{0}),$$
$$b = (J_1, J_2, J_3, J_4, J_{23}^2, \mathbf{0}),$$

(28)

with components a_i, b_i, $i = 1, \ldots, 8$.

Consider now the conditions on the contour values a, b such that the A- and B-manifolds should exist (as nonempty sets of points). The question of the dimensionality of these manifolds will be postponed to Sec. 4.4, but it turns out that their maximum (for any contour values) and generic dimensionality is 8, one half the dimension of the $4j$ Schwinger phase space. We work with the A-manifold, since the conditions for the B-manifold are completely analogous.

First, the A-manifold clearly does not exist unless $J_r \geq 0$, $r = 1, \ldots, 4$, so let us assume this condition. Then if the A-manifold exists, we can pick a point on it and evaluate the vector functions $\mathbf{J}_r$, $r = 1, \ldots, 4$, to determine the projected point in Λ_{4j}. We visualize this point as four vectors in a single copy of $\mathbb{R}^3$. In addition we compute the vector $\mathbf{J}_{12} = \mathbf{J}_1 + \mathbf{J}_2$ and plot it along with the others in $\mathbb{R}^3$. Next, we move the vectors $(\mathbf{J}_1, \mathbf{J}_2, -\mathbf{J}_{12})$ end-to-end to create a triangle with sides (J_1, J_2, J_{12}). We move the vectors by parallel transport in $\mathbb{R}^3$, that is, without rotating them. Thus, the triangle inequalities are satisfied in the triplet of lengths (J_1, J_2, J_{12}). Also, since $\mathbf{J}_{\text{tot}} = 0$, we can form a second triangle out of vectors $(\mathbf{J}_3, \mathbf{J}_4, \mathbf{J}_{12})$, so the triangle inequalities are satisfied in the triplet (J_3, J_4, J_{12}). The two triangles have the edge J_{12} in common, creating a figure like Fig. 38.

Conversely, suppose that $J_r \geq 0$, $r = 1, \ldots, 4$ and that the triangle inequalities are satisfied in triplets (J_1, J_2, J_{12}) and (J_3, J_4, J_{12}). This means that two triangles can be constructed in $\mathbb{R}^3$ with the given lengths. By translating and/or rotating the two triangles, we can bring the 12 edges into coincidence, thereby creating a figure like Fig. 38, and hence a point of Λ_{4j}. But since the map $\pi : \Phi_{4j} \to \Lambda_{4j}$ is onto, there exists an inverse image of this point in Φ_{4j}, hence the A-manifold exists.

In summary, we have shown that the A-manifold exists iff $J_r \geq 0$, $r = 1, \ldots, 4$, and the triangle inequalities are satisfied in the triplets (J_1, J_2, J_{12}) and (J_3, J_4, J_{12}). A similar result holds for the B-manifold, where the triplets are (J_2, J_3, J_{23}) and (J_1, J_4, J_{23}). The triangle inequalities imply that J_{12} and J_{23} lie in the ranges,

$$J_{12,\text{min}} \leq J_{12} \leq J_{12,\text{max}},$$

(29)

$$J_{23,\text{min}} \leq J_{23} \leq J_{23,\text{max}},$$
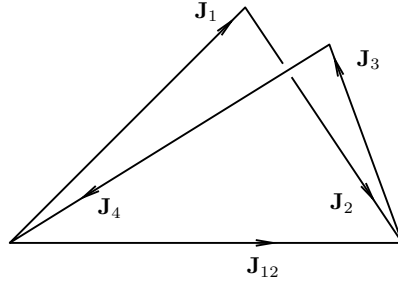
(30)

Figure 38. A point of the A- or B-manifolds in $\Phi_{4j} = \mathbb{C}^8$ projects under π onto a point of $\Lambda_{4j} = [\mathbb{R}^3]^4$ on which the four angular momenta $\mathbf{J}_r$ add to zero. We visualize this point as four angular momentum vectors in a single copy of $\mathbb{R}^3$ that add to zero. In such diagrams, the vectors need not be based at the origin; here we place them end-to-end. Also shown in the figure is the vector $\mathbf{J}_{12} = \mathbf{J}_1 + \mathbf{J}_2$.

where

$$J_{12,\text{min}} = \max(|J_1 - J_2|, |J_3 - J_4|), \qquad J_{12,\text{max}} = \min(J_1 + J_2, J_3 + J_4), \qquad (31)$$

$$J_{23,\text{min}} = \max(|J_2 - J_3|, |J_1 - J_4|), \qquad J_{23,\text{max}} = \min(J_2 + J_3, J_1 + J_4). \qquad (32)$$

These inequalities imply $J_{12}, J_{23} \geq 0$. Notice that the value 0 is not always excluded, for example, if $J_1 = J_2$ and $J_3 = J_4$ then $J_{12} = 0$ is allowed.

It turns out that the A- and B-manifolds, when 8-dimensional, are Lagrangian. According to the Liouville-Arnold theorem (Arnold 1989) the compact level sets of complete sets of Poisson commuting observables are generically Lagrangian tori. The sets of observables A or B of interest in this paper are not commuting, however, so the Liouville-Arnold theorem does not apply. In a similar situation in I we showed that the manifold in question (what we called the "Wigner manifold") was nevertheless Lagrangian. In the following section we present a general set of circumstances in which Lagrangian manifolds are obtained, which cover not only the cases considered in the Liouville-Arnold theorem but also all cases we know of in the asymptotics of spin networks, including the manifolds studied in I and the A- and B-manifolds of this paper.

4.3. Level Sets, Orbits, and Lagrangian Manifolds

We use general notation in this section that differs somewhat from that of the application to the $6j$-symbol in the rest of the paper. The basic conclusion of this section is the following. Let $\{A_i, i = 1, \ldots, m\}$ be a collection of classical observables on a phase space (symplectic manifold) P of dimension $2N$, that is, $A_i : P \to \mathbb{R}$. Let the set $\{A_i\}$ form a Lie algebra, that is, the Poisson brackets $\{A_i, A_j\}$ are linear combinations of the A_i. Let L be the level set $A_i = a_i$, for some contour values a_i, and suppose that all Poisson brackets $\{A_i, A_j\}$ vanish on L. Finally, suppose L is a smooth manifold of dimension N (thus, $m \geq N$). Then L is Lagrangian. The reader who is willing to accept this conclusion can skip the remainder of this section.

We deal with classical Hamiltonian systems with symmetry. Basic references on this subject are Abraham and Marsden (1978), Marsden and Ratiu (1999) and Cushman and Bates (1997). We make quite a few assumptions in this section, but most of them are generic. The most important one that is not is the assumption that

the momentum, in the general sense of the value of the momentum map, is a fixed point of the coadjoint action of the group, that is, it is G-invariant.

Let P be a symplectic manifold of dimension $2N$, let G be a connected Lie group of dimension m with Lie algebra $\mathfrak{g}$, dual $\mathfrak{g}^*$, and symplectic action on P. Suppose the momentum map $M : P \to \mathfrak{g}^*$ exists, that is, the action of G is generated by Hamiltonian flows of a set of Hamiltonian functions. Let $\{\xi_i, i = 1, \dots, m\}$ be a basis in $\mathfrak{g}$, and let $c^k{}_{ij}$ be the structure constants, so that $[\xi_i, \xi_j] = c^k{}_{ij}\,\xi_k$ (summation convention). Define functions $A_i : P \to \mathbb{R}$ by $A_i(x) = \langle M(x), \xi_i \rangle$ for all $x \in P$. These functions form a Lie algebra under the Poisson bracket, $\{A_i, A_j\} = c^k{}_{ij}\,A_k$, with the same structure constants as the ξ_i in $\mathfrak{g}$. Let $X_i = \omega^{-1}dA_i$ be the Hamiltonian vector fields associated with the A_i, where ω is the symplectic form on P, regarded as a map from vector fields to 1-forms.

For some point $x_0 \in P$ let $a = M(x_0)$, so the level set L of the A's passing through x_0 is given by $A = a$ (that is, $L = M^{-1}(a)$). For simplicity we assume that L has only one connected component, or else we restrict consideration to the connected component passing through x_0. Let n be the rank of the set of differential forms $\{dA_i, i = 1, \dots, m\}$, assumed to be constant over L. Then $n \le m$ and $\dim L = 2N - n$. Also let the orbit of the G-action through x_0 be B. The vectors $\{X_i, i = 1, \dots, m\}$ are tangent to B and span its tangent space at each point. Also, $\operatorname{rank}\{X_i\} = \operatorname{rank}\{dA_i\} = n$, since ω is nonsingular. Thus, $\dim B = n$.

At this point we have the basic geometry for symplectic reduction, as illustrated in Fig. 39. Shown in the figure is the intersection I of L and B, which is the orbit of x_0 under the isotropy subgroup of a under the coadjoint action of the group. Dividing L by the isotropy subgroup produces the reduced symplectic manifold.
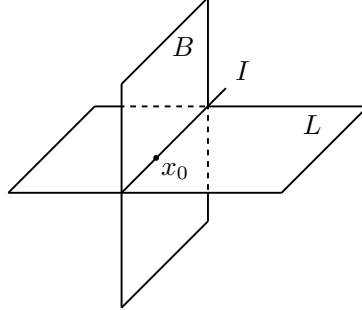

Figure 39. Schematic illustration of the basic geometry of symplectic reduction. L is the level set of the momentum map passing through x_0, B is the orbit of the group action, and I the intersection, also the orbit of the isotropy subgroup.

Now suppose that $a \in \mathfrak{g}^*$ (the generalized momentum) is a fixed point of the coadjoint action of the group, that is, $\operatorname{Ad}_g^* a = a$, $\forall g \in G$. By differentiation and contraction with an arbitrary element of $\mathfrak{g}$ this implies $\langle a, [\eta, \zeta] \rangle = 0$, $\forall \eta, \zeta \in \mathfrak{g}$, or, by setting $\eta = \xi_i$, $\zeta = \xi_j$, $c^k{}_{ij}a_k = 0$. But this implies $\{A_i, A_j\} = c^k{}_{ij}\,A_k = 0$ on the level set L, where $A_k = a_k$. In other words, the functions A_i, which may form a nontrivial Lie algebra on P, have vanishing Poisson brackets among themselves on L. This in turn implies that the A_i's are constant along each other's flows on B, that is, $X_i A_j = -\{A_j, A_i\} = 0$, so $B \subset L$. Therefore $\dim B \le \dim L$, or $n \le 2N - n$, or $n \le N$.

Finally, let us assume that n takes its maximum value $n = N$. Then $\dim B = \dim L = N$. If L is compact, then $B = L$, that is, the level set and the orbit coincide. Moreover L is Lagrangian, since the vectors X_i span the tangent space to L and $\omega(X_i, X_j) = -\{A_i, A_j\} = 0$ on L. This in turn implies that L supports locally a solution of the simultaneous Hamilton-Jacobi equations involved in finding a semiclassical eigenfunction of the operators with principal symbols A_i.

In the case of an integrable system the group is Abelian, $G = \mathbb{R}^N$, the N classical observables A_i Poisson commute everywhere in phase space, and on a generic level set $A = a$ the differentials dA_i are linearly independent everywhere. Since the group is Abelian, a is automatically a fixed point of the coadjoint action, and thus the level set is Lagrangian. Moreover, if it is compact, it is an N-torus.

In the case of the manifolds explored in I (the jm- and Wigner manifolds) and the A- and B-manifolds of this paper, the isotropy subgroup of the action of G on $x_0 \in P$ is zero-dimensional (a discrete set of points), so $\dim G = \dim B = m = n$. Moreover, $n = N$, so the manifolds are Lagrangian.

4.4. Properties of the A- and B-manifolds

We now apply the analysis of Sec. 4.3 to the A-manifold. In the following we visualize a point of Φ_{4j} as a 2×4 matrix of complex coordinates $z_{\mu r}$, referring to the r-th column as the r-th "spinor."

Here the symplectic manifold is $P = \Phi_{4j}$, and we take the group to be $G = U(1)^5 \times SU(2)$, where the action of $U(1)^5$ is generated by $(I_1, I_2, I_3, I_4, \mathbf{J}_{12}^2)$, and that of $SU(2)$ is generated by $\mathbf{J}_{\text{tot}}$. For given r, the observable I_r generates a $U(1)$ action, the multiplication the r-th spinor by $e^{-i\psi_r/2}$, where ψ_r is the evolution variable conjugate to I_r, with period 4π. See (I.27). Also, $\mathbf{J}_{\text{tot}}$ generates the diagonal $SU(2)$ action, that is, all four spinors are multiplied by the same element $u \in SU(2)$ (the 2×4 matrix is multiplied on the left by u). See (I.28) and (I.29). As for the observable $\mathbf{J}_{12}^2$, Hamilton's equations are

$$\frac{dz_{r\mu}}{dt} = \{z_{r\mu}, \mathbf{J}_{12}^2\} = 2J_{12i}\{z_{r\mu}, J_{12i}\} = \begin{cases} -i(\mathbf{J}_{12} \cdot \boldsymbol{\sigma})_{\mu\nu}\, z_{r\nu}, & \text{if } r = 1, 2, \\ 0, & \text{if } r = 3, 4, \end{cases} \tag{33}$$

where t is the variable of evolution. See (I.28) for a similar calculation, and notice that $\mathbf{J}_{12}$ is a constant of the flow generated by $\mathbf{J}_{12}^2$. Thus, $\mathbf{J}_{12}^2$ generates a $U(1)$ action that rotates spinors 1 and 2 about the axis $\mathbf{j}_{12} = \mathbf{J}_{12}/|\mathbf{J}_{12}|$, that is, it multiplies them by $u(\mathbf{j}_{12}, \theta) \in SU(2)$ (in axis-angle notation for an element of $SU(2)$, see (I.18)) while leaving spinors 3 and 4 invariant. The period is $\theta = 4\pi$ or $t = 2\pi/J_{12}$. The $U(1)$ action generated by $\mathbf{J}_{12}^2$ is not a rotation about a fixed axis, since $\mathbf{J}_{12}$ depends on where we are in Φ_{4j}, but it does commute with the other $U(1)$ actions generated by the I_r, as well as the $SU(2)$ action generated by $\mathbf{J}$. Similar statements can be made about $\mathbf{J}_{23}^2$.

Now we determine the maximum dimensionality of the A-manifold. Since there are 8 functions in the A-list and $\dim \Phi_{4j} = 16$, the answer will be 8 if the functions are independent. Functions are independent at a point if their differentials, in this case, $\{dA_i, i = 1, \ldots, 8\}$, are linearly independent. In any case, the rank of this set of differentials is the same as the rank of the set of Hamiltonian vector fields $X_i = \omega^{-1}dA_i$.

The A-manifold cannot have its maximum dimension if any $J_r = 0$, for $r = 1, \ldots, 4$, since that implies $dI_r = 0$. So we assume $J_r > 0$, $i = 1, \ldots, 4$. This means

that all four spinors z_r are nonzero, and hence the orbit of the group $U(1)^4$ generated by the I_r, $r = 1, \ldots, 4$ is a four-torus T^4. This is also the fiber of the projection $\pi : \Phi_{4j} \to \Lambda_{4j}$.

The condition $J_r > 0$, $r = 1, \ldots, 4$ also means that all four vectors $\mathbf{J}_r$, $r = 1, \ldots, 4$ are nonzero. We think of these vectors in a single copy of $\mathbb{R}^3$. When the group $SU(2)$, whose action is generated by $\mathbf{J}_{\text{tot}}$, acts on Φ_{4j}, the effect on the vectors $\mathbf{J}_r$, $r = 1, \ldots, 4$, is to rotate them by the corresponding element of $SO(3)$ (see (I.21)). If any of these vectors is moved by the $SO(3)$ rotation, then in Φ_{4j} we will have moved off the initial fiber of the projection π, hence we will have motions that are linearly independent of the $U(1)^4$ action. To make all three independent directions of rotation in $SO(3)$ give rise to linearly independent motions, we require that the isotropy subgroup of the $SO(3)$ action on the set $\{\mathbf{J}_r,\ r = 1, \ldots, 4\}$ (that is, the diagonal action) be trivial. This is at a point at which $\mathbf{J}_{\text{tot}} = \sum_{r=1}^{4} \mathbf{J}_r = 0$. This requires that the four vectors $\mathbf{J}_r$, $r = 1, \ldots, 4$ (which are nonzero) be noncollinear (otherwise the isotropy subgroup is $SO(2)$ or the whole group $SO(3)$). This in turn requires that at least one of the triangles, (J_1, J_2, J_{12}) or (J_3, J_4, J_{12}), have nonzero area.

Next there is the $U(1)$-action on Φ_{4j}, generated by $\mathbf{J}_{12}^2$. This has the effect on the vectors $\mathbf{J}_r$, $r = 1, \ldots, 4$ of a rotation of vectors $\mathbf{J}_1$ and $\mathbf{J}_2$ about axis $\mathbf{j}_{12}$, while leaving $\mathbf{J}_3$ and $\mathbf{J}_4$ invariant. In order that this motion move us off the initial fiber, we require that $\mathbf{J}_1$ and $\mathbf{J}_2$ be linearly independent, that is, that triangle (J_1, J_2, J_{12}) have nonzero area. And in order that this motion be linearly independent of overall rotation generated by $\mathbf{J}_{\text{tot}}$, we require that the triangle (J_3, J_4, J_{12}) also have nonzero area, in order that the rotation of $\mathbf{J}_1$, $\mathbf{J}_2$ about the axis $\mathbf{j}_{12}$ should change the shape of the figure created by the four vectors. (The overall rotations generated by $\mathbf{J}_{\text{tot}}$ do not change the shape of the figure.)

We conclude that at a point of the A-manifold, $\text{rank}\{dA_i, i = 1, \ldots, 8\} = 8$ iff $J_r > 0$, $r = 1, \ldots, 4$ and none of the triangle inequalities in (J_1, J_2, J_{12}) or (J_3, J_4, J_{12}), or equivalently, the inequalities in (29), is saturated. Notice in particular that this implies $J_{12} > 0$. Since these conditions depend only on the contour values and not where we are on the A-manifold, the A-manifold, under the stated conditions, is a smooth, 8-dimensional manifold.

In addition, the A-manifold is compact. It is also connected, as follows by consideration of its projection under π (see Sec. 4.5). This means that the action of the group $U(1)^5 \times SU(2)$ is transitive on the A-manifold (it is the orbit of any point on it under the group action). It then follows from the discussion of Sec. 4.3 that the A-manifold, when 8-dimensional, is Lagrangian. Similar statements apply to the B-manifold.

To find the topology of the A-manifold, we first find the isotropy subgroup of the action of $U(1)^5 \times SU(2)$ on a point x_0 on this manifold. If we denote coordinates on $U(1)^5 \times SU(2)$ by $(\psi_1, \psi_2, \psi_3, \psi_4, \theta, u)$, where $u \in SU(2)$ and where the five angles are the 4π-periodic evolution variables corresponding to $(I_1, I_2, I_3, I_4, \mathbf{J}_{12}^2)$, respectively, then the isotropy subgroup is generated by two elements, say, $x = (2\pi, 2\pi, 2\pi, 2\pi, 0, -1)$ and $y = (0, 0, 2\pi, 2\pi, 2\pi, -1)$. The isotropy subgroup itself is the Viergruppe $\{e, x, y, xy\} = (\mathbb{Z}_2)^2$. Thus the A-manifold is topologically $U(1)^5 \times SU(2)/(\mathbb{Z}_2)^2$. This is the same logic used in I to find the topology of the "Wigner manifold" of that paper. The analysis is the same for the B-manifold, which has the same topology. The isotropy subgroup would be larger in degenerate cases, for example, when some triangle inequalities are saturated.

Now it is easy to find the invariant measure on the A- or B-manifolds. It

is $d\psi_1 \wedge d\psi_2 \wedge d\psi_3 \wedge d\psi_4 \wedge d\theta \wedge du$, where du is the Haar measure on $SU(2)$ ($du = \sin\beta \, d\alpha \wedge d\beta \wedge d\gamma$ in Euler angles). Thus, the volume of the A- or B-manifold with respect to this measure is

$$V_A = V_B = \frac{1}{4}(4\pi)^5 \times 16\pi^2 = 2^{12}\pi^7, \tag{34}$$

where the $1/4$ compensates for the 4-element isotropy subgroup.

4.5. Projections and tetrahedra

We now study the projection of the A-manifold onto Λ_{4j}, for contour values such that the manifold is 8-dimensional. The projection consists of the set of four nonzero vectors in $\mathbb{R}^3$, $\{\mathbf{J}_r, r = 1, \ldots, 4\}$ of given lengths $J_r > 0$ with a sum of zero, $\mathbf{J}_{\text{tot}} = 0$, creating a closed chain of links as in Fig. 38, such that J_{12} has a given, positive value and both triangles 1-2-12 and 3-4-12 have nonzero area. We choose to place the four vectors end-to-end in the order $(\mathbf{J}_1, \mathbf{J}_2, \mathbf{J}_3, \mathbf{J}_4)$, as in Fig. 38; this is an arbitrary choice, but convenient for studying observables $\mathbf{J}_{12}^2$ and $\mathbf{J}_{23}^2$ (if we wished to examine $\mathbf{J}_{13}^2$ we would choose a different order). By filling in the lines $\mathbf{J}_{12}$ and $\mathbf{J}_{23}$, the closed chain of links becomes a tetrahedron, as shown in Fig. 40.
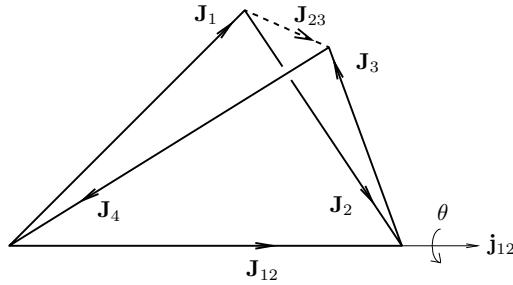

Figure 40. The function $\mathbf{J}_{12}^2$ generates a rotation about axis $\mathbf{j}_{12}$ of vectors $\mathbf{J}_1$ and $\mathbf{J}_2$, rotating triangle 1-2-12 by an angle θ while leaving triangle 3-4-12 fixed. The result is a family of tetrahedra with values of j_{23}, the length of vector $\mathbf{J}_{23}$, ranging from a minimum to a maximum.

The set of all such figures, modulo orientation, is the circle $S^1 = SO(2)$, whose angle is the dihedral angle about the edge $\mathbf{J}_{12}$. Including the orientation, we see that the projection of the A-manifold onto Λ_{4j} is topologically $SO(2) \times SO(3)$. One might imagine that this should be described as an $SO(3)$ bundle over $SO(2)$, but in fact the bundle is trivial. This is connected, so the inverse image under π, which is the A-manifold itself, is a 4-torus bundle over $SO(2) \times SO(3)$, and is also connected. An action of the group $SO(2) \times SO(3)$ on Λ_{4j} is generated by $\mathbf{J}_{12}^2$ and $\mathbf{J}_{\text{tot}}$, regarded as observables on Λ_{4j} using the Poisson structure (26). This is the projection of the action of $U(1)^5 \times SU(2)$ on Φ_{4j}. The motion generated by $\mathbf{J}_{12}^2$ is the "butterfly" motion illustrated in Fig. 40, in which the butterfly flaps one of its wings.

As the triangle 1-2-12 rotates around the edge 12, the length $|\mathbf{J}_{23}|$ varies between a maximum and minimum value. The minimum value is reached when triangles 1-2-12 and 3-4-12 lie in the same plane on the same side of line 12, and maximum when on opposite sides of line 12; these are also the minimum and maximum of $|\mathbf{J}_{23}|$ on the A-manifold in Φ_{4j}. These extremal values are reached when the tetrahedron is flat

(its volume is zero), and can be obtained in terms of the other five J's as the roots of the Cayley-Menger determinant (Berger 1987, Crippen and Havel 1988),

$$\det \begin{pmatrix} 0 & 1 & 1 & 1 & 1 \\ 1 & 0 & J_1^2 & J_{12}^2 & J_4^2 \\ 1 & J_1^2 & 0 & J_2^2 & x^2 \\ 1 & J_{12}^2 & J_2^2 & 0 & J_3^2 \\ 1 & J_4^2 & x^2 & J_3^2 & 0 \end{pmatrix} = 0, \tag{35}$$

where $x = |\mathbf{J}_{23}|$. Such determinants were an important part of the analysis of Ponzano and Regge (1968). In this case the determinant expresses the condition that the volume of the tetrahedron is zero. Expanding the determinant gives a quadratic equation in x^2 in terms of the five J's specifying the A-manifold. The same condition can be expressed in terms of a smaller (3×3) Gram matrix of dot products, as discussed in Littlejohn and Yu (2009).

A similar analysis applies to the B-manifold except that here we fix the length J_{23} of vector $\mathbf{J}_{23}$, and create tetrahedra of different shapes by varying the dihedral angle between triangles 4-1-23 and 2-3-23, that is, by rotating vectors $\mathbf{J}_2$ and $\mathbf{J}_3$ about the axis $\mathbf{j}_{23} = \mathbf{J}_{23}/J_{23}$. In this process, the length $|\mathbf{J}_{12}|$ varies from some minimum to some maximum, which can be obtained by replacing x^2 in (35) by J_{23}^2, and then J_{12}^2 by x^2 where now $x = |\mathbf{J}_{12}|$.

4.6. Quantizing the Manifolds

The A- and B-manifolds can be subjected to Bohr-Sommerfeld quantization, which selects certain contour values as quantized. The process uses the Weyl symbols or transforms (Weyl 1927, Wigner 1932, Groenewold 1946, Moyal 1949, Berry 1977, Balazs and Jennings 1984, Littlejohn 1986, Ozorio de Almeida 1998) of the lists (22) of operators, which are functions on Φ_{4j}. The Weyl symbols of selected operators are summarized in Table 2. It is important that the classical manifolds be the level sets of the Weyl symbols of the operators whose simultaneous eigenfunctions we seek (Littlejohn 1990); this holds in the present case because the Weyl symbols in the table are always equal to the corresponding classical observable (without the hat), to within an additive constant. Notationally we could have defined the classical observable (without the hat) as the Weyl symbol of the corresponding quantum observable, but the conventions in the table make it easier to establish the connections with the usual quantum numbers in physics. In particular, the zero point energy has been subtracted from the quantum observables $\hat{I}_r$, but not from the classical ones I_r, which explains the $1/2$ on the first row of the table.

To quantize the A- or B-manifold, we first determine the homotopy group, then we compute action integrals and Maslov indices along generators of the group, then we require that the action plus Maslov correction be an integer multiple of 2π. Only manifolds of full dimensionality (8) can be quantized. This is the procedure followed in I, and the analysis is very similar in this case; in particular, in both cases the homotopy group is Abelian.

We just summarize the results, speaking of the A-manifold. We find that J_r, $r = 1, \ldots, 4$ are quantized in half-integer steps, which we write in terms of the quantum numbers j_r as

$$J_r = j_r + 1/2, \tag{36}$$

operator	Weyl symbol
$\hat{I}_r$	$I_r - 1/2$
$\hat{\mathbf{J}}_r$	$\mathbf{J}_r$
$\hat{\mathbf{J}}_{\text{tot}}$	$\mathbf{J}_{\text{tot}}$
$\hat{\mathbf{J}}_{12}$	$\mathbf{J}_{12}$
$\hat{\mathbf{J}}_{23}$	$\mathbf{J}_{23}$
$\hat{\mathbf{J}}_r^2$	$\mathbf{J}_r^2 - 3/8$
$\hat{\mathbf{J}}_{12}^2$	$\mathbf{J}_{12}^2 - 3/4$
$\hat{\mathbf{J}}_{23}^2$	$\mathbf{J}_{23}^2 - 3/4$

Table 2. Weyl symbols of selected operators. In rows containing operators $\hat{I}_r$, $\hat{\mathbf{J}}_r$ and $\hat{\mathbf{J}}_r^2$, $r = 1, \ldots, 4$.

where the allowed values of j_r are $0, \frac{1}{2}, 1, \ldots$. Smaller values of j_r are not allowed because for $j_r = -1/2$ the manifolds do not have full dimensionality, while for $j_r < -1/2$ they do not exist. We choose the quantum number j_r so that it agrees with the usual notation in physics for the eigenvalues of various operators, but that is not confirmed until we compute the semiclassical eigenvalues in Sec. 4.7.

Similarly, J_{12} must be an integer or half-integer on quantized manifolds, which we write in terms of a conventional quantum number by $J_{12} = j_{12} + \frac{1}{2}$. In addition, there is the condition that $j_1 + j_2 + j_{12}$ and $j_3 + j_4 + j_{12}$ be integers, the requirement (with the usual interpretation of the quantum numbers) that the $3j$-symbols in Fig. 36 should exist. See also eq. (I.85). These imply that $j_1 + j_2 + j_3 + j_4$ must be an integer, part of the conditions that the subspace $\mathcal{Z}$ defined in Sec. 3.4 be nontrivial.

The range of the quantum number j_{12} is determined by the requirement that the A-manifold be 8-dimensional. Looking first at the upper limit, if J_{12} is quantized we have

$$J_{12} = j_{12} + \frac{1}{2} < J_{12,\text{max}} = \min(j_1 + j_2 + 1, j_3 + j_4 + 1). \tag{37}$$

Given the other conditions on j_{12}, this implies that the maximum quantized value of J_{12} is $J_{12,\text{max}} - \frac{1}{2}$. Similarly, we find that the minimum quantized value of J_{12} is $J_{12,\text{min}} + \frac{1}{2}$. The quantized values of J_{12} are separated from the maximum and minimum classical values (for given J_r, $r = 1, \ldots, 4$) by a margin of $\frac{1}{2}$, and are spaced in integer steps. These rules imply

$$j_{12,\text{max}} = J_{12,\text{max}} - 1, \qquad j_{12,\text{min}} = J_{12,\text{min}}. \tag{38}$$

They also imply the bounds (15) on the quantum number j_{12}. Similar results apply to the B-manifold and the quantized values of J_{23}.

Figure 41 is a numerical example of these quantization rules. The square in the figure is given by the bounds (29) and (30), while the spots are the quantized values of J_{12} and J_{23}. The latter are related to the usual quantum numbers by

$$J_{12} = j_{12} + \frac{1}{2}, \qquad J_{23} = j_{23} + \frac{1}{2}. \tag{39}$$

The spots form a square array because $\langle j_{23}|j_{12}\rangle$ is a square matrix. The size of the matrix (the number of rows or columns of spots) is $\dim \mathcal{Z}$, given by (16). Other features of this figure will be explained later.
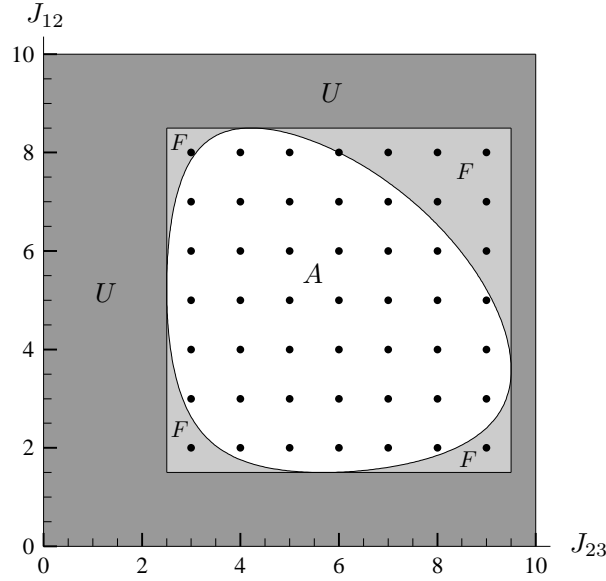
Figure 41. The J_{12}–J_{23} plane for $(J_1, J_2, J_3, J_4) = (5, \frac{7}{2}, 6, \frac{13}{2})$ (all quantized values). Region U is where either the A- or B- manifold does not exist. Inside the square both manifolds exist; A and F are the classically allowed and classically forbidden regions, respectively. Caustic curve is shown.

Note that the minimum value of J_r, $r = 1, \ldots, 4$ and of J_{12} on any quantized A-manifold is $\frac{1}{2}$, so the corresponding vectors always have a positive length. In addition, the triangles 1-2-12 and 3-4-12 always have a positive area. Similar conclusions apply to the quantized B-manifolds.

4.7. Semiclassical Eigenvalues

Once the classical manifolds are quantized, we find the semiclassical approximations to the eigenvalues of the operators in the A- or B-lists by evaluating the Weyl symbols of those operators on the classical manifold. Doing this for the operators $\hat{I}_r$, $r = 1, \ldots, 4$, we find the eigenvalue of $\hat{I}_r$ is j_r; this is the exact answer, something that was to be expected since $\hat{I}_r$ is a quadratic polynomial in the fundamental $\hat{x}$'s and $\hat{p}$'s of the system, and Weyl quantization of such operators is exact. See Littlejohn (1986) for more on classical and quantum quadratic polynomials. If we now compute the eigenvalue of $\hat{\mathbf{J}}_r^2$ by using the operator identity $\hat{\mathbf{J}}_r^2 = \hat{I}_r(\hat{I}_r + 1)$, naturally we get the exact answer, $j_r(j_r + 1)$. On the other hand, if we evaluate the Weyl symbol of the operator $\hat{\mathbf{J}}_r^2$ on the quantized level set, we get (according to the table) the eigenvalue $(j_r + 1/2)^2 - 3/8 = j_r(j_r + 1) - 1/8$, with an error of $-1/8$. There is an error because $\hat{\mathbf{J}}_r^2$ is a quartic polynomial in the fundamental $\hat{x}$'s and $\hat{p}$'s of the system, so Weyl quantization is not exact. The error is, however, of relative order $\hbar^2$, that is, $1/j^2$, which is the error expected in lowest order semiclassical approximations. The operators $\hat{\mathbf{J}}_r^2$ do not appear in the A- or B-lists, but operators $\hat{\mathbf{J}}_{12}^2$ and $\hat{\mathbf{J}}_{23}^2$ do, and here again there is an error at order $1/j^2$. Moreover, in this case there are no operators $\hat{I}_{12}$ or $\hat{I}_{23}$ which could be used to obtain the exact eigenvalues. This is a drawback of the 4j-model in comparison to the 8j- or 12j-models, where such operators exist.

It does not, however, change any of the subsequent analysis, which depends only on using the quantized manifolds to carry out the stationary phase calculation.

4.8. Time Reversal

The action of the antilinear time reversal operator $\hat{\Theta}$ on a carrier space $\mathcal{C}_j$ can be defined by

$$\hat{\Theta}|jm\rangle = (-1)^{j-m}|j,-m\rangle \tag{40}$$

(Messiah 1966). This is equivalent to $\hat{\Theta} = K_1^{-1} \circ G$, where G is the antilinear metric or map of Hermitian conjugation, and K_1^{-1} is defined in Sec. 2.7. The composition of the antilinear G with the linear K_1^{-1} is the antilinear time reversal map $\hat{\Theta}$. The map $\hat{\Theta}$ is easily extended to the full Schwinger Hilbert space $\mathcal{S}$ and tensor products thereof such as $\mathcal{H}_{4j}$.

Classically the antilinear $\hat{\Theta} : \mathcal{H}_{4j} \to \mathcal{H}_{4j}$ corresponds to an antisymplectic map $\Theta : \Phi_{4j} \to \Phi_{4j}$. In the complex coordinates, its action on all four spinors is given by

$$\Theta \begin{pmatrix} z_{1r} \\ z_{2r} \end{pmatrix} = \begin{pmatrix} -\bar{z}_{2r} \\ \bar{z}_{1r} \end{pmatrix}, \tag{41}$$

that is, $\Theta : z_r \mapsto v\bar{z}_r$, where $z_r \in \mathbb{C}^2$ and where

$$v = \exp(-i\sigma_2\pi/2) = \begin{pmatrix} 0 & -1 \\ 1 & 0 \end{pmatrix}. \tag{42}$$

We recall that in quantum mechanics, it is time reversal, not parity, that reverses the direction of angular momenta. At the classical level, this means that $\mathbf{J}_r\big(\Theta(x)\big) = -\mathbf{J}_r(x)$, where $x \in \Phi_{4j}$.

Time reversal can be projected via π onto Λ_{4j}, where its effect on the coordinates is $\Theta : \mathbf{J}_r \mapsto -\mathbf{J}_r$. It is an anti-Poisson map on Λ_{4j}.

5. Intersections and Actions

In this section we consider the intersections of the A- and B-manifolds, assuming that $J_r > 0$, $r = 1,\ldots,4$ are given. For now we treat this as a classical problem in which the J's (including J_{12} and J_{23}) are continuous variables, but we note that if J_r, $r = 1,\ldots,4$ are quantized then they are automatically positive. The motivation, however, is to find the stationary phase points of the scalar product (19), which are the intersections of the quantized manifolds.

5.1. Classically allowed and forbidden regions

A simple analogy will help to understand the results. Consider a one-dimensional harmonic oscillator, $H = (1/2)(x^2 + p^2)$ (classical or quantum). For a given value of the energy E, the classically allowed region is the interval of the x-axis between the turning points, given by $x = \pm\sqrt{2E}$, while the classically forbidden region is outside this interval. The classically allowed region can also be defined as the region of the x-axis where the two curves in phase space, $x = \mathrm{const}$ and $H = E$, have intersections. These curves are level sets of the observables x and H, which appear on the two sides of the matrix element when we write the energy eigenfunction as $\psi_E(x) = \langle x|E\rangle$. Inside the classically allowed region the intersections between the two curves consist of two points, with opposite momentum values. These are related by time reversal

$(p \to -p)$. In the classically forbidden region the two curves have no real intersections, but if we complexify phase space and the curves $x = $ const and $H = E$ (maintaining real contour values x and E), then they do have complex intersections that are related to the exponentially decaying wave function in the classically forbidden region.

We can view the classically allowed and forbidden regions in the x-E plane, in which both x and E are variables. See Fig. 42. The darkly shaded region in the figure, labeled UU, is the region $E < 0$, for which the level set $H = E$ does not exist. Above the line $E = 0$, both level sets, $x = $ const and $H = E$ exist. The unshaded region, labeled AA, is the classically allowed region, while the lightly shaded region, labeled FF, is the classically forbidden region. The quantized values of the energy $(E = n + \frac{1}{2})$ are indicated as spots on the E-axis. There is only a one-dimensional array of spots because the observable x has a continuous spectrum. The parabola $E = x^2/2$ is the caustic curve, separating the classically allowed from the classically forbidden region.
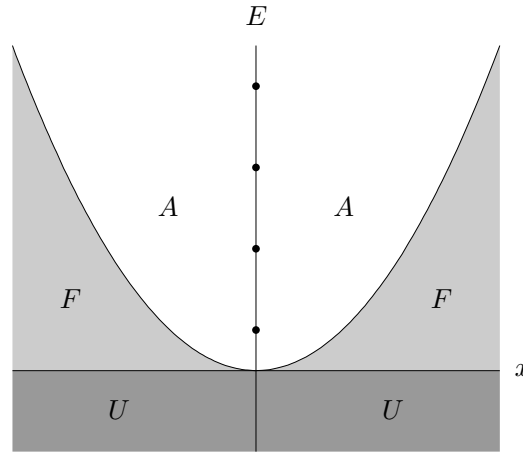

Figure 42. Regions of the x-E plane for the harmonic oscillator: UU where curves $H = E$ do not exist, and AA and FF, the classically allowed and forbidden regions, respectively. The parabola is the caustic curve.

5.2. Intersections of the A- and B-manifolds

Similarly, for positive J_r, $r = 1, \ldots, 4$, either the A- or B-manifold does not exist if J_{12} or J_{23} lies outside the bounds (29) and (30). Those inequalities define a square region of the J_{23}-J_{12} plane, as illustrated in Fig. 41. A figure like this was first given by Neville (1971). The darkly shaded region outside the square, labeled U, is where either the A- or B-manifold does not exist. In the interior of the square both manifolds exist and have full dimensionality. On the boundary of the square they exist, but have less than full dimensionality, since some triangle inequality is saturated. If the A- and B-manifolds exist and intersect, then we are in the classically allowed (unshaded) region in the interior of the square. If they exist but do not intersect, then we are in the classically forbidden (lightly shaded) region. The caustic curve is the oval curve in the figure, separating the classically allowed from the classically forbidden regions. Notice that it touches the square boundary at four points.

If we fix a value of J_{12}, we can regard the classically allowed and forbidden regions

as intervals of the J_{23}-axis. The interval within which the B-manifold exists is given by (30); this is the interval of allowed J_{23} values, given J_r, $r = 1, \ldots, 4$. The classically allowed region, on the other hand, is the interval of allowed J_{23} values, given J_r, $r = 1, \ldots, 4$ and J_{12} (equivalent to the statement that the manifolds intersect). Since this is a more restrictive condition, the classically allowed region must be a subset of the interval (30). Moreover, since the A-manifold is connected, the subset must be a connected interval, since this subset is the range of J_{23} values that occur on a given A-manifold. This is just what we see in Fig. 41: for most values of J_{12}, the interval inside the square consists of a classically allowed region, surrounded on both sides by classically forbidden regions, outside of which are the regions in which manifolds of the given J_{23} values do not exist. The bounds of the classically allowed region are given by the roots of (35), that is, they correspond to tetrahedra of zero volume. The caustic curve in Fig. 41 is the contour of $\det M = 0$, where M is the Cayley-Menger determinant (35).

The volume vanishes if the tetrahedron is flat. For most values of the parameters, this does not require that any of the triangular faces have zero area. But for certain values of J_{12}, the volume vanishes at a place where the face 2-3-23 has zero area (thus, $\mathbf{J}_2$, $\mathbf{J}_3$ and $\mathbf{J}_{23}$ are linearly dependent). This is the point where the caustic curve touches the boundary of the square on the left or right. Similarly, the caustic curve touches the boundary of the square on the top and bottom of the square, where not only does the volume vanish, but also the area of triangle 1-2-12.

The caustic curve never lies outside the bounds (30) defined by the triangle inequalities. Biedenharn and Louck (1981) appear to claim the contrary, but there is the question of whether one is talking about the classical or quantum triangle inequalities. That is, the caustic curve does pass outside the bounds given by the square array of quantized spots. It also seems to us that the interpretation of Biedenharn and Louck of Fig. 6 from Ponzano and Regge is incorrect.

If the values of J_r, $r = 1, \ldots, 4$ are quantized, then we can plot the quantized values of J_{12} and J_{23} as a square array of spots, as in the figure. See other comments on this array in Sec. 4.6. In Littlejohn and Yu (2009) we incorrectly stated that the quantized values of J_{12} and J_{23} can fall exactly on a caustic, citing the theory of Brahmagupta quadrilaterals (Sastry 2002). That theory shows that plane quadrilaterals with integer sides and integer diagonals exist, that is, flat tetrahedra with all integer edges. However, to represent a $6j$-symbol, the sums of the integers around the faces of triangles must be odd, and this condition cannot be met. (The integers divided by 2 are the values of $J_r = j_r + \frac{1}{2}$, and the sum of the j_r around the faces must be an integer.) A correct proof of the nonexistence of flat, quantized tetrahedra, credited to Adler, is given in a brief citation by Ponzano and Regge (1968).

We now examine the intersections of the A- and B-manifolds in greater detail. First, the A- and B-manifolds (assumed to exist) have an intersection in Φ_{4j} iff their projections onto Λ_{4j} intersect. Furthermore, the intersection in Φ_{4j} is the lift of the intersection of the projections in Λ_{4j}, with a T^4 fiber over every point. These statements follow from the fact that over every point $x \in \Lambda_{4j}$ there is a 4-torus fiber in Φ_{4j}, and that if x lies on the intersection of the projections of the A- and B-manifolds, then the 4-torus belongs to both the A- and B-manifolds in Φ_{4j}. This is the same logic used in I under similar circumstances.

To find the intersections of the projections in Λ_{4j} we require four vectors $\mathbf{J}_r$,

$r = 1, \ldots, 4$ that satisfy

$$|\mathbf{J}_r| = J_r, \qquad \sum_{r=1}^{4} \mathbf{J}_r = 0,$$

$$|\mathbf{J}_1 + \mathbf{J}_2| = J_{12}, \qquad |\mathbf{J}_2 + \mathbf{J}_3| = J_{23}, \tag{43}$$

for the given values of $J_r > 0$, $r = 1, \ldots, 4$ and of J_{12} and J_{23}. A nice way of constructing these vectors is given in Appendix A of Littlejohn and Yu (2009), which uses the singular value decomposition of the Gram matrix of dot products associated with the Cayley-Menger determinant (35). This method not only gives an explicit solution for these vectors at any point in the classically allowed region, it also shows that they are unique to within the overall action of $O(3)$. It is obvious in any case that if $\mathbf{J}_r$, $r = 1, \ldots, 4$ is a solution of (43), then so is $S\mathbf{J}_r$ for any $S \in O(3)$. This method was generalized to the $9j$-symbol in Haggard and Littlejohn (2010).

The group $O(3)$ is conveniently decomposed into proper rotations in $SO(3)$ and spatial inversion, which is time reversal in the present case. It is a basic fact of geometrical figures in $\mathbb{R}^3$ that spatial inversion is not equivalent to any proper rotation unless the figure is planar. Another fact is that the orbit of a geometrical figure under $SO(3)$ is diffeomorphic to $SO(3)$ itself, unless the dimension of the figure is ≤ 1. These issues are discussed by Littlejohn and Reinsch (1995, 1997) in the context of molecular configurations. They imply that except at the caustics, where the tetrahedron is flat, two tetrahedra related by time reversal are not related by any proper rotation. Therefore, except at the caustics, the solution set of (43) in Λ_{4j} consists of two disconnected subsets, each diffeomorphic to $SO(3)$, related by time reversal. Each subset consists of tetrahedra of nonzero volume related by proper rotations. At a generic point of the caustic curve, where the tetrahedron is flat but still 2-dimensional, the two subsets merge into one, which is still diffeomorphic to $SO(3)$.

The intersections in Φ_{4j} are the lifts of these intersections in Λ_{4j}. Therefore, except at the caustics, the intersection of the A- and B-manifolds consists of two disconnected subsets, related by time reversal, where each subset is a T^4-bundle over $SO(3)$. These subsets are 7-dimensional, so the A- and B-manifolds, which are 8-dimensional, intersect in two 7-dimensional submanifolds. The situation can be visualized as in Fig. 43, where $A \cap B = I_1 \cup I_2$ and where I_1 and I_2 are the connected intersection sets, related by Θ (see (41)). Each intersection set is an the orbit of the group $U(1)^4 \times SU(2)$, where $U(1)^4$ represents the phases of the four spinors and $SU(2)$ is the diagonal action (thus, the group is generated by I_r, $r = 1, \ldots, 4$ and $\mathbf{J}_{\text{tot}}$).
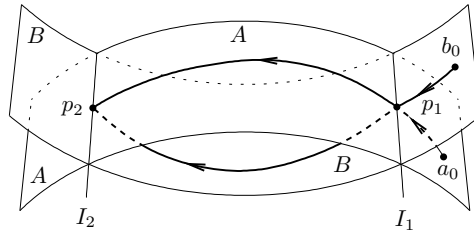

Figure 43. A schematic illustration of the intersection of the two 8-dimensional A- and B-manifolds in Φ_{4j}. The two intersections I_1 and I_2 are 7-dimensional, and are related by time reversal. Paths for computing action functions S_A and S_B relative to initial points a_0 and b_0 on the two manifolds are shown.

The isotropy subgroup of this group is $\mathbb{Z}_2$, generated by element $(2\pi, 2\pi, 2\pi, 2\pi, -1)$, in coordinates $(\psi_1, \psi_2, \psi_3, \psi_4, u)$ for group $T^4 \times SU(2)$, where $u \in SU(2)$. The volume of intersection manifold I_1 or I_2 with respect to the measure $d\psi_1 \wedge d\psi_2 \wedge d\psi_3 \wedge d\psi_4 \wedge du$ is

$$V_I = \frac{1}{2}(4\pi)^4 \times 16\pi^2 = 2^{11}\pi^6. \tag{44}$$

An interesting aspect of the method of Appendix A of Littlejohn and Yu (2009) for finding the vectors $\mathbf{J}_r$, $r = 1, \ldots, 4$ is that it also works in the classically forbidden region, where it produces complex 3-vectors that satisfy (43). These solutions are determined modulo the action of spatial inversion and $SO(3, \mathbb{C})$. In fact, as discussed in that reference, the vectors can be chosen so that two components are real and one purely imaginary, so that the symmetry group of the solution set is the Lorentz group $SO(2, 1) \subset SO(3, \mathbb{C})$. Roberts (1999) and others have referred to the tetrahedra in the classically forbidden region as living in $\mathbb{R}^3$ with a Minkowski metric, while those in the classically allowed region live in $\mathbb{R}^3$ with a Euclidean metric. This is a correct interpretation of the situation for the $6j$-symbol, but we do not think it is appropriate for generalizations to other spin networks. For example, in the $9j$-symbol (Haggard and Littlejohn 2010) the vectors in the classically forbidden region cannot be chosen so that two components are real, instead they belong to $\mathbb{C}^3$, and the symmetry group of the solution set is $SO(3, \mathbb{C})$, not some Lorentz subgroup thereof. This simply means that to explore the complex Lagrangian manifolds, complex Euler angles must be used when following the Hamiltonian flows generated by $\mathbf{J}_{\text{tot}}$. The complexified A- and B-manifolds in the $6j$-symbol support the asymptotic forms given by Ponzano and Regge (1968) in the classically forbidden region.

5.3. Actions and phases on the A- and B-manifolds

Let the x-space wave functions associated with states $|A\rangle$ and $|B\rangle$ of (21) be denoted $\psi_A(x) = \langle x|A\rangle$ and $\psi_B(x) = \langle x|B\rangle$, where $x \in \mathbb{R}^8$. The semiclassical approximations to these wave functions involve phases $e^{iS_A(x)}$ and $e^{iS_B(x)}$, where actions $S_A(x)$ and $S_B(x)$ are integrals of $p\,dx = \sum_{r\mu} p_{r\mu} dx_{r\mu}$ from some initial points on the two manifolds to some final point. The initial points on the A- and B-manifolds are denoted a_0 and b_0, respectively, in Fig. 43; they determine the overall phases of the states $|A\rangle$ and $|B\rangle$.

As explained in I, the branches of the stationary phase evaluation of the matrix element $\langle B|A\rangle$ are associated with the intersections of the A- and B-manifolds, in this case the manifolds I_1 and I_2, so the asymptotic form of the $6j$-symbol has two branches. Moreover, the phase associated with each branch is $S_A - S_B$ evaluated on the corresponding intersection manifold (see, for example, (I.3) or (I.5)), and is independent of where we evaluate it on that manifold. Figure 43 illustrates two points p_1 and p_2, on intersection manifolds I_1 and I_2, respectively, with paths that may be used for computing the actions S_A and S_B.

In the following we shall be interested in the relative phase between the two branches. Let us define

$$S_1 = S_{A1} - S_{B1}, \qquad S_2 = S_{A2} - S_{B2}, \tag{45}$$

and

$$S = S_2 - S_1 = \int_{a_0}^{p_2} - \int_{b_i}^{p_2} - \int_{a_0}^{p_1} + \int_{b_0}^{p_1} p\,dx = \oint p\,dx, \tag{46}$$

where the final integral is taken along the path that goes from p_1 to p_2 along the A-manifold and then back to p_1 along the B-manifold. The relative phase is independent of the initial points a_0 and b_0, and is moreover a symplectic invariant. The relative phase is easier to determine than the absolute phases of either branch, which are related to the overall phase convention for the $6j$-symbol. In computing the relative phase, we note that the loop integral in (46) can be evaluated with respect to any symplectic 1-form, such as the complex one used in I (see (I.64)),

$$\oint \sum_{r\mu} p_{r\mu}\, dx_{r\mu} = \mathrm{Im} \oint \sum z_{r\mu}\, d\bar{z}_{r\mu}. \tag{47}$$

The loop integral can be transformed by Stokes' theorem into an integral of the symplectic form over the enclosed area, since on $\Phi_{4j} = \mathbb{C}^8$ all cycles are boundaries.

5.4. Closing the loop in Λ_{4j}

We shall construct the closed loop giving the relative phase between the branches according to (46) by following the Hamiltonian flows of various observables. Let us define the signed volume of the tetrahedron as $V = (1/6)\mathbf{J}_1 \cdot (\mathbf{J}_2 \times \mathbf{J}_3)$, and let us take manifold I_1 to be the one on which $V < 0$, so that $V > 0$ on I_2. Time reversal changes the sign of the volume when mapping I_1 into I_2 and vice versa. Let us start at a point p of I_1, as in Fig. 44. Then by following the $\mathbf{J}_{12}^2$-flow we trace out a path that takes us along the A-manifold to a point q of I_2. We cannot use any of the other seven observables defining the A-manifold for this purpose, namely, $(I_1, I_2, I_3, I_4, \mathbf{J})$, since their flows confine us to the intersection manifold I_1.
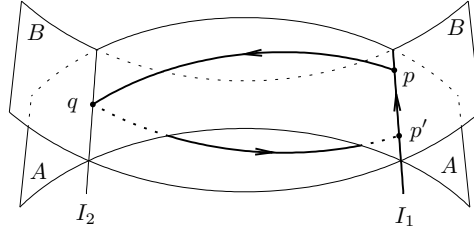

Figure 44. The $\mathbf{J}_{12}^2$-flow takes us from a point p of intersection manifold I_1 along the A-manifold to point q of manifold I_2; and then the $\mathbf{J}_{23}^2$-flow takes us back to point p' of I_1. To close the loop it is necessary to connect p' to p inside I_1.

We see that the $\mathbf{J}_{12}^2$-flow actually does take us to manifold I_2 by considering the projection of the path p-q in Fig. 44 onto Λ_{4j}. We visualize the projected path as a transformation applied to a set of four vectors in $\mathbb{R}^3$ that define a tetrahedron. The situation is illustrated in Fig. 45. In part (a) of that figure, we have four vectors $\mathbf{J}_r$ that sum to zero, defining a tetrahedron of negative volume. The lengths $J_r > 0$, $r = 1, \ldots, 4$, J_{12} and J_{23} are assumed to have the prescribed values, and vector $\mathbf{J}_{12}$ is drawn (but not $\mathbf{J}_{23}$). We take the point p of Fig. 44 to lie on the T^4 fiber above this tetrahedron. The $\mathbf{J}_{12}^2$-flow rotates the 1-2-12 triangle about the 12-axis by the right-hand rule while leaving the 3-4-12 triangle fixed (see (33)), that is, it rotates the 1-2-12 triangle into the foreground. Let the angle of rotation be $2\phi_{12}$, where ϕ_{12} is the interior dihedral angle of the tetrahedron along edge 12 in its original configuration. This brings triangle 1-2-12 through triangle 3-4-12 to the opposite side, creating a new

tetrahedron with the same lengths (the new J_{23} is the same as the old one), hence the same dihedral angles, but with the opposite signed volume. The result is illustrated in part (b) of Fig. 45, a tetrahedron that is the projection of a point $q \in I_2$ in Φ_{4j}, as illustrated in Fig. 44. Thus we see that the $\mathbf{J}_{12}^2$-flow does take us from I_1 to I_2 along the A-manifold, as claimed.
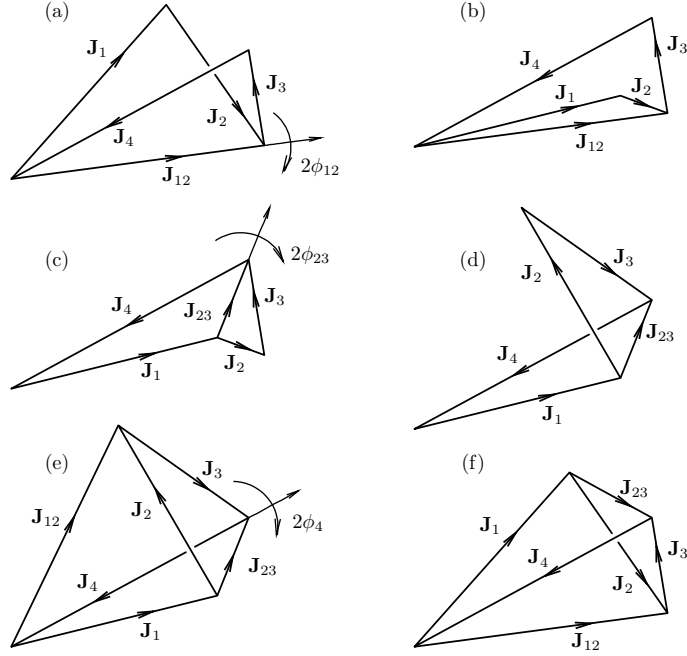

Figure 45. A cycle of rotational transformations that takes a tetrahedron in $\mathbb{R}^3$ back into itself.

Having reached point $q \in I_2$, we can go back to I_1 along the B-manifold by following the $\mathbf{J}_{23}^2$-flow, reaching point $p' \in I_1$ as illustrated in Fig. 44. The transformation in Λ_{4j} is illustrated in Fig. 45. Part (c) of that figure is the same as part (b), except that vector $\mathbf{J}_{23}$ is drawn and $\mathbf{J}_{12}$ is suppressed. The $\mathbf{J}_{23}^2$-flow rotates triangle 2-3-23 about the axis $\mathbf{j}_{23} = \mathbf{J}_{23}/J_{23}$, while leaving triangle 1-4-23 fixed. Let the angle of rotation be twice the interior dihedral angle along edge 23, that is, $2\phi_{23}$, as illustrated in part (c) of Fig. 45. The result is part (d) of that figure, a tetrahedron in which the volume has been inverted a second time, taking us back to the original (negative) volume in part (a). We arrive at point $p' \in I_1$, as in Fig. 44.

It is clear that p' is not the same as the original point p, because if it were, the orientation of the tetrahedron in part (d) of Fig. 45 would be the same as that in part (a). Thus to create a closed loop in Φ_{4j}, we must follow some path in I_1 taking us from p' to p, as in Fig. 44.

We create this path from p' to p in I_1 in two steps. First we apply an $SU(2)$ transformation to all four spinors at point p', that is, a diagonal transformation, whose projection onto Λ_{4j} is an $SO(3)$ transformation of the tetrahedron in part (d) of Fig. 45, returning it to the original orientation in part (a). This is a proper rotation of all four vectors $\mathbf{J}_r$, that is, a rigid rotation of the entire tetrahedron, and it is the final step in a cycle of rotations that transform the original tetrahedron in part (a)

into itself. That figures (a) and (d) must be related by some proper rotation is clear, since the lengths of the sides are the same and the signed volume is the same. In fact, it is easy to see that the axis of the final rotation is $\mathbf{J}_4$, since this vector is left invariant by both the $\mathbf{J}_{12}^2$- and $\mathbf{J}_{23}^2$-flows, and is the same in parts (a) and (d). As it turns out, the final rotation has axis $-\mathbf{j}_4 = -\mathbf{J}_4/j_4$ (notice the minus sign) and angle $2\phi_4$, twice the internal dihedral angle along edge 4. This is illustrated in part (e) of Fig. 45, which is the same as part (d) except that all vectors are drawn. The effect of the final rotation is illustrated in part (f), which is the same as part (a) except that all vectors are drawn.

5.5. Angle of the final rotation

To obtain the angle of the final rotation about axis $-\mathbf{j}_4$, we use the fact that the product of two reflections is rotation. Let a reflection about a plane P be $Q(P)$. There are four ways to draw the angle between the planes, one of which is denoted by α in Fig. 46. For a given choice of dihedral angle α, let the outward pointing normals of the two planes be $\mathbf{n}$ and $\mathbf{m}$, as in the figure. Then

$$Q(\mathbf{n})Q(\mathbf{m}) = R(\mathbf{a}, 2\alpha), \tag{48}$$

where we use axis-angle notation for the rotation R and where the axis $\mathbf{a}$ of the rotation is along the line of intersection of the two planes and is given by

$$\mathbf{a} = \frac{\mathbf{n} \times \mathbf{m}}{|\mathbf{n} \times \mathbf{m}|} = \frac{\mathbf{n} \times \mathbf{m}}{\sin \alpha}. \tag{49}$$

Although the angle α, the normals $\mathbf{m}$ and $\mathbf{n}$, and the axis $\mathbf{a}$ depend on which of the four choices is made for the dihedral angle, the resulting rotation does not (although it does depend on the order in which the reflections are applied).
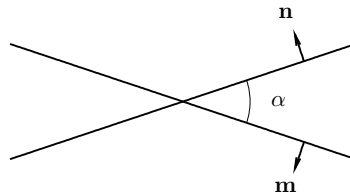

Figure 46. The product of two reflections is a rotation.

Let us denote the first rotation taking us from part (a) to part (b) of Fig. 45 in axis-angle form by $R_{12}(\mathbf{j}_{12}, 2\phi_{12})$, where the 12-subscript on R indicates that this rotation only affects vectors $\mathbf{J}_1$ and $\mathbf{J}_2$. It is obvious from Fig. 45 that the effect of this rotation on all the angular momentum vectors is to reflect them in the plane 3-4-12, that is,

$$\mathbf{J}'_r = Q(\text{3-4-12})\mathbf{J}_r, \tag{50}$$

where the prime refers to the values of the vectors after the first rotation and where $r = 1, \ldots, 4$. This applies for $r = 1, 2$ because the reflection in the 3-4-12 plane has the same effect as the rotation, and for $r = 3, 4$ because the reflection does nothing to these vectors and the rotation does not apply to them. Note that the 3-4-12 plane is the same in parts (a) and (b) of the figure (the plane is not affected by the first rotation).

Similarly, we denote the second rotation, taking us from part (c) to part (d) of Fig. 45, by $R_{23}(\mathbf{j}'_{23}, 2\phi_{23})$, where the prime on $\mathbf{j}'_{23}$ indicates that the axis is the 23-direction after the first rotation. Then the effect of the second rotation on all four $\mathbf{J}'_r$ is the same as a reflection in the plane 1'-4-2'3, that is,

$$\mathbf{J}''_r = Q(1'\text{-}4\text{-}2'3)\mathbf{J}'_r. \tag{51}$$

The planes of the two rotations intersect in edge 4 of the tetrahedron, which can be seen more clearly in Fig. 47, which is the same as part (c) of Fig. 45 except that all vectors are drawn. In Fig. 47, plane 3-4-12 is the back plane, and is also the plane of the first reflection. Plane 1'-4-2'3 (primes are omitted in the figure) is the plane of the second reflection. In comparison to (48), if we identify α with the interior dihedral angle ϕ_4 at edge 4, then $\mathbf{m}$ is the outward normal to plane 3-4-12, while $\mathbf{n}$ is the outward normal to plane 1'-4-2'3. Their cross product is in the direction $\mathbf{j}_4$, so we have

$$\mathbf{J}''_r = R(\mathbf{j}_4, 2\phi_4)\mathbf{J}_r, \qquad r = 1, \ldots, 4. \tag{52}$$

This is the rotation taking us from part (a) to part (e) of Fig. 45; to undo that rotation, we apply $R(-\mathbf{j}_4, 2\phi_4)$ to pass from part (e) to part (f) of that figure.
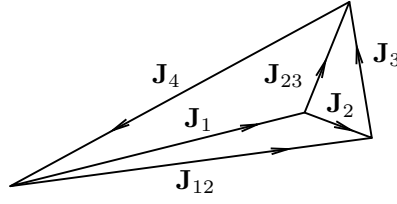

Figure 47. The plane of the first reflection is the back plane, 3-4-12, while that of the second is the plane 1'-4-2'3 (primes suppressed in the figure).

To summarize the rotational history, we have applied the rotations

$$R(-\mathbf{j}_4, 2\phi_4)R_{23}(\mathbf{j}'_{23}, 2\phi_{23})R_{12}(\mathbf{j}_{12}, 2\phi_{12}) \tag{53}$$

to the tetrahedron in part (a) of Fig. 45, taking it through a cycle of tetrahedra and returning it to its original shape and orientation. The corresponding $SU(2)$ rotations, with the same axes and angles, are applied to point p in Fig. 44, taking us along a path $p \to q \to p' \to p''$. Point p'' is not shown in Fig. 44, but it is a point of I_1 that projects onto the same tetrahedron as point p, since the projected path in Λ_{4j} is closed. Points p and p'' differ by the phases of the four spinors, that is, by transformations generated by (I_1, I_2, I_3, I_4). Thus, there is a final segment $p'' \to p$ needed to close the path in Φ_{4j}, which runs along the T^4 fiber over the initial configuration in Λ_{4j}.

5.6. Closing the loop in Φ_{4j}

There are several ways to compute the final four phases, but we will discuss just one. We start with vector $\mathbf{J}_1$. The action of the rotations (53) on this vector can be written

$$R(-\mathbf{j}_4, 2\phi_4)R(\mathbf{j}_{12}, 2\phi_{12})\mathbf{J}_1 = \mathbf{J}_1, \tag{54}$$

where we omit the subscripts on the R's because it is understood that only vector $\mathbf{J}_1$ is being acted upon, and where we omit the middle rotation in (53) since it does not

act on $\mathbf{J}_1$. The product of the two rotations in (54) is not the identity, but it is a rotation about axis $\mathbf{j}_1$ since it leaves $\mathbf{J}_1$ invariant.

To find the angle of this rotation, we use the Rodrigues-Hamilton formula (Whittaker 1960) for the product of two rotations in axis-angle form. Let $\mathbf{a}_i$, $i = 1, 2, 3$ be three unit vectors, which we can plot on the unit sphere as in Fig. 48. We join the three points on the unit sphere by arcs of great circles. On following the path $1 \rightarrow 2 \rightarrow 3 \rightarrow 1$ we regard the region to our right as the interior of the spherical triangle formed by the arcs. This gives meaning to the interior angles of the triangle, labeled ϕ_i, $i = 1, 2, 3$ in the figure. On going from point i to point $i + 1$ we can go either the long way or short way around the great circle; the interior of the triangle and the definitions of the interior angles depend on which way we go, but the formula is valid in any case. If we follow the arcs the short way around, we obtain a spherical triangle such as that shown in Fig. 48. Then the formula of Rodrigues and Hamilton is

$$R(\mathbf{a}_3, 2\phi_3)R(\mathbf{a}_2, 2\phi_2)R(\mathbf{a}_1, 2\phi_1) = I. \tag{55}$$

The proof is obtained by using (48) to write each rotation as a product of reflections, that is, $R(\mathbf{a}_1, 2\phi_1) = Q(31)Q(12)$ and cyclic permutations, where for example $Q(12)$ means reflection in the plane defined by axes $\mathbf{a}_1$ and $\mathbf{a}_2$.
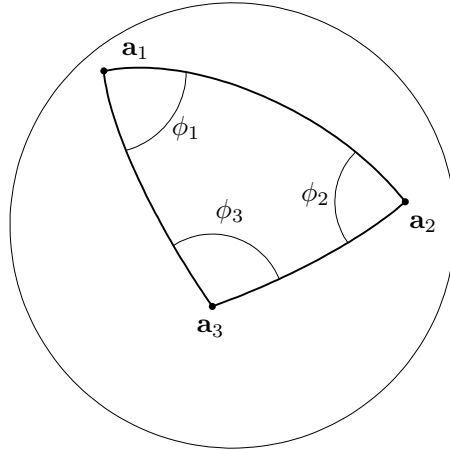

Figure 48. Axes $\mathbf{a}_i$ and angles ϕ_i, $i = 1, 2, 3$ for the product of three rotations.

To apply (55) to the rotations in (54) we imagine the vertex of the original tetrahedron (part (a) of Fig. 45) where edges 1, 4 and 12 meet as at the center of the sphere in Fig. 48, and we identify axes $(\mathbf{a}_1, \mathbf{a}_2, \mathbf{a}_3)$ with $(\mathbf{j}_{12}, -\mathbf{j}_4, \mathbf{j}_1)$. Then the ϕ's of Fig. 48 become the interior dihedral angles of the tetrahedron, and we have

$$R(\mathbf{j}_1, 2\phi_1)R(-\mathbf{j}_4, 2\phi_4)R(\mathbf{j}_{12}, 2\phi_{12}) = I. \tag{56}$$

Thus, the product of the two rotations in (54) is $R(-\mathbf{j}_1, 2\phi_1)$.

The third rotation found in this manner can be regarded as a holonomy. As the first two rotations in (54) are applied to $\mathbf{J}_1$, that vector traces out a closed curve on S^2 which is composed of the arcs of two small circles (the curve is a "small lune"). The sphere in question can be regarded as Σ_1, the symplectic manifold denoted Σ in (24) (the 1 subscript indicates that we are dealing with the first of the four copies of

Σ in Σ_{4j}). The two rotations themselves in (54) can be regarded as the lift of that curve on S^2 into $SO(3)$. The lift is an open curve starting at the identity in $SO(3)$ and ending at the product of the two rotations shown in (54). To close this curve in $SO(3)$, we apply the third rotation shown in (56).

This closed curve in $SO(3)$ may then be lifted (a second time) into $SU(2)$, by replacing each $SO(3)$ rotation by an $SU(2)$ rotation with the same axis and angle, that is, the lift is specified by the product $u(\mathbf{j}_1, 2\phi_1)u(-\mathbf{j}_4, 2\phi_4)u(\mathbf{j}_{12}, 2\phi_{12})$. This product is either $+1$ or -1, depending on the homotopy class of the closed loop in $SO(3)$. To find this class, we continuously deform the tetrahedron (see part (a) of Fig. 45), bringing dihedral angle ϕ_{12} to zero, so that the tetrahedron becomes flat. At the end of this deformation, $\phi_{12} = 0$ and one of ϕ_1 and ϕ_4 is 0 and the other is π. Thus, the closed loop in $SO(3)$ becomes an element of the noncontractible homotopy class of the homotopy group $\mathbb{Z}_2$ of $SO(3)$, so the product of the three $SU(2)$ matrices is -1. Therefore to close the loop in $SU(2)$ we apply a final rotation by an angle -2π, to obtain

$$u(\mathbf{j}_1, -2\pi)u(\mathbf{j}_1, 2\phi_1)u(-\mathbf{j}_4, 2\phi_4)u(\mathbf{j}_{12}, 2\phi_{12}) = +1. \tag{57}$$

The final rotation by angle -2π could have been chosen about any axis if all we wanted to do was to close the loop in $SU(2)$, but we choose axis $\mathbf{j}_1$ for the following reason. The first two spin rotations in (57), when applied to a spinor in $\mathbb{C}^2$ over vector $\mathbf{J}_1$, produce another spinor that projects onto $\mathbf{J}_1$ again, that is, it differs from the initial spinor only by an overall phase. This overall phase is the $U(1)$ holonomy mentioned above. The final step in closing the loop in Fig. 44 is to follow the I_r-flows to adjust the phases of the four spinors, in particular, we must follow the I_1-flow to adjust the phase of the first spinor. But the observable $\mathbf{J}_1^2 = I_1^2$ is a function of I_1, so we can follow its flow just as well. But $\mathbf{J}_1^2$ generates a rotation about the direction $\mathbf{J}_1$, that is, it is equivalent to multiplying the first spinor by an $SU(2)$ transformation with axis $\mathbf{j}_1$ and some angle. The angle required is seen in (57): it is $2\phi_1 - 2\pi$.

We remark that the final rotation in (57) could have been any angle $-2\pi + 4n\pi$. Adding a multiple of 4π to this angle is equivalent to going around some closed contour on the A-manifold (in fact, within I_1), which, when the manifolds are quantized and the Maslov phase is taken into account, changes the relative phase of the two branches by a multiple of 2π.

Next we turn to vector $\mathbf{J}_3$ and the phase needed to bring the third spinor back its original value after the rotations (53). The action of these rotations on $\mathbf{J}_3$ is given by

$$R(-\mathbf{j}_4, 2\phi_4)R(\mathbf{j}'_{23}, 2\phi_{23})\mathbf{J}_3 = \mathbf{J}_3, \tag{58}$$

where we omit the first one since it does not act on $\mathbf{J}_3$. The product of the two rotations in (58) is a third rotation about axis $\mathbf{j}_3$, which can be computed with the help of (55). This time we identify the 3-4-23 vertex of part (c) of Fig. 45, seen more clearly in Fig. 47, with the origin of the sphere in Fig. 48. We use the version of the tetrahedron after the first rotation (part (c)) since the middle rotation in (58) involves the rotated axis $\mathbf{j}'_{23}$. Thus we find

$$R(-\mathbf{j}'_{23}, 2\phi_{23})R(\mathbf{j}_4, 2\phi_4)R(-\mathbf{j}_3, 2\phi_3) = I. \tag{59}$$

Now using $R(-\mathbf{a}, \alpha) = R(\mathbf{a}, \alpha)^{-1}$ and taking the inverse of (59), we obtain

$$R(\mathbf{j}_3, 2\phi_3)R(-\mathbf{j}_4, 2\phi_4)R(\mathbf{j}'_{23}, 2\phi_{23}) = I, \tag{60}$$

which specifies a closed loop in $SO(3)$. We find the homotopy class of this loop by taking $\phi_{23} \to 0$, which makes one of ϕ_4 and ϕ_3 zero and the other π, so the loop in $SO(3)$ belongs to the noncontractible class. Thus, the lift into $SU(2)$ is not closed, but we can close it by appending a final spin rotation about axis $\mathbf{j}_3$ by angle -2π. Thus the closed loop in $SU(2)$ is specified by

$$u(\mathbf{j}_3, -2\pi)u(\mathbf{j}_3, 2\phi_3)u(-\mathbf{j}_4, 2\phi_4)u(\mathbf{j}'_{23}, 2\phi_{23}) = +1, \tag{61}$$

which when applied to the third spinor at point p in Fig. 44 returns it to its initial value. The final $U(1)$ holonomy of spinor 3, after the application of the three rotations (53), is $2\phi_3 - 2\pi$.

As for $\mathbf{J}_2$, its cycle on the sphere is specified by

$$R(-\mathbf{j}_4, 2\phi_4)R(\mathbf{j}'_{23}, 2\phi_{23})R(\mathbf{j}_{12}, 2\phi_{12})\mathbf{J}_2 = \mathbf{J}_2. \tag{62}$$

The product of the three rotations shown must be a rotation with axis $\mathbf{j}_2$. To find the angle, we first use (60) to obtain

$$R(-\mathbf{j}_4, 2\phi_4)R(\mathbf{j}'_{23}, 2\phi_{23}) = R(-\mathbf{j}_3, 2\phi_3). \tag{63}$$

Substituting this into (62) we obtain a product that we can evaluate with the help of (55) and with reference to the 2-3-12 vertex of the original tetrahedron (part (a) or (f) of Fig. 45). The result is

$$R(\mathbf{j}_2, 2\phi_2)R(-\mathbf{j}_3, 2\phi_3)R(\mathbf{j}_{12}, 2\phi_{12}) = I. \tag{64}$$

Thus the closed loop in $SO(3)$ associated with the loop traced by $\mathbf{J}_2$ on the sphere is specified by

$$R(\mathbf{j}_2, 2\phi_2)R(-\mathbf{j}_4, 2\phi_4)R(\mathbf{j}'_{23}, 2\phi_{23})R(\mathbf{j}_{12}, 2\phi_{12}) = I. \tag{65}$$

To find the homotopy class of this loop we deform the tetrahedron into a planar shape as before, and find that two of the four angles $(\phi_2, \phi_4, \phi_{23}, \phi_{12})$ are 0 and two are π. The loop in $SO(3)$ thus becomes the product of two rotations with angles 2π, which belongs to the contractible homotopy class. Therefore the lift into $SU(2)$ is closed,

$$u(\mathbf{j}_2, 2\phi_2)u(-\mathbf{j}_4, 2\phi_4)u(\mathbf{j}'_{23}, 2\phi_{23})u(\mathbf{j}_{12}, 2\phi_{12}) = 1, \tag{66}$$

which when applied to the second spinor at point p in Fig. 44 returns it to its initial value. The final $U(1)$ holonomy of spinor 2, after the application of the three rotations (53), is $2\phi_2$.

Finally, we treat vector $\mathbf{J}_4$ and the corresponding $U(1)$ holonomy. The effect of (53) on $\mathbf{J}_4$ is simply

$$R(-\mathbf{j}_4, 2\phi_4)\mathbf{J}_4 = \mathbf{J}_4, \tag{67}$$

since the first two rotations do not act on $\mathbf{J}_4$. This specifies an open curve in $SO(3)$ that can be closed (trivially) by multiplying by a rotation about axis $\mathbf{j}_4$,

$$R(\mathbf{j}_4, 2\phi_4)R(-\mathbf{j}_4, 2\phi_4) = I. \tag{68}$$

The closed loop in $SO(3)$ belongs to the contractible homotopy class, so its lift into $SU(2)$ is closed and is specified by

$$u(\mathbf{j}_4, 2\phi_4)u(-\mathbf{j}_4, 2\phi_4) = 1. \tag{69}$$

When applied to the fourth spinor at point p in Fig. 44 this sequence of spin rotations returns it to its initial value. The final $U(1)$ holonomy of spinor 4, after the application of the three rotations (53), is $2\phi_4$.

To summarize, we have succeeded in constructing the closed loop p-q-p'-p illustrated in Fig. 44 as the product of a sequence of seven spin rotations, each one generated by the Hamiltonian flow of one of the observables in the A- or B-list (in the A-list while we move on the A-manifold, and in the B-list while we move on the B-manifold). Most of these can be regarded as being generated by the square of some angular momentum vector; for example, the first and second spin rotations, specified by the axes and angles of the right-most rotations in (53), are generated by $\mathbf{J}_{12}^2$ and $\mathbf{J}_{23}^2$, respectively, while the last four rotations can be regarded as being generated by $\mathbf{J}_r^2$, $r = 1, \ldots, 4$. The third rotation in (53), about axis $\mathbf{j}_4$, is generated by $\mathbf{j}_4 \cdot \mathbf{J}$, that is, $u(-\mathbf{j}_4, 2\phi_4) = \exp(i\phi_4 \mathbf{j}_4 \cdot \boldsymbol{\sigma})$ is applied to all four spinors.

5.7. The Ponzano-Regge phase

The actions associated with these spin rotations are easily computed, using the complex 1-form (47) and the methods of Sec. I.9.2. To summarize the results, let $\mathbf{J}_p$ be a partial or total sum of the four angular momentum vectors (some range of $r = 1, \ldots, 4$ is summed over), with magnitude $|\mathbf{J}_p| = J_p$. Then the action along the path generated by $\mathbf{n} \cdot \mathbf{J}_p$ with elapsed angle θ is simply $(\mathbf{n} \cdot \mathbf{J}_p)\theta$. In particular, the third rotation in (53), the overall rotation of the tetrahedron taking us from part (e) to part (f) in Fig. 45, does not contribute to the action since in this case $\mathbf{J}_p = \mathbf{J}_{\text{tot}}$ which vanishes on the A- and B-manifolds. See also (I.74). As for the rotations generated by some $\mathbf{J}_p^2$, in this case $\mathbf{n} = \mathbf{j}_p = \mathbf{J}_p/J_p$, so the action is simply $J_p\theta$. Thus the first and second spin rotations specified by (53) contribute $J_{12}(2\phi_{12}) + J_{23}(2\phi_{23})$ to the total action. As for the last four rotations, in this case $\mathbf{J}_p$ is one of the $\mathbf{J}_r$, $r = 1, \ldots, 4$, and the four angles are summarized in Sec. 5.6. These rotations therefore contribute $J_1(2\phi_1 - 2\pi) + J_2(2\phi_2) + J_3(2\phi_3 - 2\pi) + J_4(2\phi_4)$ to the total action. Altogether, we have

$$S = \oint p \, dx = 2 \sum_{r=1}^{6} J_r \phi_r - 2\pi(J_1 + J_3), \tag{70}$$

where index $r = 5$ means $r = 12$ and $r = 6$ means $r = 23$. This can be written

$$S = -2\Psi + 2\pi(J_2 + J_4 + J_{12} + J_{23}), \tag{71}$$

where on quantized manifolds the final term is an integer multiple of 2π, and where

$$\Psi = \sum_{r=1}^{6} J_r(\pi - \phi_r). \tag{72}$$

The angle $\pi - \phi_r$ is the exterior dihedral angle, so Ψ is the phase of Ponzano and Regge.

6. The amplitude determinant and reduced phase space

Amplitude determinants are notorious for the trouble they cause in semiclassical approximations, for example, Gutzwiller's amplitude determinant (Gutzwiller 1967, 1969, 1970, 1971) has that reputation and in several studies of asymptotic approximations to spin networks the authors have resorted to numerical calculations for the amplitude determinant. In fact, amplitude determinants can be expressed in terms of Poisson brackets, which aids considerably in their evaluation. For example, Wigner's (1959) amplitude for the $6j$-symbol is a single Poisson bracket, while the

amplitude determinant for the 9j-symbol is a 2×2 matrix of Poisson brackets (Haggard and Littlejohn 2010), the derivation of which was the easiest part in the asymptotic formula for the 9j-symbol. Similarly it is easy to obtain tractable expressions for the amplitude determinant for the 15j-symbol and other more complicated cases of interest in quantum gravity.

In Sec. I.11 we presented a coordinate-based discussion of amplitude determinants in the 3j-symbol. For a more geometrical treatment of some of the issues discussed there we refer to the literature on the "quantization commutes with reduction" theorems of Guillemin and Sternberg (1982). Here we will simply review the results of I and discuss their geometrical content.

The discussion involves symplectic reduction, which in the case of the 4j-model of the 6j-symbol leads to the reduced phase space of the 6j-symbol, a 2-sphere denoted by Γ in (25). This space is essential for understanding the semiclassical mechanics of the 6j-symbol, for example, it is the phase space that underlies the 1-dimensional WKB methods used by Schulten and Gordon (1975a,b), and it played an important role in the derivation of the uniform asymptotic approximation of Littlejohn and Yu (2009), as well as in the semiclassical studies of the volume operator in quantum gravity by Bianchi and Haggard (2011).

6.1. Densities and amplitude determinants

In this section we adopt a general notation, as in Sec. 4.3, so that our results can be applied to the 4j-model of the 6j-symbol, the 12j-model of the 6j-symbol, the 9j-symbol, and many other examples. The phase space is $P = \mathbb{R}^{2N}$ with symplectic form $\omega = dp \wedge dx$. The theory of symplectic reduction usually begins with a symplectic group action on phase space, but a more natural starting point in our applications is the components of the momentum map of the group, which is a list of classical observables. Actually, there are two lists.

We assume that there exist on P an A- and a B-list of observables, $(A_1, \ldots, A_N)$ and $(B_1, \ldots, B_N)$, each of which forms a Lie algebra under the Poisson bracket. We denote contour values by a_i and b_i, so that level sets are specified by $A_i = a_i$ and $B_i = b_i$. We denote these level sets by L_a and L_b (these are the A- and B-manifolds). We assume that the A_i's and B_i's are functionally independent at most places in phase space, so that the generic dimensionality of L_a and L_b is N, although it may be less in exceptional cases. The A- and B-lists of observables correspond to two groups with symplectic actions on phase space, which we denote by G_a and G_b, with Lie algebras $\mathfrak{g}_a$ and $\mathfrak{g}_b$. We assume the groups are connected and have dimensionality N, as in Sec. 4.3. We denote the structure constants of one or the other group by $c^k{}_{ij}$, as in Sec. 4.3.

We are exclusively interested in contour values a and b that are fixed points of the coadjoint actions of the respective groups, since this implies that L_a and L_b, if N-dimensional, are Lagrangian. Only Lagrangian manifolds can support semiclassical wave functions. The restriction on the contour values means, however, that we do not have a Lagrangian foliation of P.

We will be interested in the WKB or semiclassical x-space wave function associated with the A- or B-manifold. We will work with the A-manifold, since the B-case is similar. For modern treatments of WKB theory, see for example Martinez (2002) or Mishchenko *et al* (1990). The variables x are half of the coordinates (x, p) on P; we denote "x-space" by $Q = \mathbb{R}^N$, which abstractly is best seen as the quotient

space when P is divided by the foliation into vertical Lagrangian planes, $x = \text{const.}$ We write this wave function in the form

$$\psi_a(x) = \langle x|a \rangle = K \sum_{\text{br}} |\Omega(x)|^{1/2} \exp\{i[S(x) - \mu\pi/2]\}, \tag{73}$$

where K is a normalization; where the sum is over branches of the projection $\pi : L_a \to Q$ from the Lagrangian manifold to Q, assumed to be locally invertible; where the branch index is suppressed in the sum; where S is the action computed as in Sec. 5.3; and where μ is the Maslov index.

We associate the function $\Omega(x)$ with an N-form Ω on Q by

$$\Omega = \Omega(x)\, dx^1 \wedge \ldots \wedge dx^N. \tag{74}$$

It follows from WKB theory that $\Omega(x)$ satisfies a set of amplitude-transport equations on Q, one for each observable A_i. These are conveniently expressed in terms of an N-form σ on L_a, defined by $\sigma = \pi^*\Omega$. Then the amplitude transport equations on Q are equivalent to $\mathcal{L}_{X_i}\sigma = 0$ on L_a, where $\mathcal{L}$ is the Lie derivative and where X_i, $i = 1, \ldots, N$ are the Hamiltonian vector fields on L_a associated with the A_i, that is, $X_i = \omega^{-1}dA_i$. This means that σ is invariant under the infinitesimal action of the group, hence under any finite action (recall that L_a is an orbit of the group action). These are left actions.

We express the solution σ as follows. The vector fields X_i may be chosen as a (generally non-coordinate) basis in each tangent space at each point of L_a. Let λ^i, $i = 1, \ldots, N$ be the dual 1-forms on L_a, that is, $\lambda^i(X_j) = \delta^i_j$. Then, in the case of compact groups, the solution σ is given by

$$\sigma = \lambda^1 \wedge \ldots \wedge \lambda^N, \tag{75}$$

to within a multiplicative constant. The reason is that σ is a version of the right-invariant Haar measure on the group, and for compact groups the left and right Haar measures are equal. Thus, σ is invariant under the (left) action of the group, and $\mathcal{L}_{X_i}\sigma = 0$.

The action of G_a on L_a provides two ways in which geometric structures on the group can be transferred to L_a. First, the group action implies a linear map $: \mathfrak{g}_a \to T_x L_a$ for each $x \in L_a$, which, under our assumptions, is invertible. This map can be used to push forward a standard N-form on $\mathfrak{g}_a$ to L_a. Let the basis in $\mathfrak{g}_a$ be $\{\xi_i, i = 1, \ldots, N\}$, corresponding to the observables A_i and vector fields X_i, and let $\{\alpha^i, i = 1, \ldots, N\}$ be the dual basis in $\mathfrak{g}_a^*$, that is, $\alpha^i(\xi_j) = \delta^i_j$. Then if the N-form $\alpha^1 \wedge \ldots \wedge \alpha^N$ is pushed forward to L_a in this manner, we obtain σ, defined by (75).

A second way involves picking a point $x_0 \in L_a$ to serve as an "origin" in L_a, and then identifying points x of L_a by the group element g such that $x = gx_0$. This creates a diffeomorphism between a neighborhood of the identity in G_a and a neighborhood of x_0 in L_a, which can be used to push forward differential geometric structures from G_a to L_a. It then turns out that σ given by (75) is the push forward of the right-invariant N-form on G_a associated with $\alpha^1 \wedge \ldots \wedge \alpha^N$. Thus, σ is naturally invariant only under a right action of the group; the only reason it is also invariant under the left action is that for the groups we consider, the left and right Haar measures are identical.

To see this from another standpoint, a short calculation shows that $\mathcal{L}_{X_i}\lambda^j = c^j{}_{ik}\lambda^k$, from which follows $\mathcal{L}_{X_i}\sigma = c^j{}_{ij}\sigma$. To derive this we recall that although the Poisson brackets $\{A_i, A_j\}$ vanish on L_a, the Lie brackets of the corresponding Hamiltonian vector fields do not, instead we have $[X_i, X_j] = -X_k c^k{}_{ij}$. But if the left

and right Haar measures are equal, then the adjoint representation Ad_g is volume-preserving, so the structure constants are traceless, and $\mathcal{L}_{X_i}\sigma = 0$. In our examples we deal only with compact groups, so this condition is met.

That the solution is unique to within a multiplicative constant can be seen by supposing that σ' is another N-form on L_a such that $\mathcal{L}_{X_i}\sigma' = 0$. Since all N-forms are proportional, we must have $\sigma' = f\sigma$ where f is a function on L_a. This implies $X_i(f) = 0$, or $f = \mathrm{const}$ on L_a.

Now given that (75) is the solution we want, we write $\sigma = \pi^*\Omega$ in the form,

$$\Omega(x)\,dx^1 \wedge \ldots \wedge dx^N = \lambda^1 \wedge \ldots \wedge \lambda^N, \tag{76}$$

where we write simply dx^i for $\pi^*(dx^i)$, and we evaluate both sides on the set of vectors $(X_1, \ldots, X_N)$. This gives

$$\Omega(x)\det\{x^i, A_j\} = 1, \tag{77}$$

where we use $dx^i(X_j) = \{x^i, A_j\}$. This reproduces Eq. (I.92).

Finally, as shown in I, the normalization integral, evaluated in the stationary phase approximation, implies $K = 1/\sqrt{V_a}$, where V_a is the volume of L_a with respect to σ.

6.2. The amplitude of $\langle b|a \rangle$

A coordinate-based derivation of the amplitude of the semiclassical matrix element $\langle b|a \rangle$ was presented in I for the case of the $3j$-symbol. Here we discuss the results from a geometrical point of view, using the general notation of Sec. 4.3 and the previous section. The main issue is that the stationary phase set $L_a \cap L_b$ in the evaluation of the integral $\langle b|a \rangle = \int dx \langle b|x \rangle \langle x|a \rangle$ is not a set of isolated points, as expected on the basis of a naive dimensionality count, but rather a set of manifolds of dimensionality ≥ 1. These nontrivial intersection manifolds are due to the existence of a common "intersection group" of G_a and G_b, which may be defined as follows.

The basic idea is that the A- and B-lists of observables may have some observables in common, which generate the intersection group. This is obviously the case in (27), for example. But the specific observables that occur in the A- and B-lists depend on the bases chosen in the Lie algebras $\mathfrak{g}_a$ and $\mathfrak{g}_b$, and if a basis is changed then the A- or B-observables are replaced by linear combinations of themselves. So we need a precise definition of the observables "in common."

The actions of groups G_a and G_b on P provide Lie algebra anti-homomorphisms between $\mathfrak{g}_a$ and $\mathfrak{g}_b$ and the Lie algebra of (globally) Hamiltonian vector fields on P. By our assumptions these anti-homomorphisms have full rank, so the images of these two anti-homomorphisms are two N-dimensional Lie algebras of Hamiltonian vector fields. These two Lie algebras have an intersection which itself is a Lie algebra. Let the dimension of the intersection be p, and let $p+q = N$. The intersection Lie algebra is generated by a set of Hamiltonian functions, call them $(C_1, \ldots, C_p)$. These can be regarded as the functions common to the original A- and B-lists, that is, by a change of basis in $\mathfrak{g}_a$ and $\mathfrak{g}_b$ we can bring the A- and B-lists into the form $A = (C, D)$ and $B = (C, E)$, where $D = (D_1, \ldots, D_q)$ and $E = (E_1, \ldots, E_q)$ are sets of observables that the A- and B-lists do not have in common. The common observables C generate the action of an "intersection group" G_0, that is, they are the components of the momentum map of the action of G_0 on P. The group G_0 is not uniquely determined by the C observables, only its action on P is. The same applies to G_a and G_b, which are generated by the A- and B-lists of observables. But in practice there are convenient

ways of choosing all these groups so that the kernels of their actions are discrete. This means that $\dim G_a = \dim G_b = N$ and $\dim G_0 = p$. We may assume moreover that G_0 is connected (as we have already for G_a and G_b), since we are free to take the connected identity component of any of these groups.

The level set of the momentum map of the intersection group G_0 plays an important role in what follows. We denote this level set by L_0; its equation is $C_i = c_i$, $i = 1, \ldots, p$, for some contour values c_i. We choose the c_i such that L_0 has its generic dimension $2N - p = N + q > N$.

The level set L_0 is foliated into A- and B-manifolds, where the A-manifolds are parameterized by the values d_i of the observables D_i, and the B-manifolds by the values e_i of the observables E_i, $i = 1, \ldots, q$. We will assume that the Poisson brackets $\{A_i, A_j\}$ and $\{B_i, B_j\}$ vanish on L_0, so that the generic A- and B-manifolds in L_0 are Lagrangian. This is an extension of our earlier assumption, that these Poisson brackets vanish on a specific pair of A- and B-manifolds. Thus, after removing exceptional manifolds of less than generic dimensionality, L_0 is foliated into Lagrangian manifolds in two different ways. These Poisson bracket relations imply $\{C_i, C_j\} = 0$ on L_0, so that c is a fixed point of the coadjoint action of G_0. This does not mean that L_0 is Lagrangian (the dimension is wrong), but it is coisotropic (Abraham and Marsden 1978). It also means that the isotropy subgroup of the coadjoint action is the whole group, so the reduced phase space of level set L_0 under the G_0 action is the space L_0/G_0.

This draws attention to the orbits of G_0, which generically have dimension p. Not only is L_0 foliated into orbits of G_0, so is each A- and B-manifold, since G_0 is a simultaneous subgroup of G_a and G_b. Thus, the intersections of L_a and L_b, which are the stationary phase sets, are also foliated into orbits of G_0. We will assume that $L_a \cap L_b$ is a union of a discrete set of orbits of G_0. Based on a dimensionality count, this is the generic case. It holds for example in the $4j$-model of the $6j$-symbol, where $L_a \cap L_b$ consists of two orbits of G_0, the sets I_1 and I_2 in Fig. 43. It also holds in the $12j$-model used by Roberts (1999) and in our own work on the $9j$-symbol (Haggard and Littlejohn 2010).

The orbits of G_0 appear in the stationary phase evaluation of

$$\langle b|a \rangle = \int dx \, \langle b|x \rangle \langle x|a \rangle = \frac{1}{\sqrt{V_a V_b}} \int dx \sum_{\text{br}} \frac{1}{\sqrt{|\det\{x,A\} \det\{x,B\}|}}$$
$$\times \exp\{i[S_A(x) - S_B(x) - \mu\pi/2]\}, \tag{78}$$

where we have inserted the normalized x-space wave functions for the states $|a\rangle$ and $|b\rangle$, where the sum is over all pairs of branches of both wave functions, and where μ is the cumulative Maslov index. The stationary phase set is the projection of $L_a \cap L_b$ onto Q (x-space); it is a union of the projections of the discrete set of orbits of G_0 that make up $L_a \cap L_b$.

The projection of each orbit is a subset of Q that is locally p-dimensional. As in I, we introduce a local change of coordinates $x \to (y,z)$, where $(y^1, \ldots, y^p)$ are coordinates along the projected orbits and $(z^1, \ldots, z^q)$ are coordinates transverse, with $z = 0$ being the projected orbit itself. Then the integral becomes (suppressing normalization and branch sums)

$$\int \frac{d^p y}{|\det\{y,C\}|} \int \frac{d^q z}{\sqrt{|\det\{z,D\} \det\{z,E\}|}} \exp\{i[S_A(y,z) - S_B(y,z) - \mu\pi/2]\}. \tag{79}$$

When the exponent is expanded to second order in z, the leading term $S_A(y,0) -$

$S_B(y, 0)$ is independent of y, that is, it is constant along the orbits of G_0. The second derivative matrix of $S_A - S_B$ with respect to z does depend on y, but after doing the Gaussian integral and combining with the determinants in the denominator of the z-integration, the result is expressed purely in terms of the Poisson brackets $\{E_i, D_j\}$, which are independent of y.

The fact that the z-integral is independent of y, that is, our location on the orbit of G_0, is noteworthy. It means that the integral does not depend on the detailed nature of the z-coordinates, for example, it is invariant under a coordinate transformation of the form $z' = z'(z, y)$ such that $z = 0$ implies $z' = 0$. It suggests that we are dealing with a quotient operation in which we divide by the orbits of G_0.

Another remark is that there is nothing special about the x-representation in which the integral (78) is carried out. The x-coordinates were introduced as half of the (x, p) coordinates on $P = \mathbb{R}^{2N}$, but any representation related to this one by a metaplectic transformation (Littlejohn 1986) would work as well. This amounts to foliating phase space, not by the vertical Lagrangian planes $x = \text{const}$, but rather by other Lagrangian planes related to this one by any linear, symplectic map. In this manner one can divide the orbits of G_0 into segments and do the integral over each segment in a representation in which the projection of the orbit onto the representation space has full rank. The segments into which the orbit of G_0 is divided can even be infinitesimal, effectively making the representation for the integral a function of where we are along those orbits. Similarly, one can avoid the caustics of the wave functions ψ_a and ψ_b. This is the old idea underlying the Maslov method (Maslov and Fedoriuk 1981) in WKB theory.

In any case, once the z-integral is done and is recognized to be independent of y, the remaining y-integral can be lifted to the orbit of G_0 in phase space whereupon it becomes just the integral of the Haar measure of G_0, giving the volume of the orbit. This Haar measure is normalized as in the previous section, that is, we start with the observables C_i, $i = 1, \ldots, p$, we associate these with Hamiltonian vector fields $X_i = \omega^{-1} dC_i$ (a change of notation from above, where the X's were associated with the A's), we define form λ^i dual to the X_i on the orbits of G_0, and then the Haar measure on the orbit is taken to be $\lambda^1 \wedge \ldots \wedge \lambda^p$. The final result is

$$\langle b|a \rangle = (2\pi i)^{q/2} \frac{V_I}{\sqrt{V_a V_b}} \sum_{\text{br}} \frac{1}{\sqrt{|\det\{D_i, E_j\}|}} \exp[i(S_I - \mu\pi/2)], \quad (80)$$

where now the branches refer to the discrete set of orbits of G_0 that make up $L_a \cap L_b$, where V_I is the volume of intersection manifold I (an orbit of G_0), where S_I means $S_A - S_B$ evaluated on intersection manifold I, and where μ is a cumulative Maslov index (not necessarily the same as the previous ones). The branch index could otherwise be written as I, a label of the intersection manifold, and V_I is taken out of the sum because it does not depend on which intersection manifold is taken. The volume V_I differs from the volume of G_0 because in general there is a discrete isotropy subgroup, as in (44) (one is really computing the volume of a coset space).

The result (80) contains a $q \times q$ matrix of Poisson brackets, $\{E_i, D_j\}$, whose geometrical content may be understood in terms of a variation of the discussion of densities in Sec. 6.1. First we recall that the A- and B-lists are decomposed according to $A = (C, D)$, $B = (C, E)$. Next, we fix the contour values c_i, $i = 1, \ldots, p$, so that we have a definite level set L_0 of the momentum map of G_0. Then we let "b-space" be $\mathbb{R}^q$ with coordinates $(e_1, \ldots, e_q)$ or the region of $\mathbb{R}^q$ that is the projection of L_0 onto $\mathbb{R}^q$, where coordinates e_i are interpreted as the contour values in $E_i = e_i$. The matrix

element $\langle b|a \rangle$ can be thought of as a wave function on b-space for fixed values of the a's, that is, of the c's and d's. We write the amplitude of the semiclassical approximation to this wave function as $|\Omega(e)|^{1/2}$, where $\Omega = \Omega(e)\, de_1 \wedge \ldots \wedge de_q$ is the associated density (a q-form on b-space). This density is the projection of the natural density on the A-manifold, in the following sense. Let the A- or (C, D)-observables be associated with vector fields $X_i = \omega^{-1} dC_i$, $i = 1, \ldots, p$, and $Y_i = \omega^{-1} dD_i$, $i = 1, \ldots, q$, with dual 1-forms λ^i, $i = 1, \ldots, p$ and μ^i, $i = 1, \ldots, q$. These induce a density $\sigma_0 \wedge \mu^1 \wedge \ldots \wedge \mu^q$ on L_a, where $\sigma_0 = \lambda^1 \wedge \ldots \wedge \lambda^p$ is the Haar measure on G_0. Then Ω satisfies

$$\sigma_0 \wedge \pi^*\Omega = \sigma_0 \wedge \mu^1 \wedge \ldots \wedge \mu^q, \tag{81}$$

where π is the projection from L_0 or $L_a \subset L_0$ onto b-space. Now evaluating both sides on the set of vectors $(X_1, \ldots, X_p, Y_1, \ldots, Y_q)$, we obtain

$$\Omega(e) \det dE_i(Y_j) = 1. \tag{82}$$

This gives the amplitude shown in (80), since $dE_i(Y_j) = \{E_i, D_j\}$.

   This discussion has treated the A- and B-manifolds asymmetrically, projecting from the A-manifold onto b-space, but we could have projected the density on the B-manifold onto a-space with the same result. There are really four densities, two *on* the A- and B-manifolds, and two *of* the A- and B-manifolds.

   This discussion leads us to consider the reduced phase space $\Gamma = L_0/G_0$, which is parameterized by the contour values c_i, $i = 1, \ldots, p$. As is standard in symplectic reduction, the symplectic form on Γ is obtained by pulling back vectors from Γ to $L_0 \subset P$ and evaluating them on the symplectic form on P; this is meaningful because the answer does not depend on where on the orbit of G_0 they are pulled back to, nor on the component of the pulled-back vectors along the orbit. A consequence is that the projections of the A- and B-manifolds onto Γ, which are q-dimensional since the G_0 orbits are p-dimensional, are Lagrangian on Γ. Since we are assuming that $L_a \cap L_b$ is a discrete union of G_0 orbits, the projected manifolds on Γ intersect in a discrete set of isolated points. This would be the generic case on a symplectic manifold of dimension $2q$. Also, G_0-invariant functions on L_0 project onto functions on Γ, whose Poisson brackets on Γ are the same as the Poisson brackets of the original functions on P. Such functions in the present discussion include the observables D_i and E_i, $i = 1, \ldots, q$, so the Poisson brackets $\{E_i, D_j\}$ of (80) are naturally interpreted as living on Γ.

6.3. The case of the $6j$-symbol

It is straightforward to apply the general theory of Secs. 6.1 and 6.2 to the case of the $6j$-symbol. The phase space is $\mathbb{C}^8 = \mathbb{R}^{16}$ so $N = 8$. The common observables C are I_r, $r = 1, \ldots, 4$, and $\mathbf{J}_{\text{tot}}$, so $p = 7$ and $q = 1$. The group G_0 is $T^4 \times SU(2)$. The level set L_0 of the momentum map of G_0, for $I_r = J_r$, $r = 1, \ldots, 4$, and $\mathbf{J}_{\text{tot}} = \mathbf{0}$, is the subset of Φ_{4j} upon which the four angular momenta have specified lengths and their vector sum is zero. It is logical that this would be the subset of the classical phase space Φ_{4j} that corresponds to the space $\mathcal{Z}$ of four-valent intertwiners, introduced in Sec. 3.4, on which $\hat{I}_r = j_r$, $r = 1, \ldots, 4$ and $\hat{\mathbf{J}}_{\text{tot}} = \mathbf{0}$.

   The contour values of the C's, that is, of I_r, $r = 1, \ldots, 4$ and $\mathbf{J}_{\text{tot}}$, must be chosen so that L_0 has its maximum dimensionality, namely, 9. The condition is $J_r > 0$, $r = 1, \ldots, 4$ and the polygon inequality,

$$\max\{J_1, J_2, J_3, J_4\} < \frac{1}{2} \sum_{r=1}^{4} J_r, \tag{83}$$

which as indicated must not be saturated. This is the condition that it is possible to make a noncollinear polygon in $\mathbb{R}^3$ out of vectors of four given positive lengths. If this condition is satisfied, then L_0 is foliated into A- and B-submanifolds whose generic dimensionality is 8.

There is only one observable of the D- and E-type; according to (27) we should make the identifications $D = \mathbf{J}_{12}^2$ and $E = \mathbf{J}_{23}^2$. However, since we used $d\theta$ in the volume form on the A- and B-manifolds when computing the volume (34), we should use instead $D = |\mathbf{J}_{12}|$ and $E = |\mathbf{J}_{23}|$, since these are conjugate to θ (really θ_a and θ_b, since there are two of them). Then the Poisson bracket for the amplitude is

$$\{E, D\} = \{|\mathbf{J}_2 + \mathbf{J}_3|, |\mathbf{J}_1 + \mathbf{J}_2|\} = \frac{\mathbf{J}_2 \cdot [(\mathbf{J}_2 + \mathbf{J}_3) \times (\mathbf{J}_1 + \mathbf{J}_2)]}{|\mathbf{J}_{12}||\mathbf{J}_{23}|} = \frac{6V}{J_{12}J_{23}}, \tag{84}$$

where V is the signed volume of the tetrahedron, $6V = \mathbf{J}_1 \cdot (\mathbf{J}_2 \times \mathbf{J}_3)$, where we have used (26) to evaluate the Poisson bracket, and where in the final step we have evaluated the Poisson bracket on A- and B-manifolds with contour values J_{12} and J_{23}. We see the appearance of Wigner's volume (Wigner 1959). The volume changes sign between the two intersection manifolds I_1 and I_2, but it appears with an absolute value sign in (80) so both stationary phase points in the $6j$-symbol have the same amplitude.

The amplitude $|\Omega|^{1/2}$ contains the factor

$$\sqrt{J_{12}J_{23}} = \frac{1}{2}\sqrt{(2j_{12} + 1)(2j_{23} + 1)}, \tag{85}$$

which, when evaluated as shown on quantized manifolds, reproduces the square roots seen in (19). Thus, based on the pieces of the formula we have determined so far, we can write

$$\left\{ \begin{matrix} j_1 & j_2 & j_{12} \\ j_3 & j_4 & j_{23} \end{matrix} \right\} = \frac{e^{i\pi/4}}{\sqrt{12\pi|V|}} \frac{1}{2} \left[e^{i(S_1 - \mu_1\pi/2)} + e^{i(S_2 - \mu_2\pi/2)} \right], \tag{86}$$

where S_1 and S_2 are given by (45) (they are the phases $S_A - S_B$, evaluated on the intersection manifolds I_1 and I_2 of Fig. 43). These phases contain the phase conventions for the states $|A\rangle$ and $|B\rangle$ shown in Fig. 37, which appear semiclassically as the origins for action integrals on the Lagrangian manifolds, denoted a_0 and b_0 in Fig. 43. Since we have not considered these phase conventions yet, we cannot say what S_1 and S_2 are, but the difference $S = S_2 - S_1$ is given in terms of the Ponzano-Regge phase by (71).

To return to the 9-dimensional space L_0, it projects onto what was called "b-space" in Sec. 6.2, which in the present case is the J_{23}-axis, producing the interval $[J_{23,\min}, J_{23,\max}]$, given by (32). The inverse image of a point on this interval is a B-manifold with a given value of J_{23}. Similarly L_0 projects onto "a-space", that is, the J_{12}-axis, producing the interval (31), the inverse image of a point of which is an A-manifold with given J_{12} value. The space L_0 projects onto the J_{12}-J_{23} plane producing the classically allowed region of Fig. 41; the inverse image of a point of this region is an intersection of an A- and a B-manifold of given J_{12} and J_{23} values. If the point does not lie on the caustic curve, the intersection consists of two disconnected components I_1 and I_2, each an orbit of G_0, as in Fig. 43. On the caustic curve these components merge into one. Finally, by dividing by G_0, L_0 projects onto the reduced phase space Γ, which has dimensionality $9 - 7 = 2$. We now turn to this space.

6.4. The reduced phase space Γ

Spaces of the type Γ seem to have appeared first in the work of Kapovich and Millson (1995, 1996). Those authors showed that the space of polygons of a given number of sides with fixed lengths in $\mathbb{R}^3$, modulo overall rotations, is a symplectic manifold. In fact, for quadrilaterals the space is precisely Γ. This space was recently subjected to direct geometric quantization by Charles (2008), who connected it with the $6j$-symbol and used it for a new derivation of the Ponzano-Regge asymptotic formula. The space of five-sided polygons is the analog of Γ for the $9j$-symbol; it was used by Haggard and Littlejohn (2010) in their study of the asymptotics of the $9j$-symbol.

To visualize $\Gamma = L_0/G_0$ it helps to carry out the reduction in two steps. In the first step, we choose contour values $J_r > 0$, $r = 1, \ldots, 4$, for which the level set $I_r = J_r$ in Φ_{4j} is the product of 3-spheres $(S^3)^4$, as shown in (25). The I_r, $r = 1, \ldots, 4$, generate the action of the group $U(1)^4$, corresponding to the phases of the four spinors. Dividing this level set by $U(1)^4$, we obtain the symplectic manifold Σ_{4j} shown in (25), which topologically is $(S^2)^4$, and which consists of all sets of four vectors $\mathbf{J}_r$ in $\mathbb{R}^3$, $r = 1, \ldots, 4$, with fixed lengths, $|\mathbf{J}_r| = J_r$. The space Σ_{4j} is 8-dimensional. In the second step, we consider the submanifold in Σ_{4j} upon which $\mathbf{J}_{\text{tot}} = 0$, which is a level set of the momentum map of the action of $SO(3)$ on Σ_{4j}. This manifold consists of sets of four vectors $\mathbf{J}_r$ in $\mathbb{R}^3$ of fixed lengths J_r such that $\sum_r \mathbf{J}_r = \mathbf{0}$. The vectors can be placed end-to-end to form a "closed link," that is, a four-sided polygon in $\mathbb{R}^3$. The set of closed links is denoted CL in (25). We assume the polygon inequality (83) is satisfied, so the space CL has dimensionality $8 - 3 = 5$. Since this is the level set $\mathbf{J}_{\text{tot}} = 0$, the isotropy subgroup of the $SO(3)$-action is $SO(3)$ itself, so the reduced phase space is $\text{CL}/SO(3)$, which is the space Γ in (25). This has $5 - 3 = 2$ dimensions.

The phase space Γ is parameterized by the four fixed, positive values J_r, $r = 1, \ldots, 4$ that satisfy the polygon inequality (83). A point of this space specifies a quadrilateral in $\mathbb{R}^3$ of the given lengths, modulo overall proper rotations. Once the quadrilateral has been determined, one can draw in the two remaining edges, of lengths J_{12} and J_{23}, to fill in a tetrahedron. Thus, Γ can be thought of as the shape space for a set of tetrahedra, four of whose edges have fixed, positive lengths. The two lengths that are variable are on opposite sides of the tetrahedron. Here we define "shape" as a configuration modulo proper rotations, as in Littlejohn and Reinsch (1997); two shapes related by spatial inversion are generally distinct. The lengths $|\mathbf{J}_{12}|$ and $|\mathbf{J}_{23}|$ are variable functions on Γ. In fact, any rotationally invariant quantity associated with the tetrahedron, such as the dihedral angles, the areas of the faces, the signed volume, etc, is also a function on Γ.

It is easy to find coordinates on Γ. We may take one coordinate to be J_{12}, which varies between the bounds (31). (From this point on we drop the distinction between $|\mathbf{J}_{12}|$ and J_{12}, and similarly for J_{23} and J_{13}.) For a fixed value of J_{12}, the allowed set of shapes is generated by executing the "butterfly" motion about the axis $\mathbf{J}_{12}$, that is, rotating the triangle 1-2-12 about this axis, relative to the 3-4-12 triangle. We recall this motion is the Hamiltonian flow generated by $\mathbf{J}_{12}^2$ or the magnitude $|\mathbf{J}_{12}|$ (see (33)). Thus, coordinates can be taken to be (J_{12}, ϕ_{12}), where ϕ_{12} is the interior dihedral angle about the 12-edge. For each value of J_{12} in the interior of the range (31), a circle of shapes is generated as ϕ_{12} goes from 0 to 2π; but at the endpoints there is only a single shape. For example, at the lower limit of (31), the case $J_{12,\text{min}} = |J_1 - J_2|$ is illustrated in part (a) of Fig. 49. In this case the rotation of vectors $\mathbf{J}_1$ and $\mathbf{J}_2$ about the axis $\mathbf{J}_{12}$ does not change the shape. Similarly, part

(b) illustrates the case $J_{12} = J_{12,\min} = |J_3 - J_4|$. In this case, the $\mathbf{J}_{12}^2$-action rotates the 1-2-12 triangle, but does not change the shape since the new configurations that result are related to the original ones by an overall $SO(3)$ transformation. A similar analysis applies at the upper limit of (31).

Figure 49. When J_{12} is at its lower limit for given (J_1, J_2, J_3, J_4), the shape of the tetrahedron is not changed under the $\mathbf{J}_{12}^2$-action, so the lower limit corresponds to only one point of the reduced phase space.

We see that the set of shapes generated in this manner for J_{12} in the interior of the interval (31) is a cylinder, but the two endpoints are single points that pinch the cylinder at the two ends, creating a topological sphere. Topologically, $\Gamma = S^2$.

The symplectic form on Γ may be obtained by projecting $\omega = dp \wedge dx$ on Φ_{4j} as described in Sec. 6.2 , but it is easier just to notice that ϕ_{12} is the parameter of evolution along the flow generated by J_{12}, so (ϕ_{12}, J_{12}) form a canonically conjugate (q, p) pair on the sphere. The same obviously applies to J_{23} and J_{31} and their conjugate (dihedral) angles, so we have

$$dJ_{12} \wedge d\phi_{12} = dJ_{23} \wedge d\phi_{23} = dJ_{31} \wedge d\phi_{31}, \qquad (87)$$

indicating three sets of canonical coordinates on Γ, related by canonical transformations. These are examples of the action-angle variables discovered by Kapovich and Millson (1995, 1996), which in all cases are closely related to the recoupling schemes used in angular momentum theory. The length J_{31} and the associated dihedral angle ϕ_{31} do not appear in the coupling scheme we described in Sec. 3.4 or in the tetrahedra we have discussed so far, but would appear in a different tetrahedron in which the four vectors are placed end-to-end in a different order.

So far we have described the construction of Γ as a purely classical problem, but if the J_r are quantized, $J_r = j_r + 1/2$, $r = 1, \ldots 4$, then one can speak of a quantized level set L_0 and quotient space Γ.

The area of the sphere Γ with respect to the form $dJ_{12} \wedge d\phi_{12}$ is obviously just $2\pi(J_{12,\max} - J_{12,\min})$. If Γ is quantized, then by (38) and (16) the area is $2\pi D$, where $D = \dim \mathcal{Z}$. When quantized, Γ contains one Planck cell of area 2π for every state in the Hilbert space $\mathcal{Z}$. Obviously we obtain the same area if we use either of the other symplectic forms in (87).

6.5. Quantized curves in Γ

States in $\mathcal{Z}$, such as the A- and B-states given by (21), are represented semiclassically by Lagrangian manifolds in Γ, which are quantized curves in that space. For example, the A-states are represented by quantized levels sets of J_{12}.

To plot these we map Γ into a unit 2-sphere in $\mathbb{R}^3$ with standard coordinates (x, y, z) by associating (ϕ_{12}, J_{12}) with a standard set of spherical angles (θ, ϕ), where $\phi = \phi_{12}$ and

$$J_{12} = J_{12,\min} + \frac{D}{2}(1 + \cos\theta), \qquad (88)$$

where $D = J_{12,\max} - J_{12,\min}$ (generally), or $D = \dim \mathcal{Z}$ (when Γ is quantized). Here $x = \sin\theta\cos\phi$, $y = \sin\theta\sin\phi$, $z = \cos\theta$ are understood. Then the symplectic form on the sphere is $(-1/2)D\sin\theta\,d\theta \wedge d\phi$. These coordinates make the J_{12} orbits look nice (they are small circles, as noted. The orbits do not be thought of as having any privileged role. We use them mainly for plotting figures. The x-z plane in these coordinates does have an invariant meaning, however; it is the plane upon which the tetrahedra are planar (the volume vanishes). Moreover, time reversal is a reflection in this plane ($y \to -y$).

The quantized orbits of J_{12}, on a space Γ with five Planck cells of area, are illustrated in part (a) of Fig. 50. The orbits are just small circles, as noted. The orbits are numbered $n = 0, \ldots, 4$, in order of increasing J_{12}, and enclose area $(n+\frac{1}{2})2\pi$. The minimum and maximum values of J_{12} are at the south and north poles, respectively, because of the choice (88) of coordinates, but the minimum and maximum quantized values are separated from the values at the poles by $\frac{1}{2}$, as indicated by (39), since the polar caps defined by the last quantized orbit before the poles must have area $\frac{1}{2}$.

The quantized orbits of J_{23} are illustrated in parts (b) and (c) of that figure. The function J_{23} has a minimum on the x-z plane with $x > 0$, and increases monotonically toward a maximum on the same plane with $x < 0$. The orbits are time reversal symmetric, but have no symmetry under inversion through the origin in the coordinates used (there is no reason why they should). Also shown are some quantized orbits of J_{13}, in part (d) of Fig. 50.

Another interesting observable on the reduced phase space is the signed volume $V = (1/6)\mathbf{J}_1 \cdot (\mathbf{J}_2 \times \mathbf{J}_3)$. This has been suggested by Chakrabarti (1964) and by Lévy-Leblond and Lévy-Nahas (1965) as a "democratic" alternative to the usual choices J_{12}^2, J_{23}^2, J_{13}^2 for the intermediate variable in the quantum problem of the recoupling of three angular momenta. More recently, Carbone *et al* (2002) have reconsidered the use of this observable, and have derived both recursion relations and asymptotic formulas for the matrix elements connecting the J_{12}-basis and the V-basis. The level sets (orbits) of V are plotted in part (e) of Fig. 50. The orbits plotted are not quantized, but are evenly spaced in V about $V = 0$, and labelled $n = -2, \ldots, +2$. The $V = 0$ contour is the x-z plane, which is also a quantized orbit when $\dim \mathcal{Z}$ is odd. The orbit $V = v$ is mapped by time reversal into the orbit $V = -v$.

The Bohr-Sommerfeld condition for the quantized orbits of V can be expressed in terms of complete elliptic integrals of third kind. We will report on this and other results on the spectrum of V and on the wave functions $\langle j_{12}|V\rangle$ in future publications. Preliminary results are reported in Bianchi and Haggard (2011).

6.6. The 6j-symbol on the reduced phase space

As noted below (19) the 6j-symbol is proportional to the matrix element $\langle j_{23}|j_{12}\rangle$, so on Γ it is represented semiclassically by the quantized curves, $J_{23} = j_{23} + \frac{1}{2}$ and $J_{12} = j_{12} + \frac{1}{2}$. This is illustrated in part (f) of Fig. 50 for the case $\langle j_{23}|j_{12}\rangle = \langle 0|4\rangle$, where the numbers refer to the labeling of the quantized curves in parts (a) and (b) of that figure. These curves are projections of the A- and B-manifolds in Φ_{4j}, and their intersections, the points labelled P and Q in the figure, are the projections of intersections manifolds I_1 and I_2 as illustrated in Fig. 43, respectively. This follows because we defined I_1 as the intersection manifold upon which $V < 0$, and $V < 0$ at point P since it lies in the region $y < 0$. Also, the path (with direction indicated) surrounding the shaded area in part (f) of Fig. 50 is the projection of the loop (with
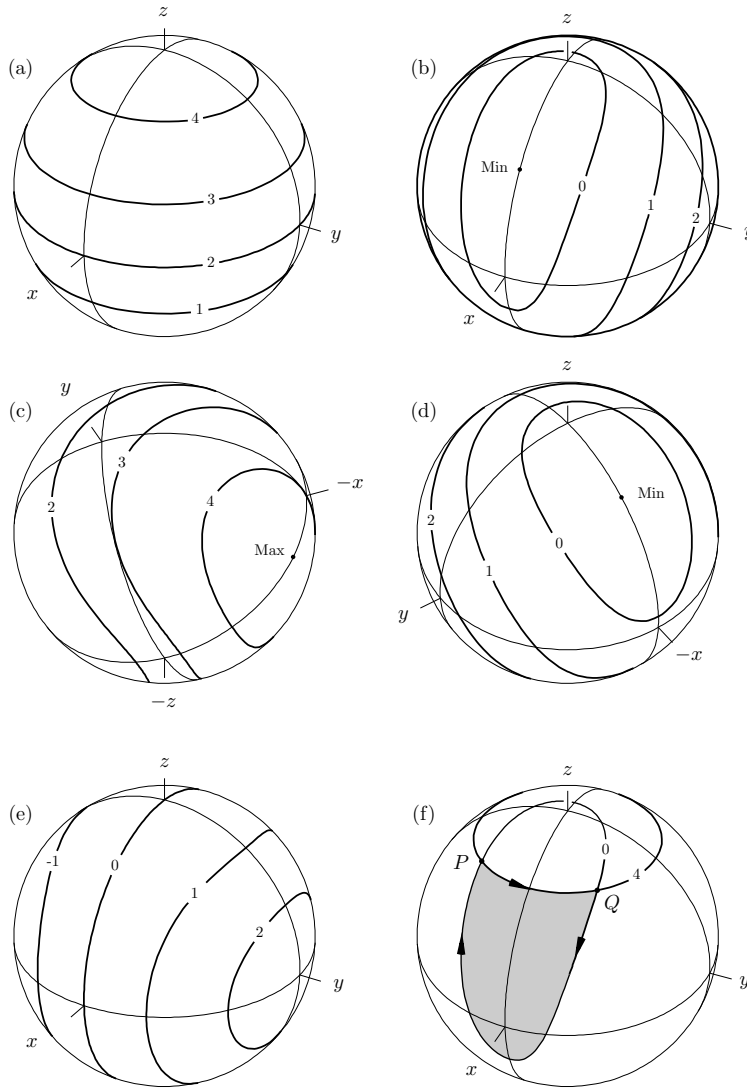
Figure 50. Orbits (or level sets) on the reduced phase space. In (a), orbits of J_{12}; in (b) and (c), of J_{23}; in (d), of J_{13}; in (e), of the volume V. Part (f) shows the orbits relevant to the 6j-symbol.

direction indicated) in Φ_{4j} illustrated in Fig. 44. We assign arrows to the path in Γ by following the flows generated by J_{12}^2 and J_{23}^2 in the direction of increasing ϕ_{12} and ϕ_{23}. Thus, the path The path $P \to Q \to P$ in part (f) of Fig. 50 corresponds to the sequence of rotations carried out on the tetrahedron in Fig. 45. On reaching point Q, the path turns down, because the rate of change of J_{12} along the J_{23}-flow is the Poisson bracket $\{J_{12}, J_{23}\}$, which is negative when $V > 0$, as follows from (84). One can also see this geometrically in Fig. 45; parts (b) and (c) of that figure correspond to point Q, and it is clear that J_{12} at first decreases, then increases again, on carrying out the rotation about $\mathbf{J}_{23}$, that is, on passing from part (c) to part (d) of Fig. 45.

The symplectic area of the shaded region in part (f) of Fig. 50 is the same as the Ponzano-Regge phase, to within a constant that depends on j_r, $r = 1, \ldots, 4$. On quantized manifolds it will not matter what region on S^2 is taken as the interior of the closed loop on the sphere (the choices differ by multiples of the total area of the sphere), but to be precise one must worry about this. The Ponzano-Regge phase is also -2 times the F_4-type generating function (Goldstein 1980, Miller 1974). Let us write $(q, p) = (\phi_{12}, J_{12})$, $(Q, P) = (\phi_{23}, J_{23})$ and $F_4(p, P) = -(1/2)S$, where S is given by (71). Then we have

$$q = -\frac{\partial F_4}{\partial P} = \frac{\partial}{\partial J_5} \sum_{r=1}^{6} J_r \phi_r, \tag{89}$$

where we use index 5 instead of 12. Here the angles ϕ_r must be interpreted as functions of the J's.

A more geometrical way of stating the same thing is to express the canonical transformation $(\phi_{12}, J_{12}) \to (\phi_{23}, J_{23})$ as a map between two spheres with symplectic forms (87). Then the graph of the canonical transformation is a Lagrangian manifold in $S^2 \times S^2$ with symplectic form $dJ_{23} \wedge d\phi_{23} - dJ_{12} \wedge d\phi_{12}$. This Lagrangian manifold is itself a sphere, whose projection onto J_{12}-J_{23} space is precisely the interior plus boundary of the oval curve in Fig. 41. The Lagrangian manifold has a double-valued projection onto the interior of the oval region, and a single-valued projection at the boundary (the caustics). The two disks fit together to form a sphere.

6.7. The Ponzano-Regge Formula

If we factor out the phase

$$\left(\frac{S_1 + S_2}{2} \right) - \left(\frac{\mu_1 + \mu_2}{2} \right) \frac{\pi}{2} \tag{90}$$

from the quantity in the square bracket in (86), we obtain a quantity proportional to

$$\cos \left[\left(\frac{S_1 - S_2}{2} \right) - (\mu_1 - \mu_2) \frac{\pi}{4} \right]. \tag{91}$$

However, in view of (45), (46), (71) and (72), this can be written as a sign times

$$\cos \left(\Psi + \Delta\mu \frac{\pi}{4} \right), \tag{92}$$

where the sign is $(-1)^{j_2 + j_4 + j_{12} + j_{23}}$ and where $\Delta\mu = \mu_2 - \mu_1$. Thus to obtain the argument of the cosine we must compute the relative Maslov index between the two branches, just as we have already computed the relative action $S = S_2 - S_1$.

This is the easiest of the Maslov index computations in deriving the Ponzano-Regged formula. We will omit details and simply remark that the calculation can be carried out entirely on the reduced phase space Γ, where it is not difficult to show that $\Delta\mu = 1$.

There remains the overall phase, which, in view of the reality of $6j$-symbol, must be a sign ± 1. This phase cannot be computed without taking into account the phase conventions for the two states $|A\rangle$ and $|B\rangle$, as well as the absolute Maslov indices on the intersection manifolds I_1 and I_2. The analogous phase for the $9j$-symbol was the most difficult part of the derivation of the results presented in Haggard and Littlejohn (2010). Since (in the case of the $6j$-symbol) the answer is known, we can see that this overall phase (combined with the $e^{i\pi/4}$ appearing in (86)) must be 1. We had no such

luxury in the case of the $9j$-symbol, nor did we find it possible to guess the answer. In any case, the final result is the Ponzano-Regge formula,

$$\left\{ \begin{array}{ccc} j_1 & j_2 & j_{12} \\ j_3 & j_4 & j_{23} \end{array} \right\} = \frac{1}{\sqrt{12\pi|V|}} \cos\left(\Psi + \frac{\pi}{4}\right). \tag{93}$$

For reasons of space we will omit the details in the calculation of these final phases, also because we have made the main points we wanted to make about the $6j$-symbol. These are the importance of the reduced phase space Γ, the geometry of symplectic reduction connecting it with higher dimensional spaces, and the manner in which elements of the semiclassical calculation (phases, amplitude determinants, etc) can be mapped from one space to another.

7. Conclusions

A glance at the calculation of Roberts (1999) shows that it is much easier and more elegant to compute the relative phase $S = S_2 - S_1$ of the $6j$-symbol in a symmetrical or $12j$-model than in the $4j$-model presented in this paper. The sum over edges times dihedral angles appears almost immediately. On the other hand, we have given a much easier way of computing the amplitude determinant, reducing it to a single Poisson bracket, whereas Roberts had to evaluate a large determinant. Obviously what is needed is a way of connecting the various models at a semiclassical level, so that actions, amplitude determinants, Maslov indices, etc, can be mapped from one model to another and computed wherever most convenient. We have investigated this question and will report on our results in the future. For now we merely make a few comments.

Already in this paper we have mapped amplitude determinants between various spaces, such as the Schwinger phase space Φ_{4j} and the reduced phase space Γ, which are connected by symplecic reduction. One might guess, therefore, that the $12j$- or symmetrical model of the $6j$-symbol and the $4j$-model are related by some kind of symplectic reduction. This is not the case, however, at least not in the way that Φ_{4j} and Γ are related. One piece of picture, however, is the following.

It is well known that a unitary map on a Hilbert space $U : \mathcal{H} \to \mathcal{H}$ corresponds semiclassically to a symplectic map or canonical transformation $T : \Phi \to \Phi$, where Φ is the symplectic manifold corresponding to $\mathcal{H}$. Also, the symplectic map T is conveniently viewed via its graph in $\Phi \times \Phi$, regarded as a symplectic manifold in its own right with symplectic form $\omega_1 - \omega_2$, where the subscripts refer to the first and second factors of $\Phi \times \Phi$ (Abraham and Marsden 1978). With this understanding, the graph of T is a Lagrangian manifold, one which supports semiclassically the operator U in the same way as a Lagrangian manifold in Φ supports a vector in $\mathcal{H}$. That is, U, which begins as a map $: \mathcal{H} \to \mathcal{H}$, is reinterpreted as a function $: \mathcal{H} \otimes \mathcal{H}^* \to \mathbb{C}$, that is, a "wave function" on a doubled space. The basic ideas inherent in this picture were developed by Hörmander (1971) and are also present in Miller (1974), while an elementary explanation of the geometrical situation is given by Littlejohn (1990).

It turns out that this picture generalizes to linear maps between Hilbert spaces $M : \mathcal{H} \to \mathcal{H}'$, where the two Hilbert spaces need not have the same dimensionality and where the map need not be unitary or even invertbible. The genralization involves again symplectic reduction, but in a different manner than that in which it appears in this paper. This situation arises in the comparison of two models of the $3j$-symbol, which is a simpler version of the comparison between the $12j$- and $4j$-models of the

$6j$-symbol. The first is a $2j$- or Clebsch-Gordan model, in which the Hilbert space is $\mathcal{C}_{j_1} \otimes \mathcal{C}_{j_2}$, where the operator $\mathbf{J}_3$ is a function of $\mathbf{J}_1$ and $\mathbf{J}_2$, that is, $\mathbf{J}_3 = \mathbf{J}_1 + \mathbf{J}_2$. The second is a symmetrical or $3j$-model, in which the Hilbert space is $\mathcal{C}_{j_1} \otimes \mathcal{C}_{j_2} \otimes \mathcal{C}_{j_3}$ and the operator $\mathbf{J}_3$ is independent, but in which we are interested only in states satisfying the constraint $\mathbf{J}_1 + \mathbf{J}_2 + \mathbf{J}_3 = 0$. We will report on these investigations in the future.

Roberts' (1999) derivation of the Ponzano-Regge formula effectively proceeded by writing the $6j$-symbol as a scalar product $\langle B|A \rangle$, where $|A\rangle$ and $|B\rangle$ are given by Fig. 33, then writing the wave functions for $|A\rangle$ and $|B\rangle$ in the Bargmann (1962) or coherent state representation to obtain an integral representation for the $6j$-symbol as an integral over $\mathbb{C}^{24}$. In the coherent state representation there is one copy of $\mathbb{C}$ for each degree of freedom, while in a $12j$-model there are two degrees of freedom for each j, hence 24 degrees of freedom total. Roberts then used the stationary phase approximation to evaluate the integral. The Bargmann representation has been used in a similar manner in several recent asymptotic studies in the quantum gravity literature.

In I and in this paper, however, we have mostly worked in a represenation-independent manner. Our emphasis on Lagrangian manifolds and other geometrical structures in phase space is part of this approach. From a certain point of view the coherent state representation is just another representation, albeit a complex one, so there is the question of whether it plays any privileged role or offers any advantages.

For some purposes it certainly does, for example, the wave functions in the coherent state representation are polynomials that can be written down explicitly, and these in turn are useful for deriving generating functions and other things, as shown by Schwinger (1952) and Bargmann (1962). Another point is that in the case of $SU(2)$, the coherent state representation appears naturally in the method of geometric quantization, that is, the holomorphic sections of Hermitian line bundles over the symplectic manifold S^2 are represented explicitly by Bargmann's entire analytic wave functions.

On the other hand, it is not obvious to us that the identification of the stationary phase set or the other aspects of the semiclassical calculation are easier or more transparent in the coherent state representation than in the representation-independent approach of this paper. Moreover, if one focuses too narrowly on the stationary phase evaluation of an integral, one misses the geometrical structures that support the representation-independent approach.

We had to assemble and extend several of the ideas presented in this paper for our derivation of the asymptotic form of the $9j$-symbol, and we have studied other extensions such as "g-inserted" spin networks, in which a group element or D-matrix is inserted in the edges of the spin network. Such g-inserted spin networks are basic amplitudes in loop quantum gravity (Rovelli 2004), taking one from the basis of spin connections to the spin network basis. The asymptotics of these amplitudes leads to piecewise flat manifolds similar to those introduced by Regge (1961).

We will report on these and other developments in the future.

Acknowledgments

References

Abraham R and Marsden J E 1978 *Foundations of Mechanics* (Reading, Massachusetts: Benjamin/Cummings)
Alesci E, Bianchi E, Magliaro E and Perini C 2008 preprint gr-qc 0809.3718
Ališauskas S 2000 *J Math Phys* **41** 7589
Anderson R W and Aquilanti V 2006 *J Chem Phys* **124** 214104
Aquilanti V, Cavalli S and De Fazio D 1995 *J. Phys. Chem.* **99** 15694
Aquilanti V, Cavalli S and Coletti C 2001 *Chem. Phys. Lett.* **344** 587
Aquilanti V and Coletti C 2001 *Chem. Phys. Lett.* **344** 601
Aquilanti V, Haggard H M, Littlejohn R G and Yu Liang 2007 *J Phys A* **40** 5637
Arnold V I 1989 *Mathematical Methods of Classical Mechanics* (New York: Springer-Verlag)
Baez J C 1996 *Adv. Math.* **117** 253
Baez J C and Barrett J W 1999 *Adv. Theor. Math. Phys.* **3** 815
Baez J C, Christensen J D and Egan G 2002 *Class. Quantum Grav.* **19** 6489
Balazs N L and Jennings B K 1984 *Physics Reports* **104** 347
Balcar E and Lovesey S W 2009 *Introduction to the Graphical Theory of Angular Momentum* (Berlin: Springer-Verlag)
Bargmann V 1962 *Rev. Mod. Phys.* **34** 829
Barrett J W 1998 *Adv. Theor. Math. Phys.* **2** 593
Barrett J W and Crane L 1998 *J. Math. Phys.* **39** 3296
Barrett J W, Dowdall R J, Fairbairn W J, Gomes H and Hellmann F 2009 preprint gr-qc 0902.1170
Barrett J W and Steele C M 2003 *Class. Quantum Grav.* **20** 1341
Barrett J W and Williams R M 1999 *Adv. Theor. Math. Phys.* **3** 209
Berger M 1987 *Geometry I* (Berlin: Springer-Verlag)
Berry M V 1977 *Phil Trans R Soc* **287** 237
Berry M V 1984 *Proc Roy Soc Lond A* **392**, 45
Bianchi E and Haggard H 2011 *Phys Rev Lett* **107** 011301
Biedenharn L C and Louck J D 1981 *The Racah-Wigner Algebra in Quantum Theory* (Reading, Massachusetts: Addison-Wesley)
Borodin K S, Kroshilin A E and Tolmachev V V (1978) *Teoreticheskaya i Matematicheskaya Fizika* **34** 110, English translation *Theoretical and Mathematical Physics* **34** 69
Brink D M and Satchler G R 1993 *Angular Momentum* (Oxford: Oxford University Press)
Brunnemann J and Rideout D 2008 preprint gr-qc 0706.0469
——2010 preprint gr-qc 1003.2348
Carbone G, Carfora M and Marzuoli A 2002 *Class. Quantum Grav.* **19** 3761
Carlip S 1998 *Quantum Gravity in 2 + 1 Dimensions* (Cambridge: Cambridge University Press)
Chakrabarti A 1964 *Ann. Inst. H Poincaré* **1** 301
Charles L 2008 preprint math 0806.1585
Conrady F and Freidel L 2008 *Phys. Rev. D* **78** 104023
Crippen G M and Havel T F 1988 *Distance Geometry and Molecular Confirmation* (Baldock, UK: Research Studies Press Ltd)
Cushman R H and Bates L 1997 *Global Aspects of Classical Integrable Systems* (Basel: Birkhäuser Verlag)
Cvitanovich P 2008 *Group Theory: Birdtracks, Lie's, and Exceptional Groups* (Princeton, Princeton University Press)
Danos M and Fano U 1998 *Phys. Rep.* **304** 155
De Fazio D, Cavalli S and Aquilanti V 2003 *Int. J. Quant. Chem.* **93** 91
Ding Y and Rovelli C 2010 preprint gr-qc 0911.0543
Edmonds A R 1960 *Angular Momentum in Quantum Mechanics* (Princeton: Princeton University Press)
El Baz E and Castel B 1972 *Graphical Methods of Spin Algebras* (New York: Marcel Dekker)
Freidel L and Louapre D 2003 *Class. Quantum Grav.* **20** 1267
Goldstein H 1980 *Classical Mechanics* 2nd ed (Reading, Massachusetts: Addison-Wesley)
Groenewold H J 1946 *Physica* **12** 405
Guillemin V and Sternberg S 1977 *Geometric Asymptotics* (Providence, Rhode Island: American Mathematical Society)
——1982 *Invent Math* **67** 515
Gurau R 2008 The Ponzano-Regge asymptotic of the 6j-symbol: an elementary proof *Preprint* math-ph 0808.3533
Gutzwiller M C 1967 J Math Phys **8** 1979

——1969 J Math Phys **10** 1004

——1970 J Math Phys **11** 1791

——1971 J Math Phys **12** 343

Hackett J and Speziale S 2007 *Class. Quantum Grav.* **24** 1525

Haggard H M and Littlejohn R G 2010 *Classical and Quantum Gravity* **27** 135010

Hörmander L 1971 *Acta Math* **127** 79

Kapovich M and Millson J J 1995 *J. Differential Geometry* **42** 133

——1996 *J. Differential Geometry* **44** 479

Kauffman L H and Lins 1994 *Temperley-Lieb Recoupling Theory and Invariants of 3-Manifolds*, (Princeton, New Jersey: Princeton University Press, New Jersey)

Kirillov A A 1976 *Elements of the Theory of Representations* (New York: Springer-Verlag)

——2004 *Lectures on the Orbit Method* (Providence, Rhode Island: American Mathematical Society)

Kurchan, Leboeuf P and Saraceno M 1989 *Phys. Rev. A* **40**, 6800

Lévy-Leblond J-M and Lévy-Nahas M 1965 *J. Math. Phys.* **6** 1372

Lewandowski J 1996 preprint gr-qc 9602035

Lindgren I and Morrison J 1986 *Atomic Many-Body Theory* (Springer-Verlag, New York)

Littlejohn R G 1986 *Phys. Reports* **138** 193

——1990 *J. Math. Phys.* **31** 2952

Littlejohn R G and Reinsch M 1995 *Phys. Rev. A* **52** 2035

——1997 *Rev Mod Phys* **69** 213

Littlejohn R G and Yu L 2009 *J. Phys. Chem. A* **113** 14904

Major S A and Seifert M D 2001 preprint 0109056

Marsden J E and Ratiu T 1999 *Introduction to Mechanics and Symmetry* (New York: Springer-Verlag)

Martinez A 2002 *An Introduction to Semiclassical and Microlocal Analysis* (New York: Springer-Verlag)

Marzuoli A and Rasetti M 2005 *Ann. Phys.* **318** 345

Maslov V P and Fedoriuk M V 1981 *Semi-Classical Approximations in Quantum Mechanics* (Dordrecht: D. Reidel)

Messiah A 1966 *Quantum Mechanics* (New York: John Wiley)

Mishchenko A S, Shatalov V E and Sternin B Yu 1990 *Lagrangian manifolds and the Maslov operator* (Berlin: Springer Verlag)

Miller W H 1974 *Adv. Chem. Phys.* **25** 69

Minkowski H 1897 *Nachr. Gess. Wiss.* 198

Moyal J E 1949 *Proc Camb Phil Soc* **45** 99

Neville D 1971 *J Math Phys* **12** 2438

——2006 *Phys Rev D* **73** 124004

Nicolai H and Peeters K 2007, in *Approaches to Fundamental Problems*, Seiler E and Stamatescu I-O eds (Berlin: Springer) (Lecture Notes in Physics v. 721) 151

Ooguri H 1992a *Nucl. Phys. B* **382** 276

——1992b *Mod. Phys. Lett. A* **7** 2799

Ozorio de Almeida A M 1998 *Phys Rep* **295** 265

Penrose R 1971 in *Combinatorial Mathematics and its Applications*, edited by D. Welsh (New York: Academic Press)

Ponzano G and Regge T 1968 in *Spectroscopy and Group Theoretical Methods in Physics* ed F Bloch *et al* (Amsterdam: North-Holland) p 1

Ragni M, Bitencourt A C P, Ferreira C da S, Aquilanti V, Anderson R W and Littlejohn R G 2010 *Int. J. Quantum Chem.* **110** 731

Regge T 1961 *Il Nuovo Cimento* **19**, 558

Regge T and Williams R M 2000 *J. Math. Phys.* **41** 3964

Roberts J 1999 *Geometry and Topology* **3** 21

Rovelli C 2004 *Quantum Gravity* (Cambridge University Press)

Rovelli C and Smolin L 1995 *Phys. Rev. D* **52**, 5743

Rovelli C and Speziale S *Class. Quantum Grav.* **23** 5861

Sastry K R S 2002 *Forum Geom* **2** 167

Schulten K and Gordon R G 1975a *J. Math. Phys.* **16** 1961

——1975b *J. Math. Phys.* **16** 1971

Schwinger J 1952 *On Angular Momentum* U.S. Atomic Energy Commission, NYO-3071, reprinted in Biedenharn L C and van Dam H 1965 *Quantum Theory of Angular Momentum* (New York: Academic Press)

Smolin L 2005 An Invitation to Loop Quantum Gravity *Preprint* hep-th/0408048

Stedman G E 1990 *Diagram Techniques in Group Theory* (Cambridge: Cambridge University Press)

Taylor Y U and Woodward C T 2004 preprint math 0406.228

Thiemann T 2007 *Modern Canonical Quantum General Relativity* (Cambridge: Cambridge University Press)

Turaev and Viro 1992 *Topology* **31** 865

Varshalovich D A, Moskalev A N and Khersonskii V K 1981 *Quantum Theory of Angular Momentum* (Singapore: World Scientific)

Van der Veen R 2010 PhD Dissertation "Asymptotics of quantum spin networks" http://www.science.uva.nl/research/math/Research/Dissertations/Veen2010.text.pdf

Voros A 1989 *Phys. Rev. A* **40**, 6814

Whittaker E T 1960 *A Treatise on the Analytical Dynamics of Particles and Rigid Bodies* (Cambridge: Cambridge University Press)

Wormer P E S and Paldus J 2006 *Adv Quantum Chemistry* **51** 59

Weissman Y 1982 *J. Chem. Phys.* **76**, 4067

Weyl H 1927 *Z Phys* **46** 1

Wigner E P 1932 *Phys Rev* **40** 749

——1940 *On the matrices which reduce the Kronecker products of representations of simply reducible groups* (unpublished), reprinted in Biedenharn L C and van Dam H 1965 *Quantum Theory of Angular Momentum* (New York: Academic Press)

——1959 *Group Theory* (Academic Press, New York)

Woodhouse N M J 1991 *Geometric Quantization* (Oxford: Oxford University Press)

Yutsis A P, Levinson I B and Vanagas V V 1962 *The Theory of Angular Momentum* (S Monson, Jerusalem)